Development and Application of Genus-Specific Peptide Arrays for Kinome Analysis

A Thesis

Submitted to the College of Graduate Studies and Research

In Partial Fulfillment of the Requirements

For the Degree of Doctor of Philosophy

In the Department of Biochemistry

University of Saskatchewan

By

Ryan Joseph Arsenault

PERMISSION TO USE

In presenting this thesis/dissertation in partial fulfillment of the requirements for a Postgraduate degree from the University of Saskatchewan, I agree that the Libraries of this University may make it freely available for inspection. I further agree that permission for copying of this thesis/dissertation in any manner, in whole or in part, for scholarly purposes may be granted by the professor or professors who supervised my thesis/dissertation work or, in their absence, by the Head of the Department or the Dean of the College in which my thesis work was done. It is understood that any copying or publication or use of this thesis/dissertation or parts thereof for financial gain shall not be allowed without my written permission. It is also understood that due recognition shall be given to me and to the University of Saskatchewan in any scholarly use which may be made of any material in my thesis/dissertation.

DISCLAIMER

Reference in this thesis/dissertation to any specific commercial products, process, or service by trade name, trademark, manufacturer, or otherwise, does not constitute or imply its endorsement, recommendation, or favoring by the University of Saskatchewan. The views and opinions of the author expressed herein do not state or reflect those of the University of Saskatchewan, and shall not be used for advertising or product endorsement purposes.

Requests for permission to copy or to make other uses of materials in this thesis/dissertation in whole or part should be addressed to:

Head of the Department of Biochemistry
University of Saskatchewan
Saskatoon, Saskatchewan S7N 5E5 Canada

OR

Dean
College of Graduate Studies and Research
University of Saskatchewan
107 Administration Place
Saskatoon, Saskatchewan S7N 5A2 Canada

ABSTRACT

Phosphorylation represents a central mechanism to regulate cell function. Protein phosphorylation is catalyzed by a class of enzymes called kinases, the cellular complement of which is referred to as its kinome. The study of the kinome has led to the development of peptide arrays as a high throughput tool. Though the approach was effective, it was limited to genera with characterized phosphoproteomes, as well as by the practice of interpreting emerging data through platforms designed for gene expression data. Within this thesis, these pivotal roadblocks are addressed through the presentation of 1) an approach for the development of custom-designed genus-specific arrays based on proteomic information and 2) a data analysis pipeline, Platform for Integrated, Intelligent Kinome Analysis (PIIKA), developed specifically for peptide array kinome data. The utility of these advances is demonstrated through the creation of the customized peptide arrays and subsequent confirmation of PIIKA-enhanced data transformation and mining. These techniques (custom array and PIIKA) were then applied to two complex host-pathogen interactions: prion diseases and *Mycobacterium avium* subsp. *paratuberculosis* (MAP) infection.

Prion diseases result from the misfolding of the widely expressed and highly conserved cellular prion protein (PrP^C) into an infectious and pathological scrapie-like conformation (PrP^{Sc}). Little is known about the function of PrP^C in either the normal or diseased states, although a role in signal transduction has been suggested. Two PrP^C protein-specific ligands, PrP 106-126 prion fragment and the prion-specific monoclonal antibody 6H4, were used to induce signalling in neuronal cells. Kinome analysis revealed distinct signalling pathways and varied signalling responses for each PrP^C ligand. This observation is consistent with the emerging concept that PrP^C interacts with multiple cellular proteins and plays a multifunctional role in regulating cellular responses.

MAP is the causative agent of Johne's disease in cattle. MAP establishes a persistent infection and has the ability to evade immune responses while replicating inside macrophages. Kinome analysis indicated that MAP is able to inhibit the interferon gamma (IFNγ)-induced JAK-STAT signalling pathway, eliminating the activation of downstream effectors. Further analysis indicated that the JAK-STAT pathway was blocked at the level of the IFNγ receptor, and JAK-STAT suppressor molecules known as SOCS were activated, both novel findings in the field of MAP pathogenesis.

Collectively, these investigations highlight the use of custom-designed and genus-specific peptide arrays to address complex biology in distinct genera.

ACKNOWLEDGEMENTS

DEDICATION

This thesis and entire Ph.D. is dedicated to my best friend and partner for life, my wife Kelly Arsenault. Without her, this Ph.D. may never have been started let alone completed. Knowing that you will be by my side throughout, whatever is in store for us, makes me look forward to every day. Regardless of where it takes us, the future is bright–as long as we experience it together.

TABLE OF CONTENTS

viii

LIST OF TABLES

LIST OF FIGURES

LIST OF ABBREVIATIONS

$\gamma^{32}P$	gamma phosphorous-32 isotope
Akt	RAC-alpha series/threonine protein kinase
ATP	adenosine triphosphate
BCR-ABL	breakpoint cluster region - Abelson murine leukemia viral oncogene homolog 1
BSA	bovine serum albumin
BSE	bovine spongiform encephalopathy
Btk	Bruton's tyrosine kinase
Bregs	regulatory B cells
CaM	calmodulin
CaMKII	calcium/calmodulin-dependent protein kinase II
CD	cluster of differentiation
CFU	colony-forming unit
X^2	chi-squared
CpG	cytosine phosphodiester guanine oligodeoxynucleotides
CWD	chronic wasting disease
DAPK1	Death-associated protein kinase-1
DEX	dexamethasone
DMSO	dimethyl sulfoxide
EDTA	ethylenediaminetetraacetic acid
EGFR	epidermal growth factor receptor
ELISA	enzyme-linked immunosorbent assay
EMEM	Eagle's Minimum Essential Medium
Erk	extracellular signal-regulated kinase
Etk	epithelial and endothelial tyrosine kinase
FBS	fetal bovine serum
FGFR	fibroblast growth factor receptor
FITC	fluorescein isothiocyanate
Fmoc	fluorenylmethyloxycarbonyl

Fura-2/AM	Fura-2-acetoxymethyl ester
GAM	goat-anti-mouse
GPI	glycophosphatidylinositol
GTP	guanosine triphosphate
H_0	null hypothesis
H_A	alternative hypothesis
HEPES	4-(2-hydroxyethyl)-1-piperazineethanesulfonic acid
HLA	human leukocyte antigen
HPK	histidine protein kinase
IFNγ	interferon gamma
IFNGR1	interferon gamma receptor 1
IFNGR2	interferon gamma receptor 2
IKK	IκB kinase
IL	interleukin
IRAK1	interleukin-1 receptor-associated kinase 1
JAK	Janus family kinase
JNK	Jun N-terminal kinase
KEGG	Kyoto Encyclopedia of Genes and Genomes
KRH	Krebs-Ringer-HEPES
limma	Linear Models for Microarray Data
log2	logarithm to base 2
logFC	logarithm to base 2 fold change
LPS	lipopolysaccharide
ManLAM	mannosylated lipoarabinomannan
MAP	*Mycobacterium avium* subsp. *paratuberculosis*
MAPK	mitogen-activated protein kinase
MEK	mitogen-activated protein kinase kinase
MHC-II	major histocompatibility complex class II
M. tuberculosis	*Mycobacterium tuberculosis*
NCBI	National Centre for Biotechnology Information
NGFR	nerve growth factor receptor

NFAT	nuclear factor of activated T-cell
NFκB	nuclear factor kappa-light-chain-enhancer of activated B-cells
OD	optical density
PP	Peyer's patch
PBMC	peripheral blood mononuclear cells
PBS	phosphate buffered saline
PBSA	phosphate buffered saline without magnesium or calcium
PCA	principal component analysis
PCR	polymerase chain reaction
PDGF	platelet-derived growth factor
PDGFR	platelet-derived growth factor receptor
PI3K	phosphoinositide-3 kinase
PI3P	phosphatidylinositol 3-phosphatase
PIIKA	Platform for Integrated, Intelligent Kinome Analysis
PKC	protein kinase C
PLC	phospholipase C
PNorm	percentile normalization
PNPP	para-nitrophenylphosphate
PrP 106-126	prion protein amino acids 106-126 peptide fragment
PrP^{C}	prion protein cellular conformation
PrP^{Sc}	prion protein scrapie-like conformation
PTP	protein tyrosine phosphatases
QNorm	quantile normalization
qRT-PCR	quantitative real-time polymerase chain reaction
R1	receptor 1
R2	receptor 2
RAMP	receptor activity modifying protein
RLT	RNeasy Lysis Buffer
RPMI	Roswell Park Memorial Institute
RT	real-time
SD	standard deviation

SHP-1	Src homology region 2 domain-containing phosphatase-1
SOCS	suppressor of cytokine signalling
Src	sarcoma
STAT	signal transducer and activator of transcription
TACO	tryptophan aspartate-containing coat protein
TAK1	mitogen-activated protein kinase kinase kinase 7
TBST	Tris-buffered saline and Tween 20
TBST-g	Tris-buffered saline and Tween 20 + 0.1% gelatin
TDM	trehalose-6-6'-dimycolate
TFA	trifluoroacetic acid
TGF	transforming growth factor
TGFBR	transforming growth factor beta receptor
T_h2	type 2 helper T cell
TLR	Toll-like receptor
TNF	tumour necrosis factor
TSE	transmissible spongiform encephalopathy
VEGF	vascular endothelial growth factor
VEGFR	vascular endothelial growth factor receptor
VSN	variance stabilization

1.0 LITERATURE REVIEW

1.1 Phosphorylation-Mediated Cellular Signalling

1.1.1 Kinases

In the mid 1950s, Edwin G. Krebs and Edmond H. Fischer described a means of enzymatic regulation based on the post-translational modification of proteins through phosphorylation. Protein phosphorylation was reversible and had a direct effect on enzymatic activity (Krebs and Fischer, 1955; Fischer and Krebs, 1955). It was subsequently determined that this phosphorylation-based protein modification was not limited to modulating enzymatic activity but affected a broad range of protein functions (Rubin and Rosen, 1975). For their role in this important advancement in cell biology, Krebs and Fischer were awarded the Nobel Prize in Physiology or Medicine in 1992. Protein kinases are now recognized as one of the largest and most important enzyme classes. Consisting of over 500 members (**Figure 1.1**), human protein kinases are responsible for modifying an estimated one third of the human proteome (protein complement of the cell) (Hunter, 1995; Manning, *et al*., 2002). The reversibility of protein phosphorylation and the generation of functional isoforms of an individual protein through complex patterns of phosphorylation at multiple sites add considerable functional diversity and complexity to the proteome.

Eukaryotic kinases catalyze the transfer of the γ-phosphate of adenosine triphosphate (ATP) or guanosine triphosphate (GTP) to hydroxyl groups. This transfer of phosphate groups generates phosphate monoesters in the case of serine- and threonine-containing proteins, or phenolic groups in the case of tyrosine-containing proteins (Hanks and Hunter, 1995). Several kinases have been found to have the capacity to utilize both ATP and GTP: ectoprotein kinase (Mastro and Sniezek, 1982), casein kinase 2 (Niefind, *et al.*, 1999) and calcium/calmodulin-dependent protein kinase II (CaMKII) (Bostrom, *et al.*, 2009). The amino acid residues that most commonly undergo phosphorylation, serine, threonine and tyrosine, do so at a ratio of 1,000:100:1 (Hunter, 1995). Protein kinases form a family of enzymes which are related due to the presence of conserved kinase domains. These domains are composed of approximately 250-300 amino acid residues and form the catalytic site. The kinase domains carry out three separate functions: 1) binding and orientation of the ATP (or GTP) phosphate donor in complex with a divalent cation, usually involving Mg^{2+} or Mn^{2+}, 2) binding and orientation of

the substrate, and 3) transferring the γ-phosphate from ATP (or GTP) to the acceptor-hydroxyl containing residue of the substrate.

Another common type of kinase is the histidine protein kinase (HPK) which is found widely outside of the animal kingdom (Wolanin, *et al.*, 2002). HPKs are transmembrane receptors which autophosphorylate a conserved histidine residue within the kinase. This phosphate group is then transferred to an aspartate residue in the receiver domain of a different protein, which carries out downstream signalling effects. Histidine kinases are part of the two-component signalling systems found in bacteria, plants and many other eukaryotes.

According to Kinbase, the online kinase database maintained by the Salk Institute and the biotechnology company SUGEN (www.kinase.com/kinbase), there are nine eukaryotic protein kinase groups: cAMP-dependent protein kinase/protein kinase G/protein kinase C extended (AGC), Calcium/Calmodulin regulated kinases (CAMK), Cell Kinase I (CK1), Cyclin-dependent Kinases and other close relatives (CMGC), Receptor Guanylate Cyclases (RGC), MAP Kinase cascade kinases (STE), Protein Tyrosine Kinase (TK), Tyrosine Kinase Like (TKL), and atypical protein kinases (Atypical). A tenth informal group, named Other, is made up of kinases which are not readily classified into any of the other established groups and is comprised of at least several hundred kinases (**Figure 1.1**).
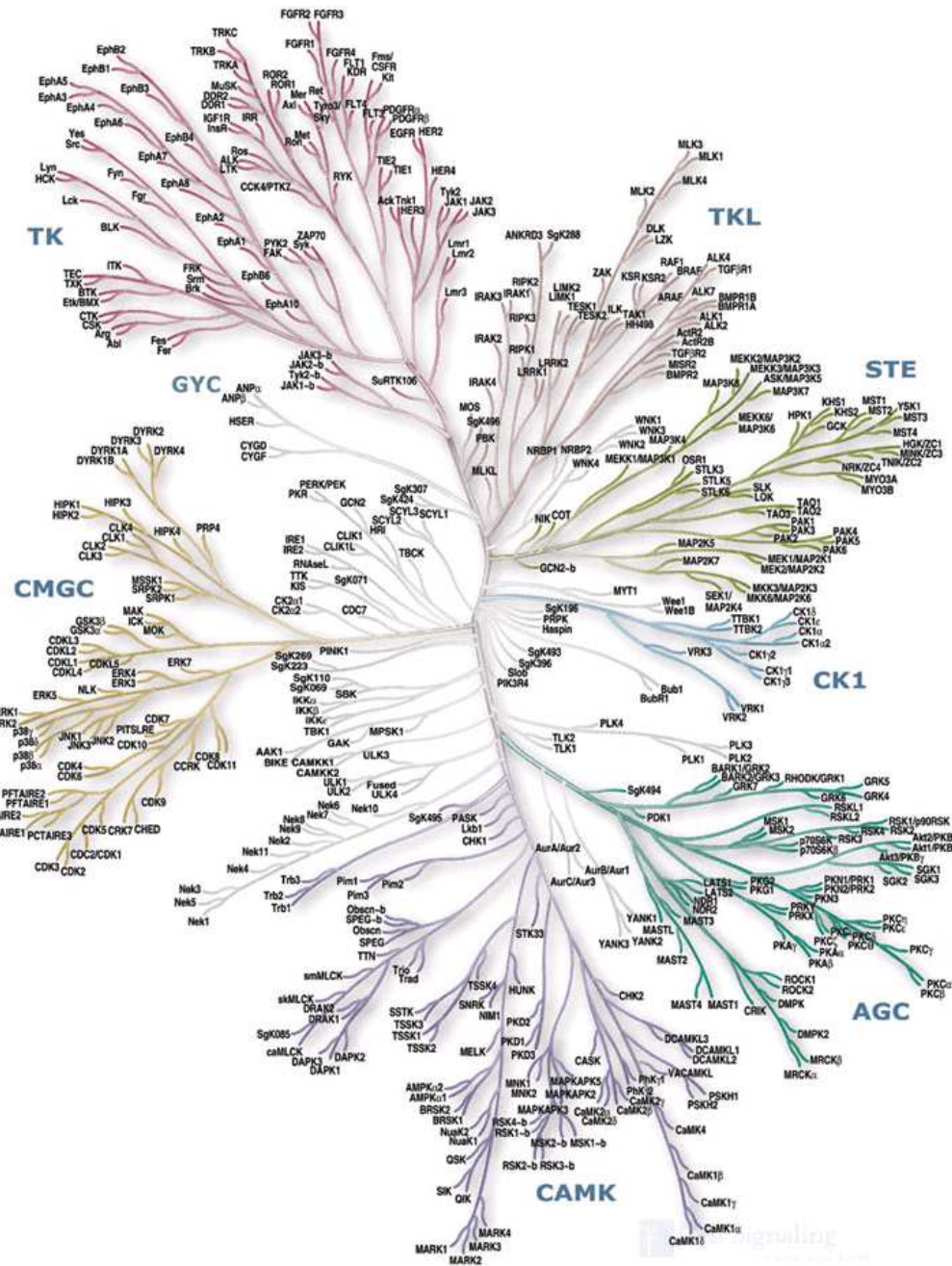
Figure 1.1. Human kinome dendrogram. The complement of kinases within the human genome as determined by Manning, *et al.*, (2002) is shown. The dendrogram shows the sequence similarity between catalytic domains. The distance along the branches between two kinases is proportional to the divergence between their sequences. Major groups of kinases are labelled and coloured distinctly. cAMP-dependent protein kinase/protein kinase G/protein kinase C extended (AGC), Calcium/Calmodulin regulated kinases (CAMK), Cell Kinase I (CK1), Cyclin-dependent Kinases and other close relatives (CMGC), MAP Kinase cascade kinases (STE), Protein Tyrosine Kinase (TK), Tyrosine Kinase Like (TKL), and Guanylate Cyclase kinases (GYC) (not considered an official kinase group). This illustration is reproduced courtesy of Cell Signalling Technology, Inc. (www.cellsignal.com).

1.1.2 Protein Kinases in Disease and as Therapeutic Targets

The disruption of phosphorylation-mediated cellular signalling is associated with a broad range of diseases including cancer, inflammation, neurological disorders and diabetes (Manning and Caenepeel, 2005). Of the approximately 500 protein kinases found in the human genome, over 250 map to disease loci (Knuutila, *et al*., 1998). The involvement of kinases in disease is often the result of improper expression/localization/activity or mutations in the protein sequence which alters any of the kinases' inherent characteristics. As will be discussed later, some pathogens produce their own enzymes to disrupt the natural pattern of host phosphorylation as a mechanism to subvert host defences (Section 1.5.2.3).

The important role of kinases in many diseases, as well as their regulatory role for cellular function, makes them potential targets for drug therapy (Cohen, 2002). Each kinase has a conserved active site with sufficient unique characteristics to allow for rational drug design targeting individual kinases or kinase groups (Hopkins and Groom, 2002). There are estimates that approximately 20-25% of the druggable genome is comprised of kinases (Keri, *et al.*, 2006). Kinase inhibitor treatment is seen as a more precise means of drug therapy than genetic manipulation, which activates or suppresses given genes. Unlike the disruption of gene expression, kinase inhibition acts proximal to the final cellular effectors; therefore, any unintended consequences can be more easily observed and managed. The central role of kinases in a variety of diseases, especially cancers, has led to considerable investment in the development of specific kinase inhibitors. Kinases are the most frequently targeted gene class in cancer therapy, and they are second only to G protein-coupled receptors in all therapeutic targets (Cohen, 2002; Hopkins and Groom, 2002).

Kinase inhibitors are an important class of drugs, and numerous examples have been employed for the treatment of a broad range of disorders. Gleevac® (imatinib), an inhibitor of the constitutively active breakpoint cluster region - Abelson murine leukemia viral oncogene homolog 1 (BCR-ABL) fusion protein, is approved for the treatment of leukemia and gastrointestinal stromal tumours (Druker, *et al*., 1996; Druker, *et al.*, 2001). Other protein kinase inhibitors, such as the epidermal growth factor receptor (EGFR) inhibitors Tarceva® and Iressa[TM], have either received FDA approval or are in late-stage clinical development to treat various cancers (Nobel, *et al*., 2004; Eglen and Reisine, 2009). However, kinase inhibitors have not only been developed for the treatment of cancer (Eglen and Reisine,

2009). Other examples include ruboxistaurin to treat diabetic retinopathy, safingol (a protein kinase C inhibitor) for the treatment of atopical dermatitis and fasudil which has received approval in Japan for treatment of cerebral ischemia (Sasaki, *et al.*, 2002; Ying, *et al.*, 2006). Anti-inflammatory drugs which suppress tumour necrosis factor (TNF)α and interleukin (IL)-1β expression function through kinase inhibition (Lee, *et al.*, 1994). Kinase involvement was determined through the study of the anti-inflammatory activity of pyridinyl-imidazole compounds. These compounds were shown to function through the inhibition of proteins referred to as cytokine-suppressive anti-inflammatory drug-binding proteins. These binding proteins were kinases which activated inflammatory cytokine responses; the kinases are now referred to as isoforms of mitogen-activated protein kinase (MAPK)14 (Gene Database, ncbi.nlm.nih.gov/gene). Two immunosuppressive drugs, cyclosporine A and rapamycin, function through broad non-specific modulation of the phosphorylation status of the cell: cyclosporine A through inhibition of phosphatases (Liu, *et al.*, 1991) and rapamycin through inhibition of kinases (Heitman, *et al.*, 1991). This disruption of the entire kinase or phosphatase class of enzyme inhibits not only immune response but also various other functions modulated by protein phosphorylation; thus, kinase inhibitors with broad activity can have extensive side effects. A partial listing of potential therapeutic kinase inhibitors and their current stage of development is presented in **Table 1.1**.

In addition to their important role as therapeutics, these kinase inhibitors are valuable experimental tools for enhancing our understanding of basic biology, cellular function, cell signalling and pathway cascades.

Table 1.1. Select therapeutic kinase inhibitors both approved and undergoing clinical trials.

Drug	Target Kinase	Status	Disease/Disorder
Avastin	VEGFR	Approved	Metastatic carcinoma, non-small cell lung cancer, breast cancer
Erbitux	EGFR	Approved	Metastatic colorectal cancer
Fasudil	Rho kinase	Approved	Cerebral vasospasm following surgery
Fostamatinib	Multikinase Inhibitor	Phase II	Colorectal, non-small cell lung, head and neck hepatocellular and renal cancer
Gleevac	ABL, KIT, PDGFR	Approved	Gastrointestinal stromal tumours, chronic myelogenous leukemia
GSK2118436	BRAF kinase	Phase II	Non-small cell lung cancer
Herceptin	Her-2	Approved	Her-2 positive breast cancer
Iressa	EGFR	Approved	Non-small cell lung cancer
MLN8237	Aurora A	Phase II	Stage III-IV melanoma
Nexavar	Multikinase Inhibitor	Approved	Renal cell carcinoma
P1446A-05	Cyclin dependent kinase	Phase I	Hematologic malignancy
Rapamune	mTOR kinase	Approved	Organ rejection in renal transplants
SB-681323	p38 MAPK	Phase II	Neuropathic pain, nerve trauma
Sprycel	TK Inhibitor	Approved	Chronic myelogenous leukemia, acute lymphoblastic leukemia
Sutent	VEGFR2, PDGFR, FLT3, KIT	Approved	Kidney cancer, gastrointestinal stromal tumours
Tarceva	EGFR	Approved	Metastatic non-small cell lung cancer
Tasigna	Abl	Approved	Chronic myelogenous leukemia
Tivozanib	VEGFR, TK	Phase II	Renal cell carcinoma
TORISEL	mTOR kinase	Approved	Advanced renal cell carcinoma
Tykerb	Her-2, others	Approved	Advanced breast cancer
Vandetanib	VEGFR, EGFR	Approved	Medullary thyroid cancer
Vectibix	EGFR	Approved	Colorectal cancer

Data sourced from Eglen and Reisine (2009), www.fda.gov and www.clinictrials.gov.

1.1.3 Phosphatases

The importance of protein phosphorylation to cellular function and its nature as a reversible post-translational modification means that the addition of phosphate groups, via the kinase, and removal, via the phosphatase, are equally important (Hunter, 1995). Interestingly, while Fischer and Krebs (1955) discovered the kinase and the chemical nature of the reaction involving inorganic phosphate (Krebs and Fischer, 1956), the phosphatase that catalyzes the reverse reaction had been reported over a decade earlier (Cori and Green, 1943). Phosphatases dephosphorylate specific amino acids much the same way as kinases phosphorylate specific residues. Phosphatases can be tyrosine-specific (Alonso, *et al.*, 2004), serine/threonine-specific (Shi, 2009), histidine-specific (Kim, *et al.*, 1993), have dual specificity (tyrosine and serine) (Camps *et al.*, 2000) or dephosphorylate lipids (Maehama, *et al.*, 2004). Tyrosine phosphatases are organized into four families: class I cysteine-based, class II cysteine-based, class III cysteine-based and aspartate-based (Alonso, *et al.*, 2004). Serine/threonine phosphatases are organized into three families: phosphoprotein phosphatases, metal-dependent protein phosphatases and aspartate-based phosphatases (Shi, 2009). While the number of tyrosine kinases and tyrosine phosphatases approximately match, the number of serine/threonine phosphatases is less than a tenth of the number of serine/threonine kinases. The human genome encodes 518 kinases in total (Manning, *et al.*, 2002). There are 107 protein tyrosine phosphatases (Alonso, *et al.*, 2004) and approximately 30 serine/threonine phosphatases (Shi, 2009). Serine/threonine phosphatases are able to maintain specificity equal to that of kinases despite their smaller numbers due to their ability to share catalytic subunits among different phosphatases regulated by a number of regulatory subunits. While traditionally kinases, rather than phosphatases, have been the target of therapeutic intervention, there is emerging appreciation of the role of phosphatases in disease (Alonso, *et al.*, 2004). One of the first studies which linked phosphatase activity with disease found the involvement of protein tyrosine phosphatase-1B in diabetic insulin sensitivity (Elchebly, *et al.*, 1999). Since that study, at least 13 phosphatases have been implicated in disease (Alonso, *et al.*, 2004).

1.1.4 "Omics" from Genes to Kinases

At the turn of this century, there was a strong focus on a genetic approach to the study of biological systems, from the individual cell to an entire complex multicellular organism. Indeed, the human genome project, which involved determining the entire DNA sequence of humans, was heralded as the means to elucidate the mechanism of nearly every human disease and condition (Collins and McKusick, 2001). When considering the complete genome sequence, functions are difficult to determine. A more focused approach that considers the transcriptionally active subset of the complete genome is a common means of studying genetics. The transcriptionally active portion of the genome in a cell is referred to as its transcriptome; transcriptomics is the most mature of the "omic" disciplines and is a widely applied technique for the global analysis of cellular responses. One of the limitations of transcriptional analysis is its inability to consider post-transcriptional events which may be important in the final phenotypic response of the cell. Specifically, transcription-based approaches are unable to consider events such as gene silencing, mRNA stability, translational efficiencies, protein turnover, sequestration of enzymes from substrates and the activation/deactivation tuning by a multitude of post-translation modifications, of which phosphorylation is a major class.

Intuitively, the transition from genetics to cellular responses closer to final effectors will reduce complicating intermediate factors. This allows a more accurate picture of what functionally relevant changes are occurring within the cell. For example, a gene encoding a protein may be transcribed but not translated; thus, it may not carry out any function within the cell. From this perspective, protein kinases may be an advantageous area to study as they are the core of signal transduction with a central role in the regulation of nearly every aspect of cellular behaviour (Manning, *et al.*, 2002). Through their ability to modulate protein conformation and functional characteristics, kinases control diverse processes such as metabolism, transcription, cell cycle progression, cytoskeletal rearrangement and cell movement, apoptosis, and cell differentiation. Considering this, an understanding of host cellular responses at the level of phosphorylation-mediated signal transduction has the potential to offer insight into cell biology that has thus far eluded the transcription-based approaches.

8

1.1.5 The Phosphoproteome and Kinome

Investigations of cellular phosphorylation can be divided into two broad categories: the kinome and the phosphoproteome (Jalal, *et al.*, 2007). Kinome analysis considers a cell's complement of kinases and subsequent phosphorylation of proteins. Phosphoproteome analysis considers the phosphorylation state of a cell's complement of protein. The phosphoproteome and kinome are intimately related since the phosphoproteome represents the total activity of the kinome as well as that of the protein phosphatases. The techniques to study the kinome and phosphoproteome are quite experimentally distinct, though the kinome and phosphoproteome are closely related biologically.

Phosphoproteome analysis is an attempt to define the subpopulation of the proteome which is modified by phosphorylation. Comprehensive characterization of the phosphoproteome involves defining which proteins undergo phosphorylation, at which residue, and the ensuing biology associated with the modification. Specific phosphorylation sites on a given protein can affect the protein's function in different ways; for example, phosphorylation at one site can activate a protein's enzymatic activity while phosphorylation at another site may inhibit this activity. A challenge to phosphoproteome analysis is that while the fraction of the proteome that undergoes phosphorylation is significant, the individual proteins involved in signal transduction are often expressed at very low levels (Mann, *et al.*, 2002). Furthermore, within the subpopulation of phosphorylated proteins, it is estimated that only 1-2% of the cellular complement of a given protein is phosphorylated at any one time. Phosphorylation of a protein can be difficult to measure due to the overwhelming amount of protein that may interfere with detection of the fraction which has undergone phosphorylation. These difficulties restrict some methods used to study the phosphoproteome. The three most common methods involve phosphospecific antibodies (Kalume, *et al.*, 2004), two-dimensional electrophoresis (Gorg, *et al.*, 2004) and mass spectroscopy (Mann, *et al.*, 2002). These methods can also be used in combination. Limitations of these techniques include availability and specificity of reagents, identification of proteins, cost, and difficulty of analysis.

The study of the kinome suffers from fewer limitations than those faced when studying the phosphoproteome. Investigation of enzymatic activities is a well-established area in biochemistry and has a greater potential for specific and sensitive analysis. The well-

defined, highly conserved chemistry of enzymatic phosphorylation allows for the characterization of kinase activity, substrate specificity and kinase targeting.

1.2 Peptide Arrays for Kinome Analysis

Peptide arrays for kinome analysis are based on the use of peptides representing protein phosphorylation target sequences, which are synthesized and spotted onto an array surface (Houseman, *et al.*, 2002). A sample containing an active kinase or kinases, such as in a cellular lysate, is applied to the array. These kinases phosphorylate their respective target sequences using the γ-phosphate from ATP, which has been added to the reaction mixture as the phosphate source. Any phosphatase activity which may inhibit or reverse peptide phosphorylation is reduced by the addition of a number of phosphatase inhibitors. These phosphorylation events are then visualized using one of a number of methods including phosphorylation-specific antibodies, radioactivity, a labelled chelator or phosphospecific stains. Quantification of the extent of phosphorylation of a given peptide target provides a measure of kinase activity within a sample. From this, the extent of phosphorylation of the represented protein can be inferred.

The distinction between a kinome array and a phosphoproteome array depends on what is being measured: the phosphorylation of array peptides by active kinases or the phosphorylation state of the endogenous cellular protein substrate acted upon by kinases and phosphatases. Thus, kinase activity in kinome analysis or phosphorylation state of protein in phosphoproteome analysis is measured. In the case of peptide arrays for kinome analysis, the data are analyzed by observing the phosphorylation state of the peptide on the array. This peptide has been phosphorylated by the active kinases applied. In the case of phosphoproteome analysis, phosphorylated proteins within a cell at a given time point are observed. In both cases, the direct measurement is the extent of peptide/protein phosphorylation. However, the distinctions are the context in which the phosphorylation occurs, on the array or within the cell, and the method of measuring, either measuring peptide phosphorylation or capturing phosphorylated protein from within the cell. A disadvantage of the peptide array technique is the assumption that the phosphorylation state of the peptide on the array is a match for the protein of interest present in a cell.

A large number of peptide arrays for kinome analysis are commercially available. These arrays range in size from dozens to thousands of peptides, representing defined phosphorylation sites. A listing of commercial peptide arrays which are currently available for kinome analysis is presented in **Table 1.2**.

Table 1.2. Commercially available peptide arrays.

Name	Technology	Company	Number of Substrates	Visualization Method
PepScan	Spotted peptide array	PepScan Therapeutics	10,000-100,000	Variable
PepStar	Custom spotted peptide array	JPT Peptide Technologies	100-1,000	Variable
PamChip	Immobilized peptide on porous surface	Pamgene	50-150	Fluorescence
Peptide Array	Unbound 96 well array	ChemPep	96	Radiolabel
CelluSpots	Custom spotted peptide array cellulose membrane	Intavis AG	1-384	Variable
Reverse-phase Protein Microarray	Sample blotting peptide array	Theranostics Health	100s	Fluorescence

1.2.1 Peptides as Kinase Substrates

While utilizing the complete protein as the substrate for a given kinase would allow investigation of the reaction under scrutiny, synthesizing the full length protein is a significant task, and proteins are often unstable in an array environment. In addition, proteins can be phosphorylated at different sites, resulting in distinct phenotypes (Sridevi, *et al.*, 2007; Smith, *et al.*, 2009). If a full-length protein were printed onto an array, it would not be possible to determine which site is being targeted. Looking at the individual site of phosphorylation rather than the phosphorylation state of a protein allows a better characterization of functional changes due to the phosphorylation. For many protein kinases, the specificity of their

substrate recognition is determined by the residues immediately surrounding the phosphorylation site rather than higher-order protein structure. Specifically, the core phosphorylated amino acid plus the four amino acids flanking each side of the phosphorylated residue is the most common recognition site (Kreegipuu, *et al.*, 1998). Synthetic peptides modelled on the phosphorylation site have been shown to be appropriate substrates with V_{max} and K_m values approaching that of the intact full-length protein (Zhu, *et al.*, 2000). Using short peptide sequences rather than full length proteins is cost-effective, displays high stability, provides site specific information and is amenable to array technologies (Ouyang, *et al.*, 2003). In addition, peptides can be custom designed to match the recognition sequence of nearly any kinase.

1.2.2 Peptide Array Design

1.2.2.1 Selection of Peptide Targets

A large number of proteins undergo phosphorylation, many of these at multiple sites. It is estimated that there are 100,000 unique phosphorylation events within the human proteome (Zhang, *et al.,* 2002) as compared to a current best calculation of 22,333 total translated human genes (Pertea and Salzberg, 2010). PhosphoSite (www.phosphosite.org) and Phospho.ELM (phospho.elm.eu.org) are publically available online databases that contain information on manually curated, literature-based serine, threonine and tyrosine phosphorylation sites. The information contained within these databases is predominantly human and mouse phosphorylation events. Search results for a specific protein return short peptide sequences corresponding to characterized phosphorylation sites. Where available, information on the corresponding kinase and descriptions of the biological function of the specific modification are listed. These databases have been used in the design of peptide arrays for kinase study (Diks, *et al.*, 2004). Once the selection process is complete, peptide synthesis and array printing can be done. If this cannot be done in-house, a number of commercially available, pre-designed and custom-designed arrays are available (**Table 1.2**).

1.2.2.2 Genus-Specific Arrays

There are techniques, tools and reagents available to conduct kinome work on the most commonly studied genera, such as human or mouse, but these resources are limited or

non-existent for other genera. The phosphorylation annotation databases are heavily biased toward human and mouse, with phosphorylation-specific reagents, like antibodies, generated predominantly to be species-specific. The limited options for kinome analysis of other genera were the impetus for the development of genus-specific peptide arrays for kinome analysis (Jalal, *et al.*, 2009). Based on the concept that specific sites of protein phosphorylation and biological activity are conserved across genera, information collected from human studies could be applied to other genera. In the initial study, the degree of amino acid sequence conservation surrounding human and bovine phosphorylation sites was investigated (Jalal, *et al.*, 2009). The investigation was done by searching nearly a thousand peptides of 15 amino acids in length, representing human phosphorylation sites, against the National Centre for Biotechnology Information (NCBI) non-redundant protein database using the Blastp program to generate orthologous bovine peptides. These results revealed that approximately half of the bovine sequences had 100% identity to the query sequences, and the majority of the remaining peptides had limited sequence divergence (**Table 1.3**). It was subsequently confirmed that these bovine peptides matched the orthologous protein found in humans. These results indicated that while a human peptide array would have substantial cross-reactivity with bovine kinases, there would be many peptide target sequences that may not match sufficiently for kinase recognition. This would limit the information generated when using human peptide arrays to analyze bovine samples.

The degree of difference in the kinase recognition sequences of the phylogenically similar human and bovine appears greater than their genetic differences (Zimin, *et al.*, 2009). These kinase recognition sequence differences indicate that human-sequence based arrays would be of less utility for more evolutionarily distinct genera. Interestingly, other labs have utilized human-based peptide arrays for genera as evolutionarily distant as the plant *Arabidopsis* (Ritsema, *et al.*, 2007), avoiding the challenge of designing a genus-specific array. Of the 184 kinase target sites on the array used by Ritsema, *et al.* (2007), only 15 showed statistically significant phosphorylation. This was considered a significant cross-reaction success. However, the relevance of kinome data based on a cross-reaction between human peptide targets and plant kinases should be interpreted with reservations. Emerging databases for economically important plant genera such as the Rice Kinase Database (phylomics.ucdavis.edu/kinase/) are simplifying the task of developing a plant-based array.

Given the availability of kinomic information found in these databases, the genus-specific design technique pioneered by our group, and the large evolutionary divergence between plants and humans, the design of genus-specific arrays for plant kinome work should be considered a more appropriate approach. Kinome analysis could be used to characterize plant responses to disease resistance/susceptibility, drought tolerance, nutrient utilization and many other important economic traits. As additional kinomic information on an increasing number of genera becomes available, the potential application of the technology is not limited to just animals and plants; rather, it is applicable to bacteria and others that use phosphorylation as a means of cellular regulation.

Table 1.3 Bovine/human phosphorylation target site comparison.

Sequence differences*	All bovine peptides[†]	Peptides on array[‡]	Comparison of bovine and human peptide[§]
0	50%	65%	Same descriptions
1	13%	15%	Same descriptions
2	7%	8%	Same descriptions
3	4%	5%	Same descriptions
4	1.5%	1%	Same descriptions
5	0.4%	1%	Same descriptions
6	0.6%	0%	Same descriptions
0 to 15	22%	5%	Different descriptions or no hits

This table shows the Blastp results against the NCBI non-redundant protein records of 880 human peptides to find orthologous bovine proteins. The number of sequence differences between human and bovine is indicated (*). The human sequences were collected from PhosphoSite and Phospho.ELM and compared to bovine peptide sequences. Of the 880 human sequences, the percent that displayed the indicated number (*) of sequence differences is shown (†). The Peptides on Array column indicates the percent of peptides which showed the indicated sequence similarity and were ultimately printed on the first-generation bovine array (‡). Some peptides with significant sequence differences between human and bovine matched a different protein between human and bovine. Whether the protein description matched (same name, function) between human and bovine is shown in the last column (§). This table is sourced from Jalal, *et al.*, 2009 and used with permission.

1.2.3 Detection of Phosphorylation Events

A number of techniques are available for the detection of protein phosphorylation status. These techniques can be used to determine the status and extent of phosphorylation of a given peptide on an array. These detection methods include the use of radioisotopes, phosphospecific antibodies, labelled chelators and phosphospecific stains (**Figure 1.2**).
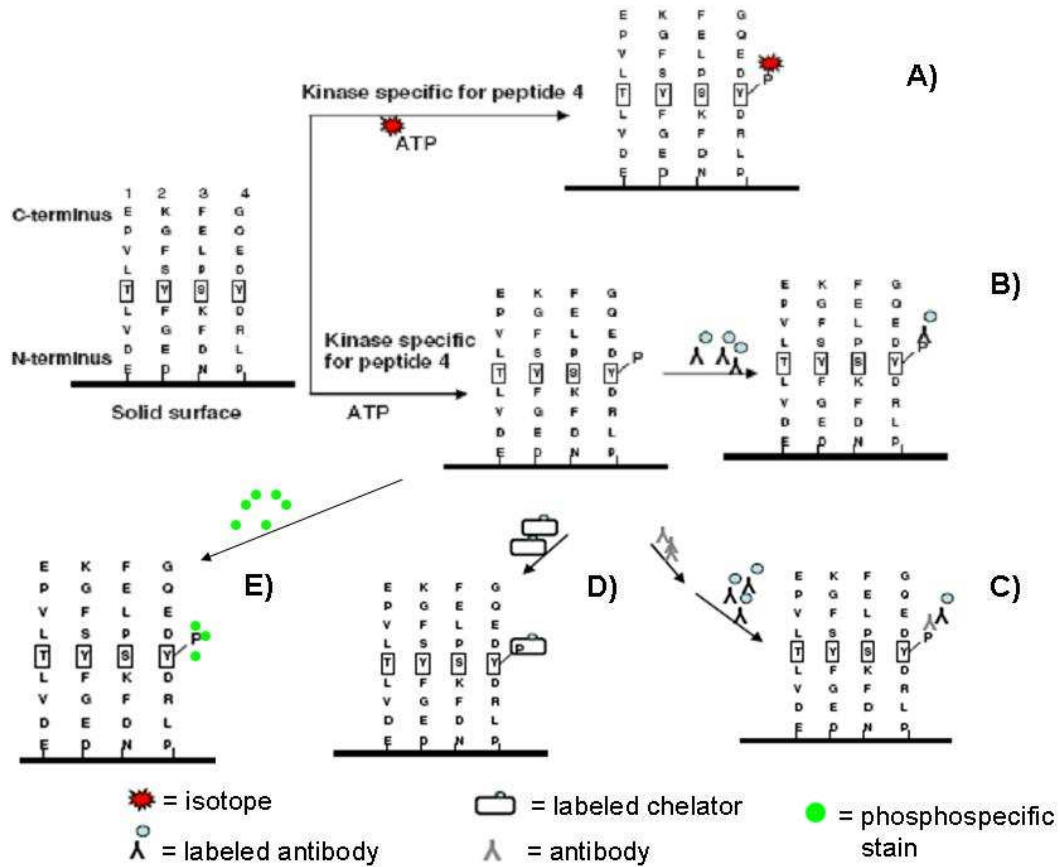
Figure 1.2. Methods of detecting phosphorylated peptides. Kinases specific for their target peptide sequence phosphorylate the appropriate residue on the array. **A)** The gamma phosphate group of ATP, which is the phosphate donor for the kinase, is radioactive. Its emissions can be visualized and quantified. **B)** Direct detection of phospho-peptides through the use of a labelled antibody specific to the phosphorylated form of the peptide is shown. The antibody can be labelled with a fluorophore. **C)** Indirect detection of the phospho-peptide through the use of a phosphospecific antibody which is then visualized by a secondary labelled anti-immunoglobulin antibody is shown. **D)** A labelled phospho-amino acid chelator is added after the kinase reaction. **E)** Fluorescent phosphospecific stain, which only binds phosphorylated peptide, can be used to directly detect the phosphorylated residues present on the array following completion of the kinase reaction. This figure was adapted from Jalal *et al.*, 2007 and used with permission.

1.2.3.1 Radioisotope Detection

The earliest detection method to be applied to phosphorylation-based peptide arrays was gamma phosphorous-32 (γ^{32}P) ATP. Kinases catalyze the transfer of the γ^{32}P group to the hydroxyl of threonine-, serine- or tyrosine-containing peptides spotted onto the array (MacBeath and Schreiber, 2000; Falsey *et al.*, 2001; Diks *et al.*, 2004). This phosphorylation event can be visualized by using a phosphorimager screen to capture the radioactive emission which can then be scanned for signal quantification (Falsey *et al.*, 2001; Diks *et al.*, 2004) (**Figure 1.3**).

The main disadvantages of using radioisotopes are the cost, time, health risks and special safety precautions required when handling these reagents. For example, it can take up to a week of exposure to an array for the phosphorimager screen to capture sufficient emissions to be detected by the scanner (Jalal, *et al.*, 2009). These factors have led many researchers to pursue alternative detection methods.
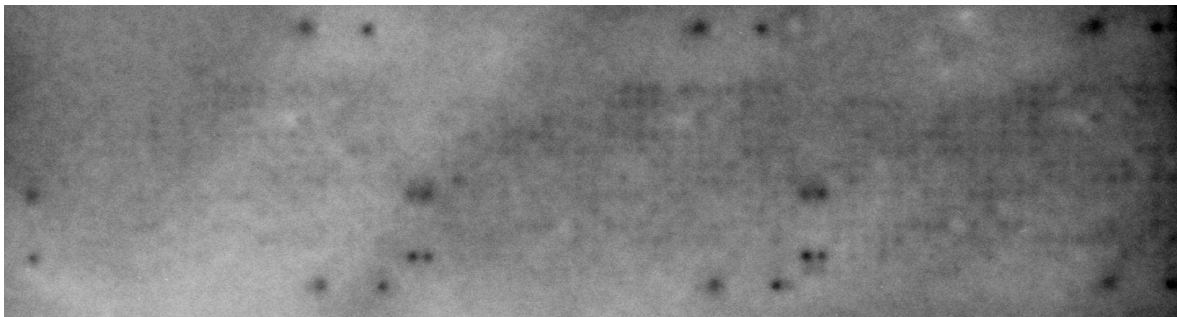
Figure 1.3. Radioisotope peptide array scan. An image of a peptide array scanned from a phosphorimager screen is shown. Bovine monocytes treated with LPS were lysed, then incubated on an array along with γ^{32}P-ATP. The array was exposed to a phosphorimager screen for one week and then scanned.

1.2.3.2 Antibodies

Shortly after the initial studies involving peptide arrays for kinome analysis, an alternative method of signal detection was developed using phosphospecific antibodies. The antibodies were generated to be specific for epitopes representing phosphorylated sites on protein (Lesaicherre, *et al.*, 2002). Use of these antibodies avoided the disadvantages of working with radioactivity. Following antibody binding to the phosphorylation site of the protein, the interaction was then visualized through the use of a fluorescence tag or a chemiluminescent system, such as those based on peroxidase activity (Schutowski, *et al.*, 2005). Generally, the phosphospecific antibody can be directly labelled with either a fluorochrome or an enzyme as indicated above (Lesaicherre, *et al.*, 2002), or a labelled secondary anti-immunoglobin can be utilized to further amplify the signal (Houseman, *et al.*, 2002) (**Figure 1.2 B** and **C**).

Antibody-based detection of protein phosphorylation eliminates the safety and time concerns of radioisotope use. In addition, antibody binding is very sensitive. In the context of a phosphorylated peptide array spot, 0.1 pmol of phosphorylated peptide is easily detectable with the potential to go 10-100 times lower in concentration (Lesaicherre, *et al.*, 2002). This sensitivity is within the range of the radioisotope γ ^{32}P system (Povey and Cooper, 1995). The major disadvantage of using antibody detection is specificity. While phosphotyrosine antibodies are generally specific, phosphoserine antibodies have at times given high rates of false positives, and phosphothreonine antibodies display high rates of cross-reactivity with phosphoserine residues (Panse, *et al.*, 2004).

1.2.3.3 Labelled Chelator

Metal-bound cyclic ring structures can be designed to specifically bind to covalently bonded phosphate groups. These are called chelators because they form a metal incorporated ring structure. It is possible to bind a fluorophore or chemiluminescent effector such as peroxidase to this chelator and expose it to a phosphorylated peptide array.

One of the disadvantages of chelators is that their binding affinity can be low, especially at physiological pH and in aqueous solution (Kinoshita, *et al.*, 2004). However, some groups have designed constructs which behave as phosphorylation sensors under physiological conditions. These constructs include an alkoxide-bridged dinuclear zinc(II)

complex (Kinoshita, *et al.*, 2004) and an anthracene zinc(II)-dipicolylamine derivative. The latter auto-fluoresces following binding to the phosphate group which induces a conformational change (Ojida, *et al.*, 2002).

1.2.3.4 Phosphospecific Stain

A small molecule fluorophore which specifically binds to phosphorylated peptides or proteins can be used to probe peptide arrays or Western blots. Extensive studies have been carried out to generally characterize these phosphospecific stains (Steinberg, *et al.*, 2003; Schulenberg, *et al.*, 2004) and specifically characterize them in the context of peptide arrays in comparison to both γ^{32}P-ATP and antibody detection (Martin, *et al*. 2003a, 2003b). The stain was found to have better sensitivity than radioactivity and was more broadly applicable than antibodies, which must be generated for each phosphorylated peptide epitope and are generally species-specific. Importantly, the study determined that a phosphorylated protein concentration of 312-625 fg and a spot diameter of 100 µm could be detected (Martin, *et al*., 2003a). This is well within the range of peptide array specifications. In addition, along with antibody and labelled chelator-based detection methods, phosphospecific stain has the potential to detect phosphorylation using GTP as the phosphate donor.

One disadvantage of phosphospecific stain is that it can non-specifically bind to the array surface. This can result in background fluorescence. Care must be taken to destain the array as much as possible, leaving only phosphorylated peptides/proteins stained. In addition, appropriate background correction can be conducted during data analysis to subtract background fluorescence from the peptide/protein signal. **Figure 1.4** shows a scan of a bovine peptide array labelled with phosphospecific stain.
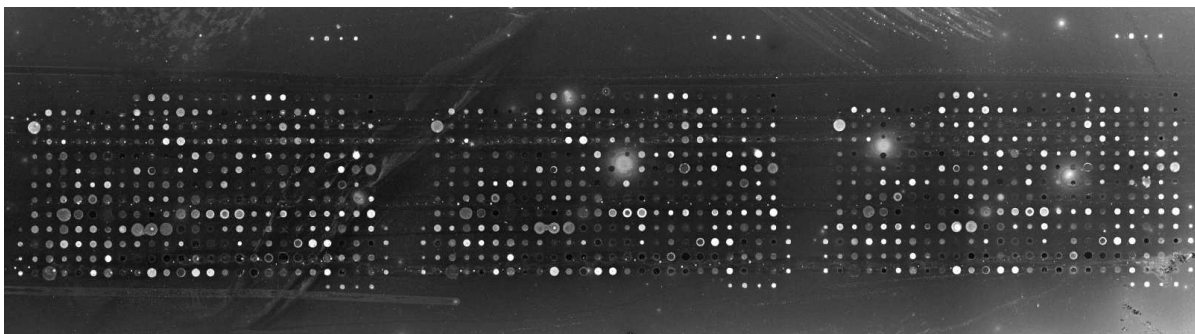
Figure 1.4. Phosphospecific stain peptide array scan. An image of a peptide array scanned using a microarray scanner at 532 nm wavelength is shown. Lysate from bovine monocytes treated with interferon gamma was incubated on an array before exposing the array to phosphospecific stain. The array was then washed and scanned for green fluorescence.

1.2.4 Data Analysis

1.2.4.1 Use of DNA Microarray Analysis Methods

Genomics, a field which adopted high throughput microarray techniques early, has dominated the development of array technology. Consequently, upon the introduction of peptide arrays for kinomic analysis, the majority of the statistical manipulation and data analysis tools developed for genomic array work were simply ported into kinome array analysis (Diks, *et al.,* 2004; van Baal, *et al.*, 2006; Schrage, *et al.*, 2009; Arsenault, *et al.*, 2009). However, peptide array data have a number of unique attributes that limit the utility of this analysis approach.

1.2.4.2 Differences Between Nucleotide and Peptide Arrays

There is concern that the tools for genomic analysis may have limitations when applied to peptide arrays, in particular phosphorylation-based peptide arrays. The two techniques are fundamentally different. A statistical analysis method should account for these differences; otherwise, data normalization will not be optimum. In the case of nucleotide arrays, a hybridization reaction takes place; with peptide arrays, the enzymatic transfer of a phosphate group occurs. The enzymatic process results in a signal response from zero to many multiples of the control. While a nucleotide array signal is limited by the number of matching nucleotides in a sample, the peptide array is limited only by the number of peptide sequences

printed on a given spot. Phosphate levels are at saturation, and the ample incubation time means a highly active kinase could theoretically phosphorylate every target sequence available virtually regardless of the number of sequences printed on the array. This makes it difficult to determine where a positive reaction cut-off should be set. Also, the variance in signal is affected by this dynamic range of phosphorylation. This makes statistical manipulations difficult when assumption of a constant variance is required, such as for Student's t-test, analysis of variance and some regression models. Data normalization is required before statistical tests can be performed; however, normalization procedures are based primarily on nucleotide microarray data and may not be the most appropriate for kinome data. Significance calculations should also be considered as the number of kinase target sequences is usually much lower than the number of nucleotide chains spotted onto an array, potentially as much as 100 times fewer. This means that each individual spot is of much greater consequence when trying to achieve coverage of a given cellular process or response. The indiscriminate discarding of data points by inappropriate statistical significance calculations is thus highly undesirable. Statistical calculations should take these differences into account when being applied to kinome data analysis.

1.2.4.3 Data Transformation

Variance stabilization (VSN) is a method of data transformation which calibrates all of the background-corrected data to a positive scale, alleviating mean-variance-dependence while maintaining the structure within the dataset (Huber, *et al.*, 2002). Mean-variance-dependence occurs when variance for individual data points is not independent of signal intensity. This is a common characteristic of peptide array kinome data as phosphorylation of peptides is not a binary signal but rather a scale increasing from zero. Because a consistent signal of zero will have a variance of zero, a replicate signal of zero phosphorylation will have no variance. Replicates with a strong signal may be relatively consistent but include a broader variance having a large absolute signal intensity value. For example, triplicate signal intensities of 0.00, 0.00 and 0.00 display no variance; signals of 25,000, 33,000 and 27,000 display much more broad variance but are relatively similar considering that the dynamic range can extend to zero. In addition to dealing with the mean-variance-dependence problem, VSN facilitates scaling of datasets to a relatively consistent value to enable comparisons

between datasets. This is important when various experiments, treatments or cell types are being compared.

1.2.4.4 Visualization Techniques

1.2.4.4.1 Hierarchical Data Clustering

Hierarchical clustering is a useful tool to organize multiple datasets based on degree of similarity. Broadly, each treatment/dataset is considered a singleton (a cluster with a single element) at the initial stage of clustering. The two most similar clusters are determined and then merged. Then, the degree of distance between this newly merged cluster and the next most similar cluster is determined. This process continues iteratively until all clusters are considered.

For hierarchical clustering, three popular independent combinations of clustering methods and distance measurement are implemented: Average Linkage + (1-Pearson Correlation), Complete Linkage + Euclidean Distance and McQuitty. The calculations of similarity/distance between the clusters and the update step are algorithm-specific. These calculations are performed on complete kinome datasets. For example, an array containing three-hundred peptides will be considered a single element; this will then be compared to a second array. The "Average Linkage + (1 - Pearson Correlation)" takes the average of the merged (i.e., the most correlated) kinome profiles and updates the distances between the merged clusters and other clusters by recalculating the correlations between them (Pearson, 1896; Eisen *et al.*, 1998). In "Complete Linkage + Euclidean Distance", the distance between any two clusters is considered as the Euclidean distance between the two farthest data points in the two clusters (Everitt, 1974; Hartigan, 1975). Finally, the "McQuitty" method updates the distance between the two clusters in such a way that, upon merging clusters C_X and C_Y into a new cluster C_{XY}, the distance between C_{XY} and each of the remaining clusters, labelled   , is calculated taking into account the sizes of   and   (McQuitty, 1966). If three arrays are to be clustered, the two most similar arrays will be merged, creating a new set representing both. This new representative set will then be compared to the third. A relative similarity/difference output will then be provided for all three arrays.

1.2.4.4.2 Principal Component Analysis

Briefly, Principal Component Analysis (PCA) is a variable reduction procedure. For example, if a dataset contains three variables between data points, PCA can reduce that to one or two variables, making the relationships between points easier to observe. The calculation performed is a singular value decomposition of the centered and scaled data matrix (Mardia, *et al.*, 1979). As a result, PCA transforms a number of possibly correlated variables into a smaller number of uncorrelated or literally orthogonal variables (i.e., principal components). An example of this is seen in **Figure 1.5**, where a hypothetical dataset is converted into two principal components by bisecting the data, thus simplifying the variables between the points. The first principal component accounts for the most variability in the data, and each succeeding component accounts for as much of the remaining variability as possible. Usually, the first three components account for more than 50% of the variability in the data and can be used as a set of the most important coordinates in a 3D plot to reveal the structure of the data.

1.2.4.5 Pathway Analysis

A number of pathway analysis databases have been developed with the goal of associating gene expression data with signalling pathways. InnateDB was originally designed for innate immune gene expression analysis but has since been significantly expanded to become a comprehensive database (Lynn, *et al.*, 2008). Kyoto Encyclopedia of Genes and Genomes (KEGG) (Kanehisa and Goto, 2000) accepts high throughput genomic data and outputs relevant pathway information. It is possible to apply these databases to peptide array kinomic data. Inputting normalized, background-corrected and comparative peptide array data produces pathways which are represented by the phosphorylated peptides on the array. This allows organization of data by functionality and provides a clearer overview of the data collected than only considering individual peptide phosphorylation events.
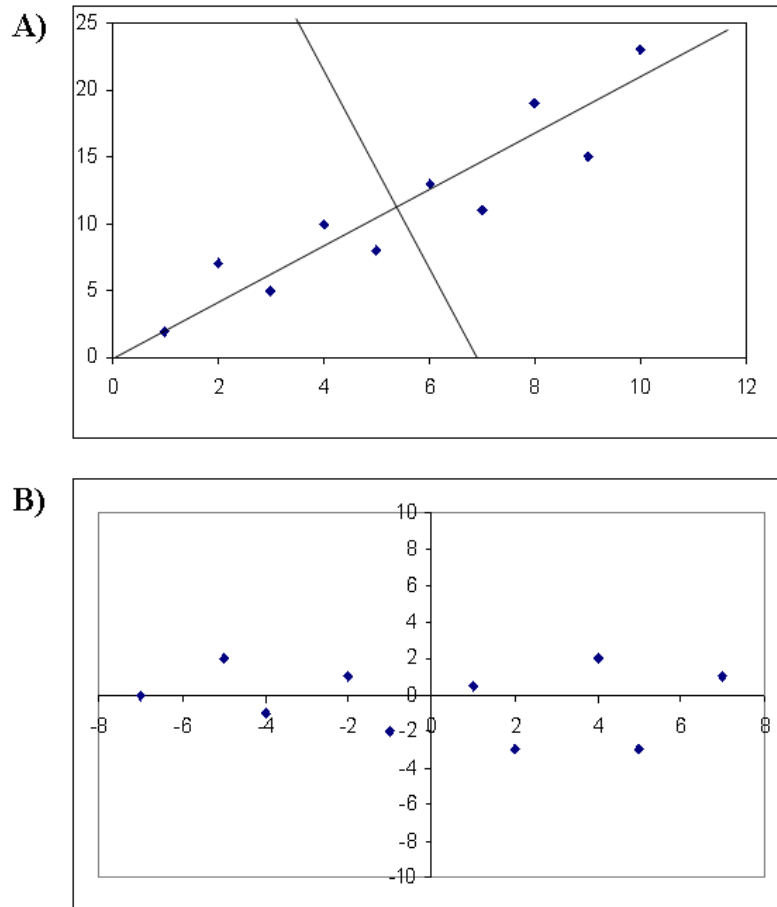
Figure 1.5. PCA example: A simplified example of how PCA works on a hypothetical dataset is shown. **A)** A hypothetical scatter plot of mean subtracted data with eigenvectors roughly drawn is shown. Eigenvectors are normally calculated from the covariance matrix of the dataset. Each eigenvector provides information about the patterns in the data. The vector with the positive slope through the dots shows how the data points relate along that line. The vector running perpendicular to the first provides another, less important pattern in the data. This second vector shows that the data are offset from the centre of the first line. The two lines together characterize the data. The vector with the highest eigenvalue, also calculated from the covariance matrix of the dataset, is the principal component. In this case, the principal component is the vector with the positive slope. **B)** A plot of the dataset in Plot A with the eigenvectors used as axes is shown. The data are now separated into two principal components by the X and Y axes. If PCA, a variable reduction procedure was used, then the values of the Y-axis could be eliminated. This is because the Y-axis in Plot B corresponds to the eigenvector with the lowest value. Eliminating this will maintain most of the information in the dataset while reducing the variables under consideration. Plot B would then appear as only the X-axis with all of the data points falling upon it.

1.2.5 Peptide Array Kinome Studies

The development and use of peptide arrays for kinomic studies is relatively new. Despite this, there have been a number of studies employing the technology which have produced novel biological insight. A number of studies employing peptide array technology for kinomic research are described below.

1.2.5.1 LPS Signal Transduction in Human PBMCs

The original study which evaluated and confirmed the efficacy of peptide arrays for kinomic analysis involved human peripheral blood mononuclear cells (PBMCs) stimulated with bacterial-derived lipopolysaccharide (LPS) (Diks, *et al.*, 2004). LPS was used since it was a well-characterized inducer of innate immune response kinases and allowed a comparison of peptide array data against known signalling events. Various peptide substrates, corresponding to proteins known to be involved in LPS-induced signaling, were found to display increased phosphorylation on the array including p44/42 MAPK, signal transducers and activators of transcription (STAT)-1α/β, nuclear factor kappa-light-chain-enhancer of activated B-cells (NFκB), Bruton's tyrosine kinase (Btk), and Tec kinase. A time course involving stimulation at 5 min, 15 min, 30 min and 60 min allowed a characterization of the time of activation of the kinases. The results were subsequently confirmed with western blot. In addition, the cells were treated with the MAPK inhibitors PD 98059 and SB 203580, and array analysis was conducted to confirm that MAPK signalling had been eliminated by the addition of inhibitors. Indeed, MAPK phosphorylation which had been observed in LPS-treated PBMCs was entirely ablated by the addition of these inhibitors.

While the goal main of this study was mainly to prove the usefulness of studying kinases using peptide arrays, novel biological results were also produced. Prior to this study, the means of activation of the Raf/MAPK kinase (MEK)/p42/p44 MAPK signalling cascade by LPS had been unknown (Diks, *et al.*, 2004). Two means of activating this pathway were considered potential options: one via p21Ras and the other by phospholipase C (PLC)β1 and protein kinase C (PKC)α/β. Peptide array data indicated an increase in the phosphorylation of peptides corresponding to proteins downstream of activated p21Ras. A subsequent p21Ras activation assay confirmed p21Ras activation. This study was the first direct identification of p21Ras activation following stimulation of a member of the Toll-like receptor (TLR) family.

This result demonstrated the utility of this technology for analyzing cell signalling events and discovering novel biology.

1.2.5.2 Glucocorticoid Receptor-Dependent Non-Genomic Inhibition of Insulin Signalling

Glucocorticoids are used as immunosuppressive agents that work in a transcriptional dependent manner through the glucocorticoid receptor (Lowenberg, *et al.*, 2006). The problem with glucocorticoid therapy is that it has resulted in insulin resistance. The mechanism by which this resistance occurs had been unknown. Evidence pointed to a rapid, genome-independent, process. Lowenberg, *et al.* (2006) attempted to uncover this mechanism by using peptide array kinome analysis to describe the cellular non-genomic effects of glucocorticoids. Their analysis indicated that several insulin-signalling intermediates were involved: p70S6k, glycogen synthase kinase-3 and Fyn. These signalling molecules were affected by the glucocorticoid dexamethasone (DEX) (all subsequently confirmed by western blot). DEX also activated Jun N-terminal kinase (JNK) signalling, an inhibitor of insulin signalling. To confirm that the insulin signalling inhibition induced by DEX was not due to a reduction in gene expression of the insulin receptor or insulin signalling intermediates, gene expression was measured and no expression-level differences were found. It was also determined that DEX was exerting its effects through the glucocorticoid receptor. The inhibition of the receptor by antibody binding eliminated the DEX dependent insulin signalling inhibition. Thus, this study uncovered the means by which glucocorticoids result in insulin resistance by a non-genomic mechanism. The hope is that this knowledge can lead to the design of immunosuppressive glucocorticoids that will not affect insulin signalling.

1.2.5.3 Chondrosarcoma with Src Activity Indicates Dasatinib as Treatment

Kinome profiling can also be used to determine the most effective treatment for various cancers by identifying specific signalling pathways that are differentially activated or inhibited in cancer cells. The activated pathways can be determined by measuring the activity of the constituent kinases within the tumour or cancerous cell. Schrage, *et al.* (2009) used this approach in the study of chondrosarcoma cancers. Treatment of chondrosarcoma of the bone

was historically restricted to surgery since the tumour was highly resistant to conventional therapies. Therefore, the only means of treatment for high grade chondrosarcomas was large-scale bone resection or amputation. Published evidence indicated that kinase inhibitors were ineffective as a means of treating conventional chondrosarcomas, which constitute over 85% of cases (Gelderblom, *et al.*, 2007). Kinome analysis of 13 chondrosarcoma samples was performed and combined to produce a representative kinome profile. Two of the top pathways indicated by the array data were platelet-derived growth factor receptor (PDGFR)B signalling and the sarcoma (Src) pathway. Two inhibitors that target these respective pathways were tested: imatinib for PDGFRB and dasatinib for Src. Imatinib had no effect on cultured chondrosarcoma cells, while it did have an effect on the positive control gastrointestinal stromal tumour cell line GIST882. Dasatinib reduced the cell viability in seven of the nine chondrosarcoma cell lines tested. Western blot analysis confirmed that dasatinib acted by inhibiting the phosphorylation of Src but had no affect either on the total level of Src protein or the activation of pro-apoptotic effector caspase-3, the mode of action of dasatinib which had been observed in other cancers. This analysis revealed the reason that Src inhibitors may not have been considered as a therapeutic treatment for chondrosarcomas: genomic and proteomic studies would not have indicated a change in the Src pathway. Src expression and total Src protein level were unchanged. Thus, peptide array kinome analysis pointed toward a potential therapy for patients suffering from chondrosarcoma where none was previously available.

1.2.6 Genus-Specific Peptide Array Kinome Studies

The use of peptide arrays for kinome analysis is still relatively new; thus, custom-designed arrays for genera such as cattle were unavailable until our group designed and validated the first bovine array in 2009 (Jalal, *et al.*, 2009). The utility of kinome technology was understood by a number of groups and was quickly applied to a variety of biological problems. While the research was outside the scope of my doctoral project, the following sections contain a review of published investigations in which I was involved, either within Dr. Napper's group or with collaborators.

1.2.6.1 Expanding Knowledge of Defined Ligand Signalling

During the development of the first custom-designed genus-specific peptide array, it was important to confirm the biological relevance of the data generated. This was first done by investigating signalling responses to ligands by receptors which activated well-defined signalling pathways. The model chosen to validate the bovine-specific arrays was purified bovine monocytes stimulated with two well characterized TLR ligands: cytosine-phosphodiester-guanine oligodeoxynucleotides (CpG) and LPS (Arsenault, *et al.*, 2009). TLRs are a family of pathogen recognition receptors ranging from TLR 1-10 in bovine that bind to pathogen-associated molecular patterns and initiate innate immune responses within the cell (McGuire, *et al.*, 2006). In this specific study, signalling by TLR4, which recognizes LPS, and TLR9, which recognizes CpG, were investigated. These ligands induce well-defined signalling responses and are of biological and medical interest. LPS is a causative agent of sepsis, and CpGs are immunomodulating agents investigated for use in immunotherapy and as vaccine adjuvants. The results from our kinomic investigation of monocyte signalling following stimulation with TLR ligands were in close agreement with signalling pathways established through alternative techniques and reported in the literature (Arsenault, *et al.*, 2009).

In addition to confirming the established TLR signalling pathways, other signalling events were identified which had not been previously described. For example, tyrosine 40 of epithelial and endothelial tyrosine kinase (Etk) (also known as Bmx) was phosphorylated in response to LPS but not CpG stimulation. This response was subsequently confirmed through the use of phosphospecific antibody and western blot analysis of human monocytes (**Figure 1.6**). Etk phosphorylation was confirmed in human monocytes because the antibody to phosphotyrosine 40 was unavailable for bovine. This lack of a bovine reagent highlights the need for an alternative kinome analysis method in non-human genera. In addition to Etk, the phosphorylation pattern of peptides corresponding to p40phox and p47phox proteins indicated that oxidative burst was activated following CpG but not LPS stimulation. A functional assay based on the production of superoxide radicals was conducted, and this bioassay confirmed the kinome data (**Figure 1.7**). Through the use of independent assays, we were able to confirm the accuracy of custom-designed bovine array data and elucidate novel ligand activities. In addition, the study using human peptide arrays to uncover human PBMC

27

response to LPS had been conducted previously (Diks, *et al.*, 2004), enabling a comparison of the conservation of TLR4 signalling responses in bovine and human cells. The strong level of similarity observed between bovine and human responses provided further validation of the bovine array results.
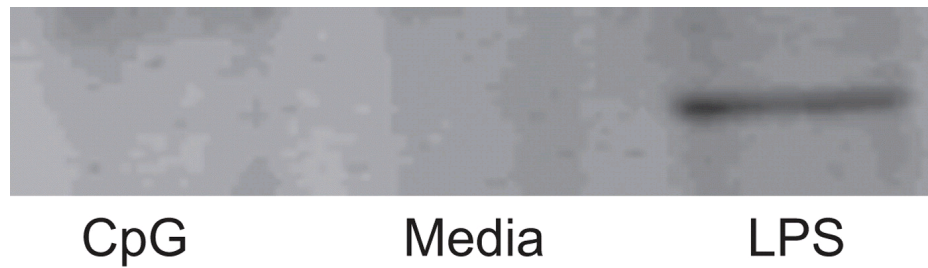
Figure 1.6. Etk phosphorylation following stimulation. An image of a western blot is shown. Monocytes were treated with CpG, LPS or media control. The cell extracts were separated by SDS-PAGE and immunoblotted using Etk Tyr40 phosphospecific antibody (Arsenault, *et al.*, 2009).
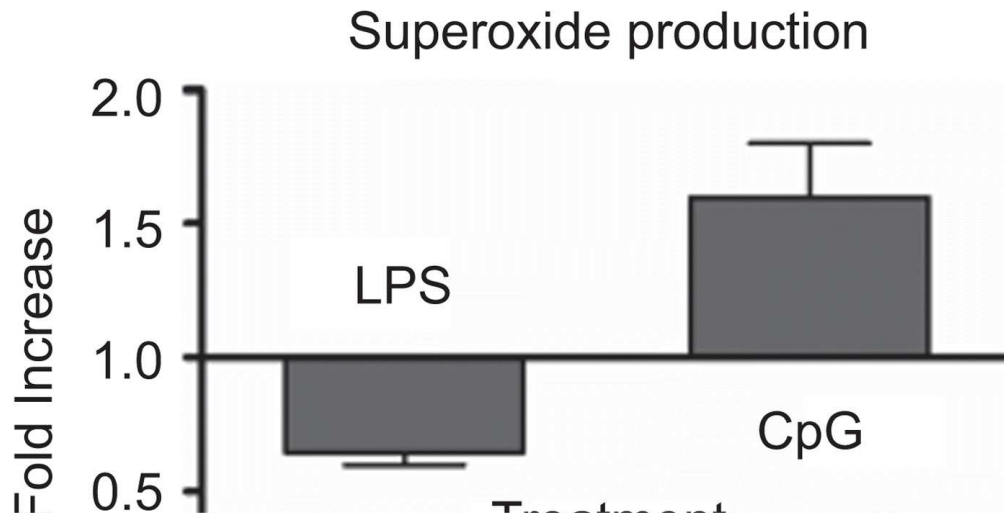
Figure 1.7. Superoxide production. The figure shows the results of a superoxide radical production assay. Monocytes were treated as indicated, and superoxide radical production was measured and calculated relative to media control (Arsenault, *et al.*, 2009).

1.2.6.2 Characterizing Phenotypically Similar But Mechanistically Distinct Signalling Events

The cytokines IL-32 and IL-17 are both involved in chronic inflammation and autoimmune disorders. It was speculated that the mechanisms by which IL-32 and IL-17 carry out their cellular effects are differentially dependent on the TNF receptor and its pathway (Turner-Brannen, *et al.*, 2011). Peptide array kinome analysis determined that a peptide corresponding to TNF receptor 1 (R1) was phosphorylated upon cell stimulation with IL-32 but not IL-17. This result was then validated through the use of an antibody to TNF-R1 used to block any TNF-R1 ligand binding, which suppressed IL-32 but not IL-17 responses. This IL-32 blockage confirmed that while IL-32 and IL-17 have similar phenotypic effects, these effects are produced by distinct cell signalling events at the level of cell surface receptors. This differential dependence may have therapeutic implications since the treatment of inflammation and cytokine induced autoimmune disorders would be ineffective if based on the suppression of the TNF-R1 rather than targeting a common downstream effector.

Considering that distinct receptors are utilized by the two cytokines but similar phenotypes are observed, similar signalling intermediates may be involved. Peptide array data indicated that p300 and death-associated protein kinase-1 (DAPK-1) were common phosphorylation targets for both IL-32 and IL-17. These phosphorylation events were subsequently confirmed by immunoblots. Known downstream responses of p300 and DAPK-1 were altered in response to both cytokines as well including activation of NFκB and the induction of chemokine production. These results allowed for the conclusion that p300 and DAPK-1 are nodes of conversion for signalling responses to IL-32 and IL-17. These nodes may be targets to disrupt the activity of both cytokines for treating chronic inflammation and autoimmunity.

1.2.6.3 Understanding the Source of Phenotypic Variability

Closely related cells may respond differently to the same stimulus producing two distinct phenotypes, but the mechanism for this differential response can be difficult to determine. For example, intestinal Peyer's patch (PP) cluster of differentiation (CD)21+ regulatory B cells (Bregs) fail to show detectable TLR9-induced immune responses. By contrast, CD21+ B cells from blood display a robust response to TLR9 stimulation (Booth, *et*

al., 2010). The apparent failure to respond to TLR9 stimulation occurs despite PP CD21+ Bregs expressing high levels of TLR9 mRNA and detectable TLR9 protein being present. It was hypothesized that CpG was unable to induce a TLR9-dependent response because of a disruption in the TLR9 signalling pathway. This hypothesis was tested by kinome analysis which showed that following stimulation with CpG, phosphorylation of downstream TLR pathway proteins was increased in blood CD21+ B cells but remained unchanged in PP CD21+ Bregs. The TLR pathway intermediates included interleukin-1 receptor-associated kinase 1 (IRAK1), mitogen-activated protein kinase kinase kinase 7 (TAK1), IκB kinase (IKK), and NF-κB-p65 (**Figure 1.8**). These results confirmed the lack of TLR9 signalling in PP CD21+ Bregs and revealed that this signalling was disrupted at or near the level of the receptor. This information could not have been determined with genetic techniques or would have been time-consuming with standard phosphorylation-based techniques.

1.2.6.4 Cancer Cell/Tumour Profiling

As described previously, cancer is very important in the field of kinome research and *vice versa*. Research on kinase drug discovery is also dominated by cancer. A large part of this research involves cancer models used to test various molecules and compounds for effect on kinases. Thus, it is of critical importance that the animal or cell model being used accurately reflects the kinase activity of the cancer under scrutiny. The development of custom-designed bovine arrays and their application along with a Bovine Leukemia Virus leukemia cancer model in sheep made it possible to study changes in kinase activities associated with B cell transformation (Van den Broke, *et al.*, 2011). It is common practice to isolate cancerous cells from a host, establish a cell line tissue culture and then use the cell lines for *in vitro* cancer research. However, our study indicated that the removal of cancer cells from the ovine host and passage of cells in tissue culture significantly altered phosphorylation patterns in these cells. Changes between host-derived and cultured cells occurred in pathways key to cancer such as growth, apoptosis and cell cycle. Thus, the external environment of these cells had a profound impact on many cell signalling pathways. This finding is one that must be considered in the fields of cancer research and drug discovery. If a cell line is used to screen potential cancer treatments, it must be a cell line

where key cancer-specific pathways or cell signalling proteins have not been significantly altered due to passage in tissue culture.
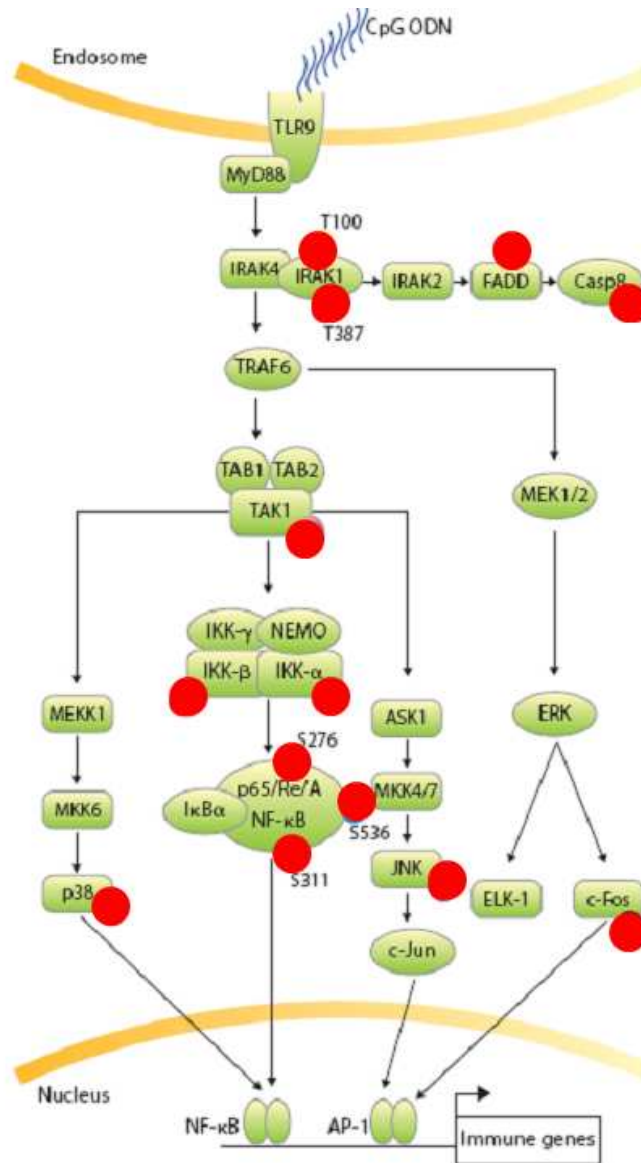
Figure 1.8. TLR9 signalling differences in related cell types. Peptide array results indicated blood derived bovine CD21+ B cells had increased activation of the TLR9 pathway upon CpG treatment. Ovine PP-derived CD21+ Bregs showed no increase in TLR9 signalling pathway phosphorylation following treatment with CpG. The red spots indicate the sites of differential phosphorylation along the pathway between the two cell types. The blood-derived CD21+ B cells displayed increased phosphorylation at these sites, and the PP-derived CD21+ Bregs displayed a lack of phosphorylation. This figure was adapted from Booth *et al.*, 2010 and is used with permission.

1.3 Host-Pathogen Interactions Involving Cell Signalling

Much of the initial work in researching the kinome, many of the kinase inhibitors and other drug discoveries developed from this work has been in the field of cancer research (Knight, *et al.*, 2010). At times perhaps overshadowed by the large role that cancer research plays in the kinome field, the importance of kinases, kinase inhibitors and cell signalling in infectious disease has been well-documented for decades (Rosenshine, *et al.*, 1992). The study of host-pathogen interactions at a cell signalling level is difficult due to the complexity of the cellular signalling networks and the challenge of separating general host stress responses from those induced by the pathogen. These responses may also include pathogen signalling events especially when studying intracellular pathogens. Despite these difficulties, the technique has provided useful insight into the biological responses to pathogen-associated ligands, CpG (Booth, *et al.,* 2010) and LPS (Diks, *et al.*, 2004; Arsenault, *et al.*, 2009).

The two infectious diseases studied in this project are uniquely suited for kinomic study: prion disease and *Mycobacterium avium* subspecies *paratuberculosis* (MAP). Prion diseases are not caused by a bacterium, virus or genetic disorder; rather, they are caused by a host protein misfolding event which is disruptive and contagious (Prusiner, 1982). The symptoms of the disease are entirely induced by a self protein and there appears to be no genetic component. Moreover, there is evidence that the prion protein has a cell signalling function. As such, a kinomic approach should be an effective technique for the study of this disease.

The second infectious disease that likely has a strong signalling component is infection where the pathogens disrupt or influence host-signalling events. MAP establishes a persistent infection which subverts host immune response, both innate and acquired. Signalling studies may provide useful information about treating these infections. In fact, some pathogens have been shown to specifically target host phosphorylation-mediated signal transduction pathways (Zachos, *et al.*, 2001; Koul, *et al.*, 2004). A fascinating example of this is the mycobacteria which produce eukaryotic-like phosphorylation effector molecules. These molecules enter the host cell and directly affect specific sites of phosphorylation (Alber, 2009). These pathogen-produced eukaryotic phosphorylation effectors have been identified as possible therapeutic targets (Schreiber, *et al.*, 2009).

1.4 Prions

Prions were discovered due to their involvement in diseases known as Transmissible Spongiform Encephalopathies (TSEs). TSEs include Creutzfeldt-Jakob disease and Kuru in humans, bovine spongiform encephalopathy (BSE) in cattle, scrapie in sheep, and chronic wasting disease (CWD) in deer and elk. These diseases represent the first class of infectious disease characterized as being mediated exclusively by a protein agent (Prusiner, 1982). TSEs result from the conversion of endogenous, cellular prion protein (PrP^C) to a misfolded, infectious, scrapie-like conformation (PrP^{Sc}) by a template-directed autocatalytic mechanism. This novel means of infection was first proposed in the early 1980s; however, fundamental questions remain regarding the physiological role of PrP^C, the mode of PrP^{Sc} transmission and the pathogenesis of prion disease. Considering the fact that PrP^C is so highly conserved, having been found in nearly every species studied (Strumbo, *et al.*, 2001), its physiological role must be important for such evolutionary fidelity to be maintained. In addition, PrP^C may play a variety of roles as it is found on various cell types and tissues. A key question in understanding TSE pathogenesis is to understand how the misfolding from PrP^C to PrP^{Sc} alters the protein's natural function, be it a gain, loss or subversion of normal function.

1.4.1 Proposed Functions of the Prion Protein

In spite of years of intensive investigation, there has been limited progress in defining the physiological function of PrP^C. PrP^C knock-out animals show minimal phenotypic effects besides a resistance to prion disease (Bueler, *et al.,* 1992). This means that researchers have been forced to look more closely at the molecular basis of prion activity. Efforts to uncover the physiological role of the protein have produced evidence of numerous and varied functions including neuronal protection (Roucou, *et al*., 2005), copper metabolism (Brown, *et al*., 1997), long-term memory creation (Shorter and Lindquist, 2005) and bone marrow renewal (Zhang, *et al*., 2006). While questions remain about the function of PrP^C, there is a strong impetus to look into its disorder of function, which occurs upon misfolding to the PrP^{Sc} conformation, and to understand the pathogenesis of this infectious disease. The protein's ability to function in two conformations adds complexity to determining function since it is not clear whether normal or disease-related activity is being studied. For example, it can be

33

unclear for a given PrP^C signalling model if the induced signalling is related to normal function or misfolded disease-state function.

1.4.2 The Prion as a Cell Signalling Molecule

PrP^C is a glycophosphotidylinositol (GPI)-anchored protein associated with lipid rafts, indicating that PrP^C is a cell-surface signalling molecule. Lipid rafts are functional hubs of cell-surface signal transduction, and GPI-anchored proteins are often part of multicomplex signalling receptors (Simons, *et al*., 2000). PrP^C does not contain a transmembrane domain; therefore, it cannot communicate directly to the interior of the cell. This is why many GPI-anchored proteins associate with secondary proteins containing a transmembrane domain (Pike, 2005). To confirm the lipid raft anchoring necessity for PrP^C function, as well as the disease potential of PrP^{Sc}, a soluble version of PrP^C was created via the removal of the GPI anchor. Removal of the GPI anchor and misfolding to the PrP^{Sc} isoform resulted in plaque formation, however, without the neuronal pathology normally observed in TSEs (Chesebro, *et al*., 2005). This observation dissociates the protein aggregation often observed in TSEs with the cell death and neuropathological symptoms of disease. It appears that pathology is a result of some type of disruption of the information transferred through the PrP^C following misfolding to PrP^{Sc}, not a disruption of cell function due to plaque deposition. The dual requirement for conversion to PrP^{Sc} and PrP^C association with lipid rafts points to a subversion of function based on alterations of cellular signalling events (Aguzzi, 2005).

Subsequent investigations of PrP^C and PrP^{Sc} from the perspective of signalling analysis have implicated a number of intracellular kinases and signalling pathways including Src (Nixon, 2005), MAPK (Lee *et al*., 2005; Marella, *et al*. 2005), phosphoinositide-3 kinase (PI3K)/RAC-alpha serine/threonine protein kinase (Akt) (Vassallo, *et al*., 2005), JNK (Carimalo, *et al*., 2005) and extracellular signal-regulated kinase (Erk) (Monnet, *et al*., 2004). It is clear that PrP influences intracellular kinase activity, though the specific details of how and for what purpose have yet to be elucidated. The diversity of conflicting functions that have been ascribed to the PrP$^{C/Sc}$ protein may be partially due to the limited scope of the investigations carried out thus far. This may also reflect the functional diversity of the PrP$^{C/Sc}$ protein. When undertaking a prion signalling/function study, experimental design is complicated by numerous variables including species, cell type, primary or cultured cell,

conformational isomer, and the interacting partner/ligand chosen. It is essential to achieve as broad a cellular picture as possible to eliminate the biases and limitations inherent in studying a complex protein such as this.

1.4.2.1 Putative Prion Interacting Partners

The PrP^C protein is GPI-anchored, and its apparent ability to influence cell signalling suggests that PrP^C must have cell surface interacting partners that contain transmembrane domains. Alternatively, PrP^C may interact with intracellular partners during protein trafficking to enable the transmission of signals from the PrP^C to the intracellular environment. No fewer than 45 potential interacting partners have been proposed for the prion protein (Aguzzi, *et al.*, 2008). Some well-cited examples of proposed PrP^C interacting partners are shown in **Table 1.4**.

Table 1.4. Putative prion interacting partners.

Interacting Partner	Subcellular Localization	Interaction Detection Method	Reference
Hsp60	Mitochondria	Yeast-2-hybrid	Edenhofer, *et al.*, 1996
Laminin	Extracellular	Binding assay	Graner, *et al.*, 2000
N-CAM	Plasma membrane	Formaldehyde cross-linking	Schmitt-Ulms *et al.*, 2001; Maness and Schachner, 2007
STI-1	Cytoplasm, plasma membrane	Co-IP	Chiarini, *et al.*, 2002; Zanata *et al.*, 2002
Fyn kinase	Cytoplasm	Co-IP	Mouillet-Richard, *et al.*, 2000; Mattei *et al.*, 2004
Insulin Receptor	Plasma membrane	Co-IP, Equilibrium Binding	Ostlund, *et al.*, 2001
NMDA	Plasma membrane	Co-IP	Khosravani, *et al.*, 2008

1.4.2.2 Ligands for Inducing a Prion Signalling Event

While there are many theories, there are no definitive conclusions about the interacting partners of PrP^C or PrP^{Sc}. To study the intracellular effects produced by the prion protein, two characteristics are essential: 1) the ligand or interacting molecule must be prion-specific in that it must bind to the prion protein to the exclusion of all other cell surface proteins, and 2)

it must induce a response within the cell. Prion-specific antibodies and prion peptide fragments are two types of prion ligands that are available and do not have the negative side effect of producing protease-resistant infectious prions. Research groups have used prion antibody to dimerize PrP^C on the cell surface inducing intracellular signalling events (Mouillet-Richard, *et al.*, 2000; Schneider, *et al.*, 2003; Solforosi, *et al.*, 2004). The prion peptide fragment composed of amino acids 106-126 (PrP 106-126) is a well characterized *in vitro* model for inducing TSE-like effects on cultured cells (Tagliavini, *et al.*, 1993; Fabrizi, *et al.*, 2001; O'Donovan, *et al.*, 2001; Thellung, *et al.*, 2002; Carimalo, *et al.*, 2005; Pietri, *et al.*, 2006). Numerous studies have confirmed that this peptide interacts with PrP^C and induces cellular effects strikingly similar to infection with scrapie material. Therefore, antibody cross-linking may be considered a model for endogenous PrP^C signaling, while peptide binding may model the disease-like effects of PrP^{Sc} infectious material.

1.5 *Mycobacterium avium* subspecies *paratuberculosis*
1.5.1 MAP and Johne's Disease

Mycobacterium avium subsp. *paratuberculosis* (MAP) is a gram-positive, acid fast organism that is the causative agent of Johne's disease, a severe gastroenteric disorder in ruminant animals. The disease has been known to veterinary medicine for well over a hundred years; H.A. Johne and L. Frothingham initially reported the disease in Germany in 1894. It wasn't until 1910 that MAP was proven to be the causative agent when F.W. Trowt fulfilled Koch's postulates (Chiodini, *et al.*, 1984). Johne's disease is extremely important to the dairy industry since it is responsible for estimated losses of over $1.5 billion per year to the United States industry alone (Stabel, 1998). MAP is the cause of the highest production losses among the five major production-limiting diseases (Chi, *et al.*, 2002). There have been reports that MAP is also the cause, trigger or an aggravating factor in a number of human diseases including Crohn's disease (Eltholth, *et al.*, 2009; Olsen, *et al.*, 2009; Shin, *et al.*, 2010), type-1 diabetes (Rani, *et al.*, 2010) and ulcerative colitis (Pierce, 2010). Evidence for a causal link with these diseases remains circumstantial. Despite the amount of time MAP has been under scientific scrutiny and the economic imperative for an effective treatment, limited success has been achieved in controlling MAP infections. The intracellular survival and the chronic nature of MAP infection are thought to be a result of substantial immune evasion abilities.

1.5.2 Immune Evasion Capabilities of MAP

MAP invades the host through M cells of the ileal Peyer's Patch (PP) where it subsequently enters macrophage cells of the immune system (Momotani, *et al.*, 1988). This invasion via M cells is through the formation of a fibronectin bridge with host integrins (Secott, *et al.*, 2004). There is evidence indicating that MAP can invade the intestinal mucosa without PP through enterocytes, but even these studies indicate that the preferred invasion route of MAP is through the M cells (Siguroardottir, *et al.*, 2005). It is in the macrophages that MAP resides and proliferates, effectively shielded from the host immune system. Macrophages' normal function is to internalize and destroy bacteria as well as present antigen to the immune system. For MAP to be able to invade and survive within these cells, it must disrupt normal immune functions (Woo, *et al.*, 2007; Weiss and Souza, 2008). A number of mechanisms have been described which explain how MAP evades the natural immune defences. MAP is able to block the maturation of phagolysosomes (Fratti, 2001). It is believed that components of the *Mycobacterium* cell wall have immune-evasion and immune-disruption properties (Karakousis, *et al.*, 2004). The bacterium is also able to interfere with other immune defences related to pathogen clearance including the blocking of interferon gamma (IFNγ)-induced immune signalling events (Robertson and Andrew, 1991). In addition, MAP is known to produce tyrosine phosphatases. Since the MAP genome encodes no tyrosine kinases and its intracellular phosphorylation dependent signalling is serine/threonine-based, it is believed the role of these phosphatases is to disrupt host signalling (Koul, *et al.*, 2000; Singh, *et al.*, 2003).

1.5.2.1 The Phagolysosome

Phagolysosomes are acidic organelles that are rich in hydrolytic enzymes which digest bacteria and other particles (Koul, *et al.*, 2004). Phagosomes, which engulf extracellular particles or bacteria, merge with lysosomes containing acid hydrolysases to form the phagolysosome. Mycobacteria are able to inhibit the merger of phagosome and lysosome protecting the bacteria from hydrolysis and other immune effector molecules such as oxidases. There have been several proposed mechanisms by which mycobacteria are thought to disrupt membrane fusion. One proposed mechanism involves tryptophan aspartate-containing coat protein (TACO) which is released from the membrane of the phagosome and

allows fusion with the lysosome (Ferrari, *et al.*, 1999). In mycobacteria-infected cells, the TACO protein is not released from the phagosome; thus, membrane fusion is inhibited. A mechanism discovered in *Mycobacterium tuberculosis,* but may equally apply to other mycobacteria species due to the conserved genes involved, is the use of the lipid phosphatase SapM to hydrolyze phosphatidylinositol 3-phosphate (PI3P) (Vergne, *et al.*, 2005). In normal phagosome development, PI3P is an essential membrane-trafficking regulatory lipid which allows for phagosomal acquisition of lysosomal constituents. It was found that PI3P was retained in cells infected with dead bacteria, but PI3P is continuously eliminated by the action of SapM in cells infected with live bacteria. This mechanism may be shared with MAP since the MAP genome encodes a phosphoesterase protein very similar in amino acid sequence to SapM (based on NCBI-NR Blastp results). Whatever the mechanism(s) used, MAP is able to survive within the phagosome and replicate without elimination by normal immune effector molecules, allowing for establishment of a chronic infection.

1.5.2.2 Cell Wall

Components of the mycobacterial cell wall are potent immune modulators affecting the responses of both the innate and adaptive immune systems (Karakousis, *et al*, 2003). The four main components of the bacterial cell wall that have immune modulating activity are mannosylated lipoarabinomannan (ManLAM), sulpholipids, mycolic acid-containing glycolipid trehalose-6-6'-dimycolate (TDM) and the 19 kDa lipoprotein.

In the case of ManLAM, there is evidence that it may directly inhibit macrophage activity and promote intracellular survival. Specifically, ManLAM attenuates TNFα and IL-12 expression and induces host expression of Src homology region 2 domain-containing phosphatase-1 (SHP-1), a tyrosine phosphatase that down-regulates macrophage immune responses (Knutson, *et al.*, 1998). ManLAM is also able to inhibit the expression of IL-12 in dendritic cells (Nigou, *et al.*, 2001). In experiments involving isolated M. *tuberculosis* and *M. Bovis* bacille Calmette-Guérin, when cells were exposed to ManLAM, there was no detectale TLR-dependent activation (Means, *et al.*, 1999). The failure to activate TLR responses and the down-regulation of IL-12, thus T-cell activation, may be a key strategy for immune avoidance by mycobacteria. ManLAM also has been found to inhibit IFNγ-mediated macrophage activation (Adams, *et al.*, 1993) and induce transforming growth factor (TGF)β

production (Takeuchi, *et al*., 1998). This may inhibit macrophage and T-cell activation and lead to a switch from a Type 1 helper T-cell (T_h1) immune response to a T_h2 immune response, which is ineffective against mycobacteria (Takeuchi, *et al*., 1998).

Sulpholipid immune modulation has been linked to the inhibition of phagosome activation (Goren, *et al.*, 1987), a key step in the ability of macrophage to destroy intracellular bacteria. Purified sulpholipids of mycobacteria were found to block priming of human monocytes by LPS or IFNγ, resulting in no detectable increase in superoxide production as compared to control cells (Pabst, *et al.*, 1988; Zhang, *et al.*, 1988).

Evidence for the role of TDM in mycobacteria immune evasion and survival came from a study involving the delipidation of *M. tuberculosis*. When delipidated *M. tuberculosis* was used to infect macrophages, bacterial survival was severely impaired. However, upon reconstitution with TDM, bacterial survival was restored, indicating a role for TDM in intracellular macrophage survival (Indrigo, *et al.*, 2002). It has been speculated that this survival enhancement has something to do with TDM's role in the arrest of phagosome development (Karakousis, *et al*, 2003).

The 19 kDa lipoprotein has been linked to reduced production of TNF-α and IL-12 (Post, *et al.*, 2001) and the inhibition of major histocompatibility complex class-II (MHC-II) molecule expression (Noss, *et al.*, 2001). The mechanism by which MHC-II levels are reduced is through the 19 kDa lipoprotein-dependent activation of TLR2, which inhibits IFNγ receptor signalling by down regulating human leukocyte antigen (HLA)-DR. This results in decreased MHC-II processing and reduced recognition of antigens by CD4+ T cells (Gehring, *et al.*, 2003), potentially allowing the bacteria to actively evade the adaptive immune surveillance systems and maintain chronic infection.

1.5.2.3 Disruption of Host Cell Signalling
1.5.2.3.1 IFNγ Response

IFNγ is a key cytokine involved in the immune response to a number of intracellular pathogens including mycobacteria (Dorman and Holland, 1998; Doffinger, *et al*., 2000). Mice deficient in IFNγ display increased susceptibility to intracellular pathogens (Cooper, *et al*., 1993; Dalton, *et al*., 1993). Humans with mutations in the IFNγ receptor display an increased prevalence to infection with low-virulence environmental mycobacterial strains and suffer

from recurrent bouts of tuberculosis (Jouanguy, *et al*., 1999; Dupuis, *et al*., 2000). IFNγ is released from T cells and natural killer cells to activate target cells through a high-affinity receptor composed of two chains: IFNγ receptor 1 (IFNGR1) and IFNγ receptor 2 (IFNGR2). Signal transduction by IFNγ is most commonly associated with the Janus family kinase (JAK)-STAT signalling cascade (Bach, *et al*., 1997; Darnell, 1997). IFNγ binds to its receptor which induces dimerization of the receptor activating JAK1 and JAK2, which phosphorylate IFNGR1 (Igarashi, *et al*., 1994; Bach, *et al*., 1996). This phosphorylation of IFNGR1 causes the recruitment of STAT1, which itself is phosphorylated. Phosphorylated STAT1 translocates to the nucleus to activate the transcription of IFNγ-inducible genes (Greenlund, *et al*., 1995). One of the main actions of IFNγ is the induction of genes encoding proteins to kill intracellular pathogens.

Since the IFNγ immune response is so important to the clearance of intracellular pathogens, a number of viruses and bacteria have evolved means to block cells' ability to respond to IFNγ stimulation. There are a number of points along the IFNγ signalling cascade, from receptor-ligand binding to internal signal transduction to gene expression to protein activity, which are potential points of disruption. At the level of the receptor, several pathogens decrease the expression of one or both of the IFNGR1 and IFNGR2 chains. For example, *Trypanosoma cruzi* (Kierszenbaum, *et al*., 1995) and *Leishmania donovani* (Ray, *et al*., 2000) decrease IFNGR1 expression, adenoviruses decrease IFNGR2 expression (Joseph and Look, 2001), and *Mycobacterium avium* decreases expression of both IFNGR1 and IFNGR2 (Hussain, *et al*., 1999). Disruption of intracellular signalling events downstream of the IFNGR will also eliminate IFNγ responsiveness. For example, human *cytomegalovirus* targets JAKs for degradation (Miller, *et al*., 1998), Mumps virus reduces levels of STAT1 (Fujii, *et al*., 1999), Varicella-zoster virus reduces levels of JAK2 and STAT1 (Abendroth, *et al*., 2000), and *Leishmania donovani* activates the protein tyrosine phosphatase SHP-1 to dephosphorylate and deactivate JAK2 (Blanchette, *et al*., 1999). Transcriptional effectors' expression and translation are induced by IFNγ, and these can also be targets for pathogens since without effector activity, there is no immune response. *Adenovirus* inhibits IFNγ-induced gene expression through a direct interaction with cellular transcription factors (Eckner, *et al*., 1994; Look, *et al*., 1998).

The diverse mechanisms employed to disrupt the IFNγ response clearly demonstrate that knowledge of a given pathogen subverting an immune response is not adequate information to design an effective treatment. The exact mechanism by which the IFNγ response is deactivated must be known. For example, the treatment will be ineffective if a given pathogen disrupts the IFNγ response by down-regulating IFNγ receptor expression and a treatment is given to stimulate the IFNγ receptor. A rationally designed treatment approach based on the specific mechanism of host-pathogen interaction may have a greater chance of success.

It is clear from numerous studies that an IFNγ response is important in Johne's disease. It has been shown that cattle in the excretory, subclinical stage of Johne's disease have increased IFNγ at the site of infection (Sweeney, *et al.*, 1998) and increased IFNγ production after *in vitro* re-stimulation of PBMCs with MAP antigens (Coussens, *et al.*, 2004). Macrophages pre-treated with IFNγ are able to clear mycobacterial infections (Flynn, *et al.*, 1993; Bonecini-Almeida, *et al.*, 1998), while macrophages treated with IFNγ post-infection are unable to achieve effective bacterial clearance (Denis, *et al.*, 1990; Robertson and Andrew, 1991). Taken together, these results indicate that one of the immune evasion mechanisms of MAP is to block cellular responses to IFNγ but not the production of IFNγ. To date, the mechanism by which MAP blocks the IFNγ response has not been determined.

1.5.2.3.2 MAP Tyrosine Phosphatases

Most *Mycobacterium* genomes contain genes for two proteins which act as functional protein tyrosine phosphatases (PTPs): PtpA and PtpB (Koul, *et al.*, 2004). This discovery was surprising, considering that mycobacteria do not contain any tyrosine kinases encoded in their genome, and their internal cell signalling is based on serine/threonine phosphorylation. Based on these observations, it was hypothesized that these phosphatases may be involved in disruption of host cell signalling, and the fact that they are secreted from the bacteria strengthened this hypothesis. When the *mptpB* gene of *M. tuberculosis* was disrupted, it was found that the bacteria were as able to survive in macrophages as wild type. However, when macrophages were activated with IFNγ, bacterial survival was highly impaired (Singh, *et al.*, 2003), indicating that PtpB may dephosphorylate key signalling proteins in the active IFNγ pathway. Specifically in MAP, PtpA was characterized as an active, secreted phosphatase that

41

carries out its function on defined substrates (Bach, *et al.*, 2006). It was also determined that PtpA is actively secreted by MAP in both *in vivo* and *in vitro* infection models. MAP PtpA had dephosphorylation kinetics similar to the well defined *M. tuberculosis* PtpA. This indicates that the phosphatases may be conserved in both sequence and function across mycobacteria species and most likely play an important role in infection. In light of the importance of PTPs in *Mycobacterium* infections, and with the development of more phosphatase specific inhibitors, it is believed that a future treatment for *Mycobacterium* infections may involve the use of phosphatase inhibitors specific for one or both of PtpA and PtpB. The first species this specific phosphatase inhibitor treatment will be applied to will most likely be in *M. tuberculosis* infections targeting PtpB (Koul, *et al.*, 2004).

2.0 HYPOTHESIS AND OBJECTIVES

Hypothesis

Custom-designed genus-specific peptide arrays, in conjunction with customized data analysis methods, represent a valuable strategy to determine host signalling responses induced by a variety of stimuli, including infection.

Objectives

1) To develop and validate custom-designed genus-specific peptide arrays for kinome analysis

2) To develop and validate customized strategies to analyze and interpret peptide array kinome data

3) To apply peptide arrays and associated data analysis methods to understand host signalling responses to prion and MAP infection

3.0 MATERIALS AND METHODS

3.1 Reagents and Chemicals

The chemical reagents required to carry out experiments throughout this thesis are listed in **Table 3.1**.

3.2 Peptide Array Development

3.2.1 Protein Selection and Target Site Identification

The original bovine peptide array contained peptides corresponding to phosphorylation targets of proteins selected on the basis of known cell signalling pathways and was biased toward innate immune-related signalling events. Despite this bias, a broad range of signalling proteins were chosen to facilitate novel discovery and provide a broad overview of signalling events. Many proteins undergo phosphorylation at multiple sites to allow discrete control of various aspects of protein function and interactions. Therefore, many target proteins were represented more than once on the array by peptides corresponding to multiple phosphorylation sites within the protein. This allowed a more detailed exploration of cellular response. The first generation bovine array contained a total of 300 phosphorylation target sequences corresponding to 194 proteins. A custom-designed human/porcine array, in which the majority of peptide sequences were homologous to both genera, contained 300 phosphorylation target sequences corresponding to 152 proteins. The phosphorylation target sites were determined through the use of PhosphoSite (www.phosphosite.org) or Phospho.ELM (phosphor.elm.eu.org).

Table 3.1 List of selected reagents, chemicals and suppliers.

Reagent/Chemical	Supplier
[5-(4-Fmoc-aminomethyl-3,5-dimethyloxyphenoxy) valeric acid]-polyethylene glycol-polystyrene resin	Applied Biosystems
Acetonitrile	EMD Biosciences, VWR
Acid destain	Sigma Aldrich
Amino acids	VWR
Anisole: ethylmethyl sulfide: 1,2-ethanedithiol	Sigma Aldrich
Aprotenin	Sigma Aldrich
Adenosine triphosphate (ATP)	New England Biolabs
Beta-mercaptoethanol	Qiagen
Bovine serum albumin (BSA)	Biorad Laboratories
Brij-35	ICN Biomedicals
Camptothecin	Sigma Aldrich
Carbol fuchsin	Sigma Aldrich
CD14 microbeads	Miltenyi Biotec Inc.
CpG 2007	Merial
Diethyl ether	VWR
Eagle's Minimum Essential Medium (EMEM)	Cedarlane Laboratories
Entellen New Rapid Mounting Medium	EMD Chemicals
Ethanol (molecular grade)	Sigma Aldrich
Ethylene glycol tetraacetic acid (EGTA)	Sigma Aldrich
Ethylenediaminetetraacetic acid (EDTA)	Sigma Aldrich
F12K medium	Cedarlane Laboratories
Fetal bovine serum (FBS)	Seracare
Fura-2, AM	AnaSpec Inc.
Gentamicin	Gibco, Invitrogen Corp.
Glycerol	GE Healthcare
Immulon 2 96U plates	Thermo Scientific

Leupeptin	Sigma Aldrich
Lipopolysaccharide (LPS)	Sigma Aldrich
MACS buffer	Miltenyi Biotec Inc.
Magnesium chloride	Sigma Aldrich
Methylene blue	Sigma Aldrich
Middlebrook 7H9 broth	Difco Labs
Middlebrook 7H10 agar	Difco Labs
Mycobactin J	Allied Monitor Inc.
Oleic acid albumin dextrose complex enrichment medium	Difco Labs
Para-Nitrophenylphosphate (PNPP)	Invitrogen
Percoll	GE Healthcare
Phenylmethylsulphonyl fluoride (PMSF)	Sigma Aldrich
Piperidine	VWR
Polyoxyethylene lauryl ether (Brij-35)	MP Biomedicals
ProQ Diamond Phosphoprotein Stain	Invitrogen
Recombinant bovine IFNγ	Novartis
Reverse transcriptase buffer	Invitrogen
Reverse transcriptase enzyme	Invitrogen
RNase H (*E. coli*)	Invitrogen
RNeasy lysis buffer (RLT)	Qiagen
Roswell Park Memorial Institute (RPMI) medium	Gibco, Invitrogen Corp.
Sodium acetate	Sigma Aldrich
Sodium fluoride	Sigma Aldrich
Sodium orthovanadate	Sigma Aldrich
Sodium pyrophosphate	Sigma Aldrich
Streptavidin alkaline phosphatase	Jackson ImmunoResearch
SYBR Green master mix	BioRad Laboratories
Trifluoroacetic acid (TFA)	Fischer Scientific
Tris + Tween 20 (TBST)	Sigma Aldrich

Gelatin	Sigma Aldrich
Triton X-100	Sigma Aldrich
Trypan blue	Gibco-Invitrogen
Tween 80	Sigma Aldrich
Recombinant VEGF	Invitrogen
Antibodies	**Supplier**
6H4	Prionics
Goat anti-mouse (GAM) IgG1	CALTAG Laboratories
GAM fluorescein isothiocyanate (GAM-FITC)	BD Biosciences
Goat anti rabbit IgG biotin	Zymed, Invitrogen
IgG1 isotype control	CALTAG Laboratories
Kits	**Supplier**
RNeasy mini kit	Qiagen
Supplier Name	**Supplier Address**
Allied Monitor Inc	Fayette, Missouri, USA
Applied Biosystems	Foster City, California, USA
Difco Labs	Detroit, Michigan, USA
EMD Biosciences	Mississauga, Ontario, Canada
VWR	Mississauga, Ontario, Canada
Sigma Aldrich	Oakville, Ontario, Canada
Gibco-Invitrogen Corp.	Burlington, Ontario, Canada
New England Biolabs	Pickering, Ontario, Canada
Qiagen	Mississauga, Ontario, Canada
Biorad Laboratories	Mississauga, Ontario, Canada
ICN Biomedicals	St. Laurent, Quebec, Canada
Miltenyi Biotec Inc.	Auburn, California, USA
Merial	Baie d'Urfé, Quebec, Canada
Cedarlane Laboratories	Burlington, Ontario, Canada
EMD Chemicals	Mississauga, Ontario, Canada
Seracare	Milford, Massachusetts, USA

AnaSpec Inc.	Fremont, California, USA
GE Healthcare	Baie d'Urfé, Quebec, Canada
Thermo Scientific	Nepean, Ontario, Canada
Invitrogen	Mississauga, Ontario, Canada
MP Biomedicals	Solon, Ohio, USA
Novartis	Mississauga, Ontario, Canada
Qiagen	Mississauga, Ontario, Canada
Jackson ImmunoResearch	West Grove, Pennsylvania, USA
Fisher Scientific	Ottawa, Ontario, Canada
Prionics AG	Lincoln, Nebraska, USA
CALTAG Laboratories	Mississauga, Ontario, Canada
BD Biosciences	Mississauga, Ontario, Canada
Zymed, Invitrogen	Mississauga, Ontario, Canada

3.2.2 Genus Ortholog Identification

The PhosphoSite and Phospho.ELM phosphorylation databases contain predominantly human or mouse phosphorylation sites. These human sequences were converted to the genus of interest, originally bovine. The NCBI program Blastp (blast.ncbi.nlm.nih.gov) was utilized to find orthologous target sequences in the genus of interest. The first step in scrutinizing the Blastp-generated results was to ensure that the identified protein matched the human query protein by ensuring the annotations matched. Then, the number of amino acid differences between the human peptide and target was determined by comparing the two 15 amino acid sequences, query and match. In the bovine array design, target sites with substantial sequence differences between human and bovine were purposely limited. Limiting sequence differences meant more confidence that the peptide sequences represented a true kinase target, since the human sequences were well characterized. In addition, with fewer sequence differences, more cross-reactivity between bovine and human samples could be expected. For the human/porcine array, 268 of the 600 human sequences were exact matches with the porcine sequence, and the remaining sequences contained at least one amino acid difference. For

human and porcine peptides that did contain sequences differences, it was decided that the human sequence would be printed on the array. This would allow the array to be used in studies with both human and porcine cell lysate since the majority of the sequences were 100% identical. Of the 300 peptides printed on the array, 206 had 100% homology, and the remainder had at most 2 amino acid sequence differences.

3.2.3 Peptide Synthesis and Spotting

All peptides were synthesized and printed according to the protocol developed and performed by JPT Peptide Technologies (www.jpt.com). Amino-oxy-acetylated peptides were synthesized on cellulose membranes in a parallel manner using SPOT synthesis technology (Frank, 1992; Wenschuh, *et al*., 2000). Following side chain deprotection, the solid-phase bound peptides were transferred into 96-well microtiter filtration plates (Millipore, Bedford, USA) and treated with 200 μL of aqueous triethylamine (0.5 % v/v) to cleave the peptides from the cellulose. Peptide-containing triethylamine solution was filtered off, and solvent was removed by evaporation under reduced pressure. The resulting peptide derivatives (50 nmol) were re-dissolved in 25 μL of printing solution (70% dimethyl sulfoxide (DMSO), 25% 0.2 M sodium acetate pH 4.5 and 5% glycerol v/v) and transferred into 384-well microtiter plates. Two droplets of 0.5 nL peptide solution were deposited per spot on aldehyde functionalized glass slides using the non-contact printer Nanoplotter of GESIM (Großerkmannsdorf, Germany) equipped with 8 piezoelectric NanoTips (GESIM, Großerkmannsdorf, Germany). Printed peptide microarrays were kept at room temperature for 5 hours, washed with deionised water, quenched for 1 hour with 50% aqueous hydroxylamine, washed extensively with water followed by ethanol, and dried under a stream of nitrogen. The peptide microarrays were then stored at 4°C and maintained reactivity for more than 18 months. To determine intra-assay variability in substrate phosphorylation, each block of 300 peptides was printed in triplicate. The physical dimensions of the array were 19.5 x 19.5 mm. Each peptide spot had a diameter of ~350 μm, and the distance between the peptide spots was 750 μm.

In the case of the bovine array, a total of 298 bovine peptides and 2 negative control peptides of 15 amino acids in length were printed within each block of the array. The layout of one block is presented in **Figure 3.1 A**. Seven positive control proteins (Histone 1-4, Myelin basic protein-maltose binding protein bovine and alpha/beta Casein) were printed

outside the margins of each block on the array. The layout of the entire array is shown in **Figure 3.1 B**. For the human/porcine array, a total of 297 human/porcine peptides and 3 negative control peptides were printed in blocks similar to the bovine arrays. The same seven positive control proteins were used. Each positive control was a full-length protein which is known to be phosphorylated in cells in the presence of ATP. Signals from the controls were not included in the peptide array analysis, but these proteins were used to orient the slide for visualization and gridding of the blocks. The layout of the human/porcine array was similar to that shown in **Figure 3.1.**

A)

B)
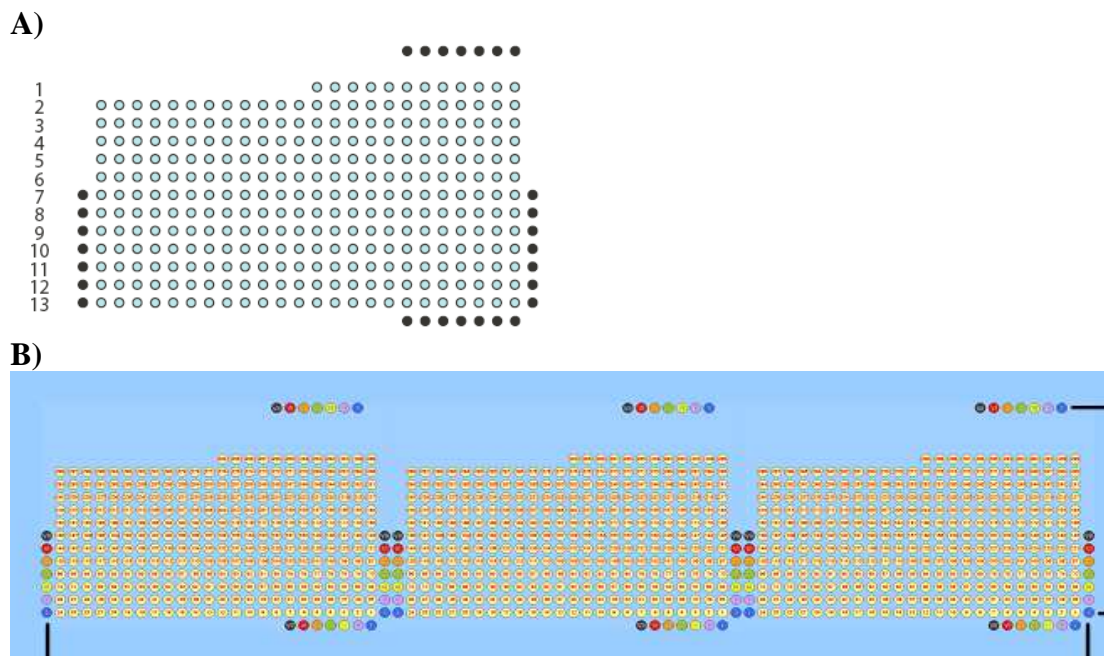
Figure 3.1. Peptide array diagram: Shown are representations of a custom peptide array from JPT Peptide Technologies. Three hundred peptides are printed within each block which is then printed in triplicate. Control spots are printed outside of these blocks to ease array orientation and gridding during analysis. **A)** A single block of peptides is shown. Blue spots indicate custom-designed peptides, and black spots indicate positive control proteins. **B)** Shown here is an entire peptide array chip with each block printed in triplicate. Light yellow spots containing red indicate custom-designed peptides. Coloured and black spots located around the custom-designed spots indicate control proteins. This figure was adapted from the JPT schematic.

3.3 Human Neuronal BE(2)M17 Culture

Human neuronal cells, BE(2)M17, (Cedarlane Laboratories Burlington, ON) were maintained in a 1:1 mixture of Eagle's Minimum Essential Medium (EMEM) (Cedarlane Laboratories) containing Earle's Balanced Salt Solution, non-essential amino acids, 2 mM L-glutamine, 1 mM sodium pyruvate, and 1500 mg/L sodium bicarbonate, and F12K Medium (Cedarlane) containing gentamicin (Gibco-Invitrogen, Burlington, ON) with 10% fetal bovine serum (FBS) (Seracare, Milford, MA). The cells were cultured in T-75 culture flasks (Corning, Lowell, MA) at 37ºC in an atmosphere of 5% CO_2 and 95% air. The cells grew as an adherent monolayer and were detached from the plastic with 0.5% trypsin in versene when passaged every 3-4 days.

3.4 Flow Cytometric Analysis of PrP^C Expression on BE(2)M17 Cells

Monoclonal antibody 6H4, specific for PrP, was purchased from Prionics AG (Lincoln, NE). Fluorescein isothiocyanate (FITC)-conjugated, isotype specific, goat anti-mouse Ig antibodies (GAM-FITC) were purchased from BD Biosciences (Mississauga, ON), and IgG1 isotype control antibodies were purchased from CALTAG Laboratories (Mississauga, ON). One-million cells resuspended in 50 μL phosphate buffered saline (PBS) and 50 μL of primary antibody (10 μg/mL) were mixed and incubated on ice for 15 minutes before the cells were washed 3 x with 200 μL phosphate buffered saline (PBS). The cells were then resuspended in 100 μL secondary GAM-FITC (10 μg/mL) and incubated for 15 minutes on ice. The cells were again washed 3 x with 200 μL PBS and resuspended in 200 μL PBS. Phenotypic analysis of the cells was performed using a FACSCalibur (Becton Dickinson, San Jose, CA) flow cytometer to collect data, and the CellQuest (Becton Dickinson) software program was used for data analysis.

3.5 BE(2)M17 Prion Stimulation
3.5.1 Peptide Synthesis

Peptide PrP 106-126, sequence N terminal - KTNMKHMAGAAAAGAVVGGLG – C terminal (O'Donovan, *et al.*, 2001), and scramble peptide of identical amino acid composition, sequence N terminal – NGAMAKMAGGHAVATVAGKGL – C terminal, were synthesized by VIDO Chemistry Services using the following protocol. Peptides were

synthesized on a Pioneer solid-phase peptide synthesizer (PerSeptive Biosystems. Foster City, CA) using 9-Fluorenylmethyloxycarbonyl (Fmoc) chemistry. The peptide chain was synthesized by the addition of amino acids (VWR, Mississauga, ON) from the carboxyl terminus to the amino terminus onto [5-(4-Fmoc-aminomethyl-3,5-dimethyloxyphenoxy) valeric acid]-polyethylene glycol-polystyrene resin (Applied Biosystems, Foster City, CA). The Fmoc protecting group at the amino terminus was deprotected with piperidine (VWR). The peptide was cleaved from the resin with concurrent deprotection of the side-chain protecting groups by treating the resin-bound peptide with trifluoroacetic acid (TFA) (Fisher Scientific, Ottawa, ON) (9.3 parts) in the presence of the scavengers anisole, ethylmethyl sulfide and 1,2-ethanedithiol (Sigma Aldrich, Oakville, ON) (3:3:1) for 3 hours. The crude peptide was filtered from the resin, and the TFA evaporated. Diethyl ether (VWR) was added to the residue to precipitate the crude peptide. The peptide was isolated and purified by high performance liquid chromatography on Vydac Protein C-4 column (1.0 x 25 cm) eluting with a linear gradient of 15% (water, 0.1% TFA) - 90% B (acetonitrile (VWR):water (90:10), 0.01% TFA) for 40 minutes at a flow rate of 3 mL/minute. The molecular weight of the peptides was measured by matrix-assisted laser desorption/ionization time of flight mass spectrometry on PE Biosystems Voyager System 4068 (Plant Biotechnology Institute, National Research Council, Saskatoon, SK).

3.5.2 Peptide Stimulation

Human neuronal cells were stimulated with a prion protein fragment PrP 106-126, and a scrambled peptide of identical amino acid composition was used as a negative control. The peptides were dissolved in distilled H_2O at a concentration of 5 μg/mL. This solution was then added to cultured cells at a final concentration of 80 μM, and the cells were incubated at 37ºC, 5% CO_2 and 95% air for 4 hours. The cells were then harvested as described in Section 3.11.1.

3.5.3 Antibody Stimulation

Antibody cross-linking was done as per the cell phenotyping procedure with the following alterations: cells were suspended in culture media, GAM without conjugated FITC (CALTAG) was used as the secondary to cross-link the antibody, 5 μg/mL of primary and 2

μg/mL of secondary was used, only 1 wash following the addition of the primary was done, and no washes were performed after GAM addition.

3.6 MACS Isolation of Bovine Monocytes

Fifty mL of blood was collected from three 9-month-old Charolais-cross steers, animal numbers 89, 136 and 148. Blood was collected by venupuncture into tubes containing ethylenediaminetetraacetic acid (EDTA) (Sigma Aldrich, Oakville, ON) as an anti-coagulant (performed by VIDO Animal Care staff). Blood was transferred to 50 mL polypropylene tubes (Corning) and centrifuged at 1,400 x g for 20 minutes at 20°C. Mononuclear leukocytes were isolated from the buffy coat and mixed with phosphate buffered saline without Mg^{2+} or Ca^{2+} (PBSA) to a final volume of 35 mL. The cell suspension was then layered onto 15 mL of 54% isotonic Percoll (GE Healthcare, Baie d'Urfe, QC) and centrifuged at 2,000 x g for 20 minutes at 20°C. Peripheral blood mononuclear cells (PBMC) from the Percoll-PBSA interface were then collected and washed three times with ice-cold PBSA. Monocytes were purified from isolated PBMCs by MACS purification using anti-CD14 microbeads (Miltenyi Biotec, Auburn, CA), as per Miltenyi Biotech Protocol Sheet 130-050-201. Monocytes were then plated at $4x10^6$ cells/well in 12-well culture cluster plates (Corning) using RPMI medium (Gibco-Invitrogen) supplemented with 10% heat-inactivated FBS (Gibco-Invitrogen) and rested overnight at 37ºC in 5% CO_2 prior to infection.

3.7 MAP Culture

MAP K10 was incubated at 37ºC on Middlebrook 7H10 agar (Difco Labs, Detroit, MI) with oleic acid albumin dextrose complex enrichment medium (Difco Labs) and mycobactin J (Allied Monitor Inc., Fayette, MO). After 3-4 weeks of growth, a large loopful of bacteria was collected and transferred to 50 mL Middlebrook 7H9 broth (Difco Labs) containing 0.05% Tween 80 (Sigma Aldrich), oleic acid albumin dextrose complex enrichment medium and mycobactin J. The culture was incubated at 37ºC with gentle agitation for 5 days to achieve log phase growth. A 50 mL tube (Corning) was weighed, and bacteria culture was transferred to the tube. The tube was then centrifuged at 3,400 x g for 30 minutes. The supernatant was decanted, and the pellet was allowed to drain upside down on sterile filter paper for 30 minutes. The tube containing the pellet was then weighed. A

calculation of colony-forming units (CFU) was then performed (1 mg = 10^7 CFU) as per Hines, *et al.* (2007). The pellet was resuspended in an appropriate amount of RPMI medium (Gibco-Invitrogen) to achieve the desired concentration.

3.8 MAP Infection of Monocytes

MAP bacteria were added to cultured monocytes at a ratio of 10 bacteria to 1 monocyte. Following MAP addition, the culture plate (Corning) was centrifuged at 300 x g for 2 minutes to ensure contact between the bacteria and monocytes. The monocyte culture was then incubated at 37ºC in 5% CO_2 for 3 hours. The cells were washed 3 x with fresh RPMI (Gibco-Invitrogen) + 10% FBS (Seracare), and if required for the given assay, incubated for additional time at 37ºC in 5% CO_2.

3.9 Monocyte and MAP Acid Fast Staining

Following infection, media containing the monocytes was removed. The monocytes were lifted from the plastic using 0.5% trypsin in versene. The monocytes were prepared for cytospins by centrifugation at 325 x g for 5 minutes. The cells were then resuspended in 200 µL PBSA + 0.1% EDTA (Sigma Aldrich). Cytospins were performed by adding 100 µL cell suspensions to the cytospin cone before centrifuging at 300 x g for 3 minutes to deposit cells onto a glass slide. The slides were allowed to dry overnight in a fume hood. The cells were heat-fixed to the slides by briefly passing them through flame. The slides were then placed over boiling water, stained with carbol fuchsin (Sigma Aldrich) for 5 minutes and rinsed. Acid destain (Sigma Aldrich) was briefly added to each slide before rinsing with water. The slides were counterstained using methylene blue (Sigma Aldrich) for 1 minute and rinsed with water. The slides were dried overnight in the fume hood. The next day, each cytospot was fixed using Entellen New Rapid Mounting Medium (EMD Chemicals, Mississauga, ON) with a coverslip. The cells were observed under a light microscope using oil immersion (100X power).

3.10 Treatment of Monocytes

Purified monocytes (uninfected and MAP-infected) were prepared as described earlier. In the case of CpG treated monocytes, 5 µg/mL CpG 2007 (Merial, Baie d'Urfé, QC) was added to the well. In the case of LPS treated monocytes, 100 ng/mL of LPS (*E. coli* 0111:B4) (Sigma Aldrich) was added to the well. In the case of recombinant bovine IFNγ treatment, IFNγ (Novartis, Mississauga, ON) was added to cultures at a final concentration of 10 ng/mL, and the cells were incubated for time required for the individual assays at 37ºC in 5% CO_2.

3.11 Peptide Array Technique
3.11.1 Cell Harvesting

Approximately $10x10^6$ cells were stimulated/infected for the desired time period: 4 hours for prion, CpG, LPS studies and 3 hours for MAP studies. The media was removed and discarded. Approximately 1 mL mixture of 0.5% trypsin-versene was added to each well for 30 seconds. Trypsin-versene was removed and discarded. The cultures were placed in an incubator for 5 minutes at 37ºC. To remove adherent cells, the plates were then washed with the appropriate media: EMEM-F12K for prion study or RPMI for studies involving monocytes. The cells were then collected, spun down and pelleted at 300 x g for 8 minutes. The media was removed, and the pellet was frozen in a freezer block at -80ºC overnight. The cells were then removed from the block and stored at -80ºC until used in peptide array analysis.

3.11.2 Peptide Array Exposure/Incubation/Washing Procedure

The cells were thawed and lysed by the addition of 100 µL lysis buffer [20 mM Tris-HCl pH 7.5, 150 mM NaCl,1 mM EDTA, 1 mM Ethylene glycol tetraacetic acid (EGTA), 1% Triton X-100, 2.5 mM sodium pyrophosphate, 1 mM Na_3VO_4, 1 mM NaF, 1 µg/mL leupeptin, 1 g/mL aprotinin and 1 mM Phenylmethylsulphonyl fluoride] (all products from Sigma Aldrich unless indicated). The cells were incubated on ice for 10 minutes and spun in a microcentrifuge at 1,000 x g for 10 minutes at 4ºC. An approximate protein concentration of 1.3-1.5 mg/mL was present in the 100 µL of lysate. A 70 µl aliquot of this supernatant was mixed with 10 µl of activation mix [50% glycerol (GE Healthcare), 500 µM ATP (New England Biolabs, Pickering, ON), 60 mM $MgCl_2$, 0.05% v/v Brij-35 (ICN Biomedicals, St.

Laurent, QC) and 0.25 mg/mL BSA (BioRad Laboratories, Mississauga, ON)] which was incubated on the array for 2 hours at 37ºC. Custom-designed bovine peptide array was used for all array experiments. Following incubation, the slides were washed once with PBS-(1%) Triton, submerged in stain (ProQ Diamond Phosphoprotein Stain, Invitrogen) and agitated for 1 hour. Arrays were then washed twice in 50 mL tubes (Corning) containing destain [20% acetonitrile (EMD Biosciences, Mississauga, ON) and 50 mM sodium acetate (Sigma Aldrich) at pH 4.0] for 10 minutes, with the addition of new destain before each wash. A final wash was done with distilled H_2O, and the arrays were dried.

3.11.3 Signal Detection

The arrays were read using a GenePix Professional 4200A microarray scanner (MDS Analytical Technologies, Toronto, ON) at 532-560 nm with a 580 nm filter to detect dye fluorescence. Images were collected using the GenePix 6.0 software (MDS). Signal intensity values were collected using the GenePix 6.0 Software (MDS) with the following settings: scanner saturation level 65535, background calculation done using local feature background, signal mean and background mean intensity values used for analysis, local background features excludes 2 pixels, and width of background was set to 3 feature diameters. Intensity values for the spots and background were collected for each array.

3.12 Peptide Array Data Analysis
3.12.1 Statistical Analysis

The statistical analysis pipeline and data mining steps were developed as a collaborative effort with Dr. Tony Kusalik and his student Yue Li of the Department of Computer Science, University of Saskatchewan.

3.12.1.1 Data Pre-Processing

For all datasets, the specific value for each peptide spot was calculated by subtracting local background intensity from foreground intensity. The resulting data were transformed using a variance stabilization (VSN) model (Huber, *et al*., 2002). The transformation calibrated all the data to a positive scale while maintaining the structure within the data and alleviating mean-variance-dependence. In addition, the data across various experiments were

brought to the same scale by VSN to enable comparison of arrays between experiments, cell types or treatments. To facilitate subsequent analysis, the dataset was rearranged so each row contained all the replicates of a unique peptide. The R software environment (www.r-project.org) function *vsn2* from the package *vsn* was used for the VSN transformation (Huber, *et al.*, 2003). Only in the subsequent clustering analysis was the average for each of the peptide replicates in a single treatment taken, otherwise replicates were left as separate values.

3.12.1.2 Spot-Spot Variability Analysis

A chi-squared (X^2) test was used to examine the variability of each peptide spot across technical replicates (Draghici, 2003), that is, replicates on the same chip or multiple chips for the same subject under the same treatment.

For each peptide, the null hypothesis (H_0) claimed that there was no difference among intensities from the replicate spots, and the alternative hypothesis (H_A) stated that there existed significant variation among the replicates. The X^2 test statistic (TS_1) was:

$$TS_1 = \frac{(n-1)s^2}{\sigma^2} \tag{3.1}$$

where n is the number of replicates for each peptide in the treatment,

$$s^2 = 1/n \sum_{i=1}^{n}(y_i - \bar{y})^2 \tag{3.2}$$

is the sample variance of the replicates for each peptide in a treatment,

$$\bar{\sigma}^2 = 1/M \sum^{M} \quad _2 \tag{3.3}$$

is the mean of all the variances for the replicates of the   peptides in the treatment (i.e., total number of distinct peptides included in an array), and

$$\text{-value} = \tag{3.4}$$

57

The peptides with *p*-values less than a set threshold were considered inconsistently phosphorylated across the array replicates. A confidence level (e.g., 0.01) was used to retain as much data as possible. The *p*- value was calculated using the R function *pchisq* from the *stats* package.

If applicable, the remaining intensities induced by the treatments were adjusted by subtracting the intensities of the biological control of the same subject.

3.12.1.3 Subject-Subject Variability Analysis

Subject-subject variability analysis was done after biological background subtractions (if applicable) and was only applied to datasets where there was a concern of animal (subject) variation. Thus, subject-subject variability analysis was performed on the MAP peptide array data but not the prion array data. For each of the peptides, an F-test was used to determine whether there were significant differences among the subjects under the same treatment condition. Data for inconsistently phosphorylated peptides were eliminated from subsequent analysis.

As a description, let *a* be the number of subjects, *n* the number of intra-array replicates, N the total number of replicates for each peptide for each treatment and u_i the mean response of each peptide in the ith subject for each treatment. The null hypothesis (H$_0$) claimed that $u_1 = u_2 = \ldots = u_a$, or that the mean phosphorylation intensities elicited by the identical peptide among the subjects were the same. The alternative hypothesis (H$_A$) stated that not all subject means were equal. The F-statistic (TS_2) was calculated as:

$$TS_2 = \frac{MS_B}{MS_w}$$

(3.5)

where

(mean squared between subjects)   (3.6)

58

and

$$MS_W = \frac{SS_W}{df_W} = \frac{\sum_{i=1}^{a} \sum_{m=1}^{n} (y_{im} - \bar{y}_i)^2}{N - a} \quad \text{(mean squared within subjects)} \tag{3.7}$$

Above, $\bar{y}_i \equiv \hat{u}_i$ is the sample mean for the ith subject, $\bar{y} \equiv \hat{u}$ the grand mean of all the subjects and y_{im} the individual response of the mth replicate in the ith subject. For the p-value calculation:

$$p\text{ - value} = P[TS_2 > F(a-1, N-a)] \tag{3.8}$$

Under the same treatment condition, the peptides with p-value less than a threshold were considered inconsistently phosphorylated among the subjects and were eliminated from subsequent analysis. A confidence level (e.g., 0.01) was used so that as much data as possible was retained.

3.12.1.4 Treatment-Treatment Variability Analysis

All peptides identified as having consistent patterns of response to various treatments across the subjects were the objects of one-sided paired t-tests. T-tests were conducted to compare signal intensities under a treatment condition with those under control conditions. The t-test statistic (TS_3) was calculated as:

$$TS_3 = \frac{\bar{D}}{S_D / \sqrt{N}} \tag{3.9}$$

where is the mean of the differences between responses for the same peptides induced by two different treatments, the standard deviation of the differences and N the number of differences between each treatment and control. Finally,

$$\text{ - value} = \text{(phosphorylation)} \tag{3.10}$$

and

$$p\text{ - value} = P[TS_3 < -t(N-1)] \quad \text{(dephosphorylation)} \tag{3.11}$$

Thus, each peptide had two *p*-values: one associated with the peptide being differentially phosphorylated and the other with it being dephosphorylated. The peptides with a *p*-value less than a threshold (e.g., 0.1) were considered as differentially (de)phosphorylated and were used for the subsequent analyses. To retain as much data as possible, no adjustment (as for multiple hypotheses testing) was made to the *p*-value. The paired t-test was performed using the R environment function *t.test* from the *stats* package with *paired = True*.

The paired t-test was used because it takes into account the interdependence between the same peptides under treatment and control conditions. Also, note that the t-test was able to account for the variability (in terms of S_D) among the replicates; thus, replicates with significant *p*-value from the X^2-tests automatically had insignificant *p*-value from the t-test. However, this did not apply to datasets with multiple subjects because significant variation for the same peptide among the subjects under the same treatment condition might have been biologically meaningful. It may have confounded the analysis if these peptides were treated as if they came from the same source.

3.12.1.5 Data Visualization

The results from the treatment-treatment variability analysis were recorded in tables and also presented in pseudo-images. The latter were generated based on the *p*-values from the one-sided t-tests for phosphorylation or dephosphorylation of each peptide. Each peptide was represented by one small coloured circle. The intensity of the colouration in red and green were inversely related to the corresponding *p*-values. For example, if the *p*-value for phosphorylation was 0.001, then the redness in percentage was 100% x (1 - 0.001) = 99.9%. The same rationale was applied to dephosphorylated peptides and the intensity of the green colour. Thus, the combined colour intensity of red and green represented the phosphorylation status of each peptide in the microarray. In addition, each circle in the plot was partitioned into sectors, each of which represented a different treatment. Moreover, the circles were arranged in such a way that, going downwards by column from left to right, the consistently

phosphorylated peptides across treatments were presented first, and the inconsistent ones followed. Within the consistently phosphorylated peptides the ones with the most significant *p*-values for (de)phosphorylation on average over the treatments being compared, were presented first, and the less significant ones followed. Similarly, the inconsistent ones with the largest *p*-values when compared to the treatment were presented first, and the smaller *p*-values followed. The original numbering for a peptide (i.e., the label below each circle) from the physical array layout was unchanged for indexing detailed information of the peptide. The plots were generated using R environment functions *plot* (for plotting the circles in different coordinates), *rgb* (for 13 colouration) and *polygon* (for drawing sectors to represent treatments). This visualization of the results from differential analysis facilitated the identification of conspicuous intensities of peptides, or patterns of intensities, across treatments.

3.12.1.6 Cluster Analysis

Peptides with consistent intensities in technical and biological replicates were determined in the previous spot-spot and subject-subject variability analyses. For each such peptide, an average intensity was taken over the technical replicates. The averaged data, with or without biological control subtractions, was subjected to hierarchical clustering and PCA to cluster peptide-response profiles across treatments or subject-treatment combinations. The dendrograms from the hierarchical clustering were augmented by heatmaps showing the averaged (de)phosphorylation intensities.

The R environment function *heatmap.2* from the *gplots* package was used for hierarchical clustering, and the *prcomp* function from *stats* was used for PCA. The 3D plot for the PCA using the first three principal components was produced by the R function *scatterplot3d* from package *scatterplot3d*.

In the case of the prion dataset, heatmap clustering was based on complete linkage plus Euclidean (Everitt, 1974; Hartigan, 1975). The distance between any two clusters was considered as the Euclidean distance between the two farthest data points in the two clusters. Formally, the Euclidean distance between two animal/treatment vectors, X and Y, was calculated as:

$$dist(X,Y) = \sqrt{(x_1 - y_1)^2 + (x_2 - y_2)^2 + ... + (x_{300} - y_{300})^2} \qquad (3.12)$$

For the MAP study dataset, the clustering was average linkage plus Pearson correlation (Pearson, 1896; Eisen *et al.*, 1998), and the calculation of two vectors of treatment, X and Y, were computed as follows:

$$rXY = \frac{\sum_{i=1}^{300}(x_i - \bar{x})(y_i - \bar{y})}{\sqrt{\sum_{i-1}^{300}(x_i - \bar{x})^2 \sum_{j=1}^{300}(y_j - \bar{y})^2}} \qquad (3.13)$$

3.12.2 Statistical Method Comparison

To compare our pipeline, three previously published workflows for microarray analyses were implemented in R and applied to the same datasets. Those were percentile normalization (PNorm) + fold change (Lowenberg, *et al.*, 2006; van Baal, *et al.*, 2006; Jalal, *et al.*, 2009), quantile normalization (QNorm) + Linear Models for Microarray Data (*limma*) (Schrage, *et al.*, 2009) and VSN + *limma* (Fletcher, *et al.*, 2009). All three methods operated on background-corrected data. The PNorm procedure was implemented in R based on the algorithm reviewed by Fundel *et al.* (2008). The 90th percentile was used, as in the kinome analysis by Lowenberg *et al.* (2006). Briefly, after background correction, intensities in each array were divided by the 90th percentile of the data points from the same array in order to achieve a uniform intensity at the 90th percentile across all the arrays. The QNorm and VSN steps were carried out using the R environment *limma* package function *NormalizeBetweenArrays* by setting the parameter *method* to *quantile* and *vsn*, respectively (Smyth and Speed, 2003). Note that the *NormalizeBetweenArrays* provided the VSN method. After VSN, however, the function further scaled the transformed data by taking the logarithm to base 2 (log2), which was not carried out in our pipeline.

In the PNorm + fold change approach, data from the same array with standard deviation (SD) larger than 1.96 (approximated as 2 x SD) of the mean were deemed inconsistent and excluded from subsequent analysis (Lowenberg, *et al.*, 2006; van Baal, *et al.*, 2006). In QNorm + *limma* and VSN + *limma*, a function called *duplicateCorrelation* in the *limma* package was used to estimate the correlation between the replicates within an array

(Smyth, *et al.*, 2005). The resulting correlations for each peptide were used as a weighting factor for the subsequent differential analysis. Finally, an F-test provided by the *limma* package was used to compare the log2 fold change (logFC) of each peptide across biological replicates. The log scale ratios given by *limma* were converted to fold change values by using the R function *logratio2foldchange* from the *gtools* library.

In the differential analysis, the PNorm + fold change approach identified differentially phosphorylated peptides by comparing their combined fold change to an arbitrary threshold (*td*). The peptides with fold change larger than *td* were deemed significantly phosphorylated, and those with fold change less than *td* were deemed significantly dephosphorylated. The two other comparison methods involving *limma* used the function *eBayes* (Schrage, *et al.*, 2009) to determine the *p*-values associated with the moderated t-statistics. A peptide was determined as differentially phosphorylated if its *p*-value was less than 0.1.

3.12.3 Pathway Analysis

Differentially phosphorylated peptides, as determined by the differential analysis step (Section 3.12.1.4), can be used to probe the database InnateDB (Lynn, *et al.*, 2008). Because InnateDB requires fold change values as input (with *p*-values optional), the differences between the VSN-transformed intensities under control and treatment were converted to fold change values by the formula:

$$\text{Fold Change} = 2^d \tag{3.14}$$

where

$$d = \text{average}_{\text{treatment}} - \text{average}_{\text{control}} \tag{3.15}$$

The fold change value and one of the *p*-values from the one-sided t-test for each of the 300 peptides (less those removed during the subject-subject variability analysis) were input into InnateDB. If a peptide had a positive calculated fold change value, then the *p*-value associated with phosphorylation was chosen; otherwise, if the calculated fold change value was negative, the *p*-value associated with dephosphorylation was chosen.

Other inputs to InnateDB were *p*-value threshold and fold change threshold. These thresholds allow specified cut-offs for the input dataset. InnateDB eliminated from analysis all peptides with a *p*-value greater than the set *p*-value threshold and fold change values less than the set fold change threshold. For the prion and MAP dataset analysis, the *p*-value threshold was set to 0.2, and the fold change threshold was set to 1. The latter threshold is non-selective since the fold change values will always be equal to or greater than 1, or equal to or less than -1. This non-selectivity was a deliberate choice. Since the *p*-value was a calculation of how significant the difference was between treatment and control, it was the preferred basis for determining whether a peptide should be included rather than relying on fold change.

For the comparison methodologies, pathway identification was again performed using InnateDB. All peptides except those determined to have inconsistent intensities were considered. Thresholds were the same as for our method (*p*-value of 0.1 and fold change of 1). For QNorm + *limma* and VSN + *limma* methods, identifiers of the peptides along with *p*-values and fold change values were again input. For PNorm + fold change, only peptide identifiers and fold change values were input as no *p*-values were available from this method.

Pathways identified by InnateDB for each methodology and each dataset were then visualized using the Cerebral plugin (Barksy, *et al.*, 2007) for the interaction viewer Cytoscape (Shannon, *et al.*, 2003).

3.13 Phosphospecific Antibody Array

3.13.1 Cell Preparation

BE(2)M17 cells (10 x10^6) were stimulated for 4 hours with 80 µM of the prion protein fragment PrP 106-126 or scrambled control peptide in media. The cells were then centrifuged at 300 x g for 8 minutes, washed in PBS and centrifuged a second time. The supernatant was removed, and the pellet was frozen at -80°C before shipping for commercial analysis.

3.13.2 Array Procedure

The antibody array procedure was performed as per Pelech and Zhang (2008) by Kinexus Bioinformatics (Vancouver, B.C.). Cell lysates at a protein concentration of 2 mg/mL were labelled with a fluorescent dye. Unincorporated dye was removed by ultrafiltration. Purified, labelled proteins from the control and treatment samples were

incubated separately on opposite sides of a Kinex KAM 1.0 antibody microarray. The microarray contained two identical fields of antibody grids. Each field contained 604 antibodies printed in duplicate. Pan-specific and phosphospecific antibodies were printed at a concentration of 100 µg/mL at 10 nL per spot. The internal variation for the spot printing between chips in the same print run is less than 4%. After antibody binding, arrays were scanned using a ScanArray scanner (Perkin-Elmer, Wellesley, MA) with a resolution of 10 µm. Images were quantified to determine the binding signal using ImaGene software (BioDiscovery, El Segundo, CA). The values were the means of the measurements from each antibody spot pair. Means were converted to fold change by dividing treatment mean by control mean.

3.14 Camptothecin Treatment of BE(2)M17

Human neuronal cells were plated in 24-well plates (Corning) in 1 mL of media. Ten µM camptothecin (Sigma) was added to the wells which were incubated at 37°C in 5% CO_2 and 95% air overnight. The cells were then harvested and assayed, as indicated in Section 3.11.1 but without freezing.

3.15 VEGF Treatment of BE(2)M17

Human neuronal cells were plated in 24-well plates (Corning) in 1 mL of media. Fifteen ng/mL recombinant vascular endothelial growth factor (VEGF) (Invitrogen) was added to wells which were incubated at 37°C in 5% CO_2 and 95% air overnight. The cells were then harvested and assayed as indicated in Section 3.11.1, but without freezing.

3.16 Viable Cell Assay

Neuronal cells ($5x10^5$) were plated in triplicate in 24-well plates (Corning) at a concentration of $1x10^6$ cells/mL and left overnight. The cells were then treated with peptide or antibody as described in Sections 3.5.2 and 3.5.3 respectively, with or without the addition VEGF (Invitrogen) (Section 3.15). The cells were left for an additional 24 hours to allow stimulation to have effect. The cells were harvested as described in Section 3.11.1, but without freezing. Cell viability was determined by trypan blue (Gibco-Invitrogen) dye

exclusion, and cell count was determined using a hemocytometer. Fold change and standard error of mean were calculated from replicate means.

3.17 Calcium Release

Triplicate cell samples at a concentration of $1x10^6$/mL were treated with the appropriate stimulation for 4 hours, harvested and resuspended at $2x10^6$ cells/mL in modified Krebs-Ringer-HEPES (KRH) buffer at pH 7.4 containing 0.1% BSA (BioRad), 118 mM NaCl, 4.6 mM KCl, 24.9 mM $NaHCO_3$, 1.0 mM KH_2PO_4, 11.1 mM glucose, 1.1 mM $MgSO_4$, 5.0 mM HEPES, and 1.0 mM $CaCl_2$ (Sigma Aldrich, unless indicated). The cells were incubated with 2 µM Fura-2-acetoxymethyl ester (Fura-2/AM) (AnaSpec Inc., Fremont, CA) fluorophore at 37°C in 5% CO_2 for 30-40 min. The cells were then centrifuged at 300 x g for 8 min, resuspended in KRH buffer and incubated for an additional 20 min at a concentration of $1x10^6$ cells/mL. Fluorescence was measured at 339 nm excitation and 505 nm emission using a Victor[3]V 1420 Multilabel Counter (PerkinElmer, Woodbridge, ON).

3.18 TNFα ELISA

Purified monocytes (uninfected and MAP-infected) were prepared as described in Section 3.8 and incubated for an additional 24 hours. Recombinant bovine IFNγ (Novartis) was added at a final concentration of 10 ng/mL. The cultures were returned to the incubator (37°C in 5% CO_2 and 95% air) overnight. Supernatant was collected from each well, diluted (1:2), and bovine TNFα concentration was quantified using an antibody capture Enzyme-linked immunosorbent assay (ELISA).

The ELISA was performed as per Ellis, *et al.* (1993). Briefly, mouse-anti-bovine TNFα antibody (Clone 1D11-13) was diluted 1:1000 in coating buffer (0.1 M PBS). The diluted antibody was applied to Immulon 2 96U plates (Thermo Scientific, Nepean, ON) at 100 µL per well. The plates were left at 4°C overnight and then washed 4 x with Tris-Buffered Saline and Tween 20 (TBST) (Sigma Aldrich). Samples were serially diluted, and 100 µL was added per well. Samples were diluted with TBST + 0.1% gelatin (TBST-g) (Sigma Aldrich). Known concentrations of TNFα were added for the establishment of a standard curve. The plates were incubated for 2 hours at room temperature and then washed 4 x with TBST. Rabbit-anti-bovine TNFα Pool 88 was diluted 1/1500 in TBST-g, and 100 µL

added per well. The plates were incubated for 1 hour at room temperature and then washed 4 x with TBST. Goat-anti-rabbit IgG (H+L) biotin (Zymed-Invitrogen, Mississauga, ON) was diluted 1/10,000 in TBST-g, and 100 μL was added per well. The plates were incubated for a minimum of 1 hour at room temperature and then washed 4 x with TBST. Streptavidin alkaline phosphatase (Jackson ImmunoResearch, West Grove, PA) in 50% glycerol was diluted 1/5000 in TBST-g, and 100 μL was added per well. The plates were incubated for a minimum of 1 hour at room temperature and then washed 4 x with TBST. Para-Nitrophenylphosphate (PNPP) (Invitrogen) substrate was diluted in PNPP buffer to 1 mg/mL, and 100 μL was added per well. The plates were incubated approximately 1 hour at room temperature. The reaction was stopped by the addition of 30 μL 0.3 M EDTA (Sigma Aldrich) when the optical density (OD) of the first dilution of the standard curve reached an OD of approximately 2.00 at a wavelength of 405 nm. The plates were then read at 405 nm, reference 490 nm. The TNFα concentration of the samples was determined from the standard curve of known concentrations.

3.19 IFNGR and SOCS RT-PCR

Purified monocytes (uninfected and MAP-infected) were prepared as described in Section 3.8 and incubated for 1 hour or 18 hours. Total RNA extraction was performed as per the RNeasy Mini Kit Protocol (Qiagen, Mississauga, ON). Briefly, 1 mL of RNeasy Lysis Buffer (RLT) + beta-mercaptoethanol (Qiagen) was added to each well for 5 minutes. The cells were collected in a 2 mL tube, vortexed briefly and stored at -80°C until further processing. Samples were homogenized by running lysate through a QIAshredder (Qiagen). Molecular grade ethanol (Sigma Aldrich) was added to each sample before running the sample through an RNeasy mini spin column (Qiagen). DNase treatment was performed on each sample by adding a DNase solution (Qiagen) to the column and allowing the solution to sit for 15 minutes. Three washes were performed, followed by elution in nuclease-free water. Each sample was quantified and checked for purity using a 2100 Bioanalyzer (Agilent Technologies, Mississauga, ON).

RNA (200 ng) was converted to cDNA by adding 8 μL 2 x real-time (RT) buffer and 2 μL RT Enzyme (Invitrogen) to a total volume of 10 μL. A master mix of buffer and enzyme was made to eliminate pipetting error. Samples were placed in a thermocycler under the

following conditions: 25°C for 5 minutes, 50°C for 60 minutes and 70°C for 15 minutes. The RNA template was removed by adding 1 μL *E. coli* RNase H (Invitrogen) for 20 minutes. The cDNA was stored at -20°C.

Each reaction for qRT-PCR included 9 μL iQ SYBR Green Master Mix (BioRad Laboratories, Mississauga, ON), 3 μL primer mix (3.3uM), 2 μL nuclease-free water and 1 uL cDNA, for a total of 15 μL reaction. Thermocycler conditions were as follows: cycle 1 55°C for 2 minutes, cycle 2 95°C for 8.5 minutes, cycle 3 step 1 - 95°C for 15 seconds, step 2 - 55°C for 30 seconds, and step 3 - 72°C for 30 seconds, and cycle 4 55°C for 10 seconds with an increased set-point temperature after cycle 2 by 1°C. Results were analyzed using the $2^{-\Delta\Delta CT}$ method described in Applied Biosystems User Bulletin No. 2 (P/N 4303859).

4.0 RESULTS

4.1 Peptide Array Design

In the first generation bovine array (Jalal, *et al.*, 2009), sixty-five percent of the bovine peptides exactly matched the orthologous human sequences. This sequence similarity was not by design. During the development of the human/porcine array, a different approach was utilized. A search was done to specifically identify porcine peptide sequences with exact matches to human sequences, and these peptide targets were the majority of sequences chosen. Out of the 600 human sequences screened, 268 were exact matches to orthologous porcine peptides. The remaining peptides contained at least one amino acid difference (**Table 4.1**). In choosing peptides for the human/porcine array, if there were sequence differences, the human peptide was chosen rather than the porcine sequence. Of the 300 peptides ultimately printed on the array, 206 had 100% homology between human and porcine. The majority of the remaining peptides had a maximum of two amino acid sequence differences. As the majority of the sequences were 100% identical, the array could be used in human and porcine studies.

Human phosphorylation target sites were compared with those of a number of diverse genera. Thousands of human phosphorylation target sites were investigated using the protocol described for peptide array design (Section 3.2.2), but the process was computer automated. This high-throughput method allowed a comparison of phosphorylation target site sequences across several mammalian genera, as well as rice, fruit fly and yeast (**Table 4.2**). Individual peptides showed variable degrees of sequence conservation across genera. The significant number of differences observed between genera highlights the importance of designing genus-specific peptide arrays for evolutionarily divergent genera.

Table 4.1. Porcine/human phosphorylation target site comparison.

Sequence Difference	# of Peptides	Human-Porcine Protein Match
0	268	Same protein
1	165	Same protein
2	39	Same protein
3	29	Same protein
4	6	Same protein
5	7	Same protein
6	4	Same protein
7	5	Same protein
8	2	Same protein
9	4	Same protein
10	6	Same protein
11	2	Same protein
12	1	Same protein
13	0	N/A
14	0	N/A
15	62	Different protein

Six-hundred human peptide sequences were analysed using the Blastp program and the NCBI porcine proteome database. Sequence Difference indicates the number of amino acid differences when comparing the porcine and human kinase target site sequences. # of Peptides indicates the number of peptides out of the 600 human sequences screened. Human-Porcine Protein Match indicates whether the porcine protein was identified as being orthologous to the human protein by protein name and description.

Table 4.2: Phosphorylation target site differences between various genera.

Sequence Difference	% of Proteins vs. Human						
	Cow	*Chicken*	*Mouse*	*Pig*	*Rice*	*Fruit Fly*	Yeast
0	34.82%	12.78%	27.29%	26.82%	0.03%	0.54%	0.07%
1	15.86%	8.56%	15.04%	11.35%	0.03%	0.66%	0.08%
2	9.66%	6.71%	9.58%	7.07%	0.02%	0.86%	0.16%
3	6.43%	5.33%	6.39%	4.50%	0.03%	1.00%	0.16%
4	4.59%	4.62%	4.60%	3.20%	0.04%	1.01%	0.17%
5	3.09%	3.82%	3.10%	2.41%	0.07%	1.15%	0.19%
6	1.63%	2.74%	1.61%	1.11%	0.05%	1.10%	0.18%
7	0.51%	1.33%	0.47%	0.42%	0.02%	0.84%	0.12%
8	0.08%	0.33%	0.05%	0.08%	0.01%	0.42%	0.03%
No similarity	23.34%	53.75%	31.88%	43.03%	99.69%	92.31%	98.83%

The table shows the differences in the phosphorylation target site amino acid sequences of various genera. Comparison was done between human sequences collected from PhosphoSite (www.phosphosite.org) and the proteome of the comparative genera using Blastp. At the time of analysis, there were over 100,000 non-redundant phosphorylation sites in the PhosphoSite database.

4.2 Standard Array Data Analysis and PIIKA Comparison

Often, the data normalization and analysis techniques used for the analysis of peptide array kinome data were lifted directly from the processes used to analyze nucleotide arrays. Our group questioned whether these previously developed methods were adequate since these methods cannot take into account the distinct nature of peptide array data. In conjunction with bioinformatics collaborators, Dr. Anthony Kusalik and Yue Li, a new analysis pipeline was developed. This pipeline, specifically designed for the data collected from peptide arrays, was entitled Platform for Integrated, Intelligent Kinome Analysis (PIIKA) (**Figure 4.1**). Initial results produced with this pipeline appeared to provide superior results: the data displayed enhanced statistical significance, the pipeline was able to handle negative values and it did not distort the raw data. Despite this early evidence, it was decided that a comprehensive comparison between the new analysis pipeline and other established methods based on nucleotide arrays was required to objectively evaluate the value of PIIKA.

The datasets used to conduct the comparison were collected from three different treatment conditions. All experiments were done on bovine monocytes treated with one of three different ligands or untreated control samples. Two sets, CpG-treated and LPS-treated, were done as a single set of array experiments. The third set of IFNγ-treated monocytes contained samples collected from three different animals and was performed as a separate experiment. Thus, CpG and LPS datasets contained 300 peptides printed in triplicate on the array, totaling 900 data points per treatment. The IFNγ-treated experiment had 300 peptides printed in triplicate for three animals, totaling 2,700 data points per treatment.
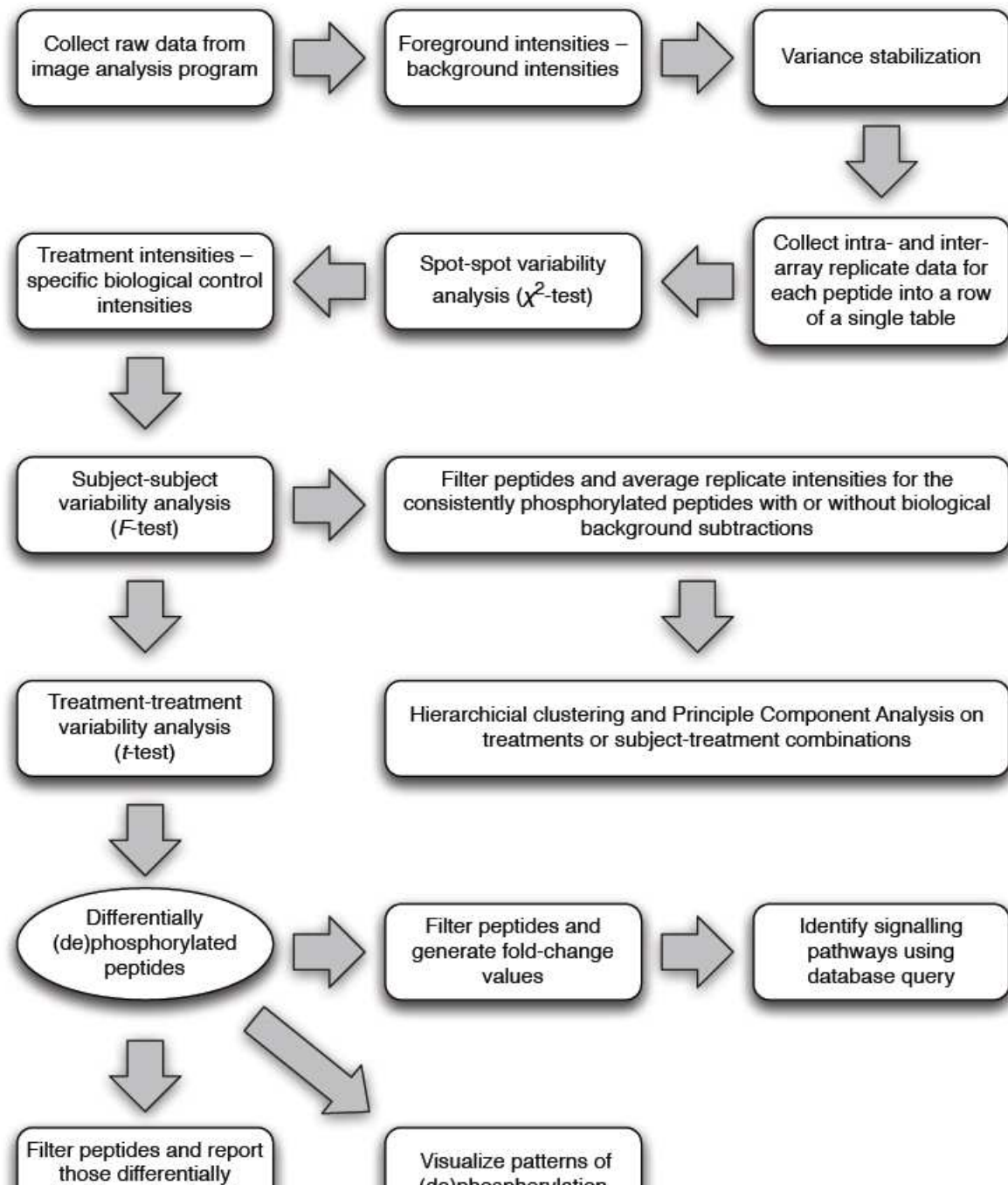
Figure 4.1. PIIKA workflow. Shown is a general workflow of the PIIKA process pipeline. The flow chart starts from the top left and follows the arrows. Rectangles represent procedures, and ovals represent intermediate results.

4.2.1 Data Processing Prior to Analysis

The raw data collected from the scanned array image displayed noticeable signal mean-variance-dependence for each phosphorylated spot (**Figure 4.2**). This dependence was observed as an increase in the standard deviation on these plots. This was an important aspect of the peptide array data that needed to be taken into account. The peptide array data being a measure of target site phosphorylation means that the greater the phosphorylation, the greater the variance. Correspondingly, a lack of phosphorylation or signal will display limited or no variance. The mean-variance-dependence characterisitic of peptide array data is described extensively in Section 1.2.4.3. The goal was to eliminate this mean-variance-dependence by using appropriate normalization techniques (**Figure 4.2**). The relative success of each normalization technique was determined by the slope of the line in the plots. Raw data which have not undergone normalization had the greatest slope. Following Log2 transformation, a jagged line was produced which indicated significant change in the variance of the spots as signal increases. As observed by the upward slope of the line in the top right plot, PNorm did not eliminate the mean-variance-dependence at the highest levels of signal intensity. QNorm caused the opposite effect where the variation was greatest at the lower signal levels, as indicated by the negative slope of the line. The VSN transformations, VSN alone and VSN with log-scaling provided the best results, as indicated by the limited slope of the lines in the VSN plots. PNorm standard deviation increased from approximately 0.25 to 0.75. VSN standard deviation increased from approximately 0.6 to 0.8, and VSN log-scaled standard deviation stayed at approximately 0.09 across peptides.

With any data normalization technique, a key concern was that the final results are not skewed by the manipulation. **Figure 4.3** shows scatter plots displaying the signal intensities of the CpG data compared to their own media control. These plots showed a pattern of response matching the raw data in both PNorm and VSN without log-scaling methods (**Figure 4.3**). This pattern can be observed by the location and distribution of the spots along the line of best fit. Raw Data, PNorm and VSN displayed a similar pattern, while the other plots, Log2, QNorm and VSN (log-scaled), displayed different patterns and did not preserve the biologically relevant phosphorylation data. This lack of data preservation can be seen by the colour-coded negative or positive spot signal following background subtraction. Only PNorm and VSN maintained the distribution of positive and negative spots along the axis seen in the

raw data. This negative and positive spot distribution is very important since any normalization should maintain the relative signal intensity of a given spot compared to another. If negative spot intensities, which indicate no phosphorylation when compared to background, are altered to show significant signal following transformation, this altered data distribution would significantly skew further data analysis. Considering the signal intensity plots, PNorm and VSN appeared to be the best methods to normalize data while not altering data relevance.

Taking into account both the mean-variance-dependence correction (**Figure 4.2**) and the data preservation ability (**Figure 4.3**) of the normalization method, VSN transformation was the best method. VSN and VSN log-scaled were the best methods for correcting mean-variance-dependence, while PNorm and VSN were best at preserving raw data patterns. Thus, VSN transformation, which was among the best at both, was the better overall method.
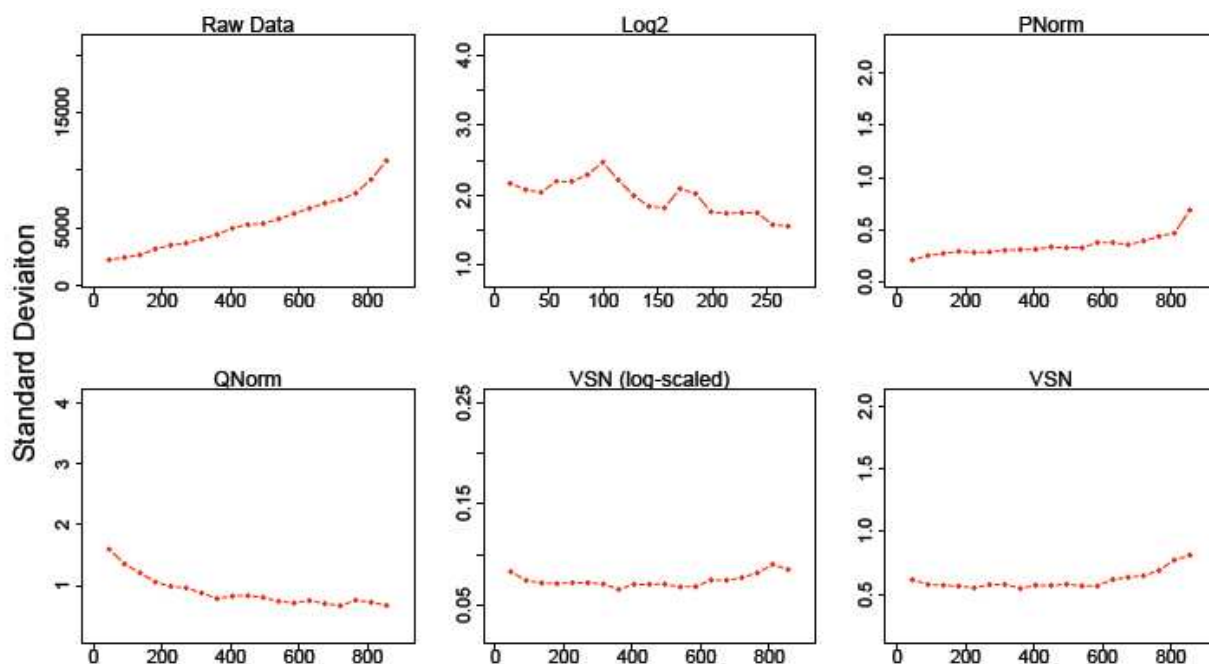
Figure 4.2. Mean-variance-dependence plots. These data plots show before (Raw Data) and after normalization by log2 (Log2), percentile normalization (PNorm), quantile normalization (QNorm), transformation by variance stabilization (VSN) and transformation by VSN with log2 scaling (VSN (log scaled)). Rank of the mean signal intensities was plotted against the standard deviation of the corresponding peptide intensities. If there was no variance-mean-dependence, then the line formed by the dots should display no slope.
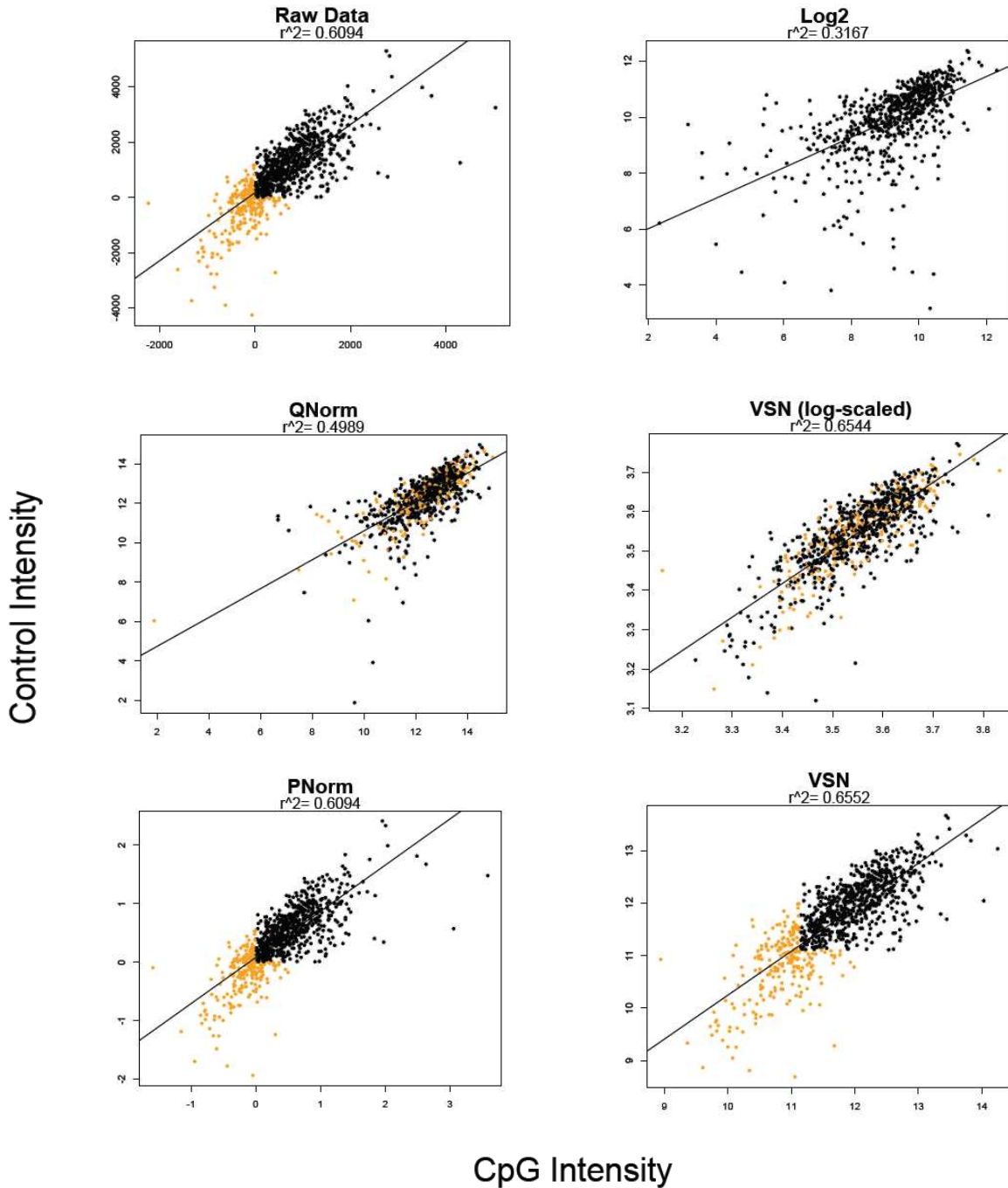
Figure 4.3. Signal intensity scatter plot. Shown are scatter plots of the signal intensities for monocyte responses to CpG against the corresponding intensities in the media control. The raw data were preprocessed in the following ways: no processing (top left panel), logarithm to base 2 of the positive intensities while discarding the negative signal (top right), QNorm (middle left), VSN (log-scaled) (middle right), PNorm (bottom left) VSN (bottom right). The dots in each plot represent signal intensities after background subtraction and taking the average across intra-slide replicates. If the resulting intensity for treatment was negative, an orange dot was used. Otherwise, the average intensity for both conditions was positive, and the dot was coloured black.

4.2.2 Treatment-Treatment Variability Analysis and Phosphorylation Significance

When considering normalized peptide array data, the significantly phosphorylated or dephosphorylated peptides relative to control are important. The greater number of significant peptides, the easier it is to assign pathways and functions to a treatment. **Table 4.3** lists the number of statistically significant peptides under a given treatment condition for all the normalization methods except PNorm. PNorm was not applicable since this method does not provide a means of calculating statistical significance for a given peptide. The peptide significance cut-off was set at 90% confidence. Given the ligands used in the experiments and the design of the array, a large number of peptides were expected to display significant levels of phosphorylation relative to control. However, both QNorm (QNorm + *limma*) and VSN log-transformed (VSN + *limma*) displayed a very limited number of significant peptides for each treatment. By contrast, the VSN + paired *t*-test method (PIIKA) provided a large number of peptides considered significant. For a given experiment, the more data considered, the more powerful the biological analysis. For example, in the case of VSN log-transformed data, only three peptides were indicated as significantly differentially phosphorylated in CpG-treated cells. With three peptides, no functionality could be assigned to the effect of CpG on bovine monocytes. By contrast, VSN + paired *t*-test (PIIKA) identified 85 significant peptides, providing a better overview of phosphorylation events following treatment.

Table 4.3. Normalization method comparison.

Treatments	QNorm + *limma*			VSN + *limma*			VSN + paired *t*-test (PIIKA)		
	↕	↑	↓	↕	↑	↓	↕	↑	↓
CpG	11	8	3	3	3	0	85	44	41
LPS	17	11	6	9	5	4	55	28	27
IFN	16	7	9	8	4	4	133	71	62

Table shows the number of statistically significant peptides (*p*-value $\leq$ 0.1) identified by the various normalization techniques. The results are generated from peptide array data for bovine monocytes treatmented with one of CpG, LPS or IFNγ. ↕ indicates the total number of differentially phosphorylated peptides relative to control. ↑ indicates the number of peptides with increased phosphorylation. ↓ indicates the number of peptides with decreased phosphorylation. The PNorm + fold change method was not included in the above table, since it did not allow for a calculation of significance.

4.2.3. Pathway Analysis of Normalized Data

Previous steps in the analysis generated a list of peptides that were differentially phosphorylated under the various treatment conditions. For each of the normalization methods, fold change and *p*-value information from this list of peptides were input into the online pathway database InnateDB (Lynn, *et al.*, 2008). The output generated from this database was a list of over-represented pathways and associated pathway *p*-values calculated from the input peptide array data. The model pathways for the various treatments, CpG, LPS and IFNγ, were TLR (Hemmi, *et al.*, 2000), IL-2 (Holter, *et al.*, 1987) and JAK-STAT (Darnell, *et al.*, 1994), respectively. **Table 4.4** shows the number of peptides present on the array that fit into each of these pathways (Pep), the number of those that were identified by the various methods and the significance level for the pathway. Results indicated that our custom-designed pipeline increased statistical significance without a considerable loss in sensitivity. When comparing PIIKA to the next best method, the improvement in pathway *p*-value for the TLR pathway was from 0.019 to 0.008 over QNorm, for the IL-2 pathway from 0.405 to 0.002 over VSN and for the JAK-STAT pathway from 0.122 to 0.003 over PNorm. Part of this improvement may be due to the increased number of peptides deemed

significantly differentially phosphorylated by our method versus the others. This, however, is not a complete explanation, as the PNorm method generates comparable numbers of peptides but lower pathway significance levels. As mentioned previously, the PNorm method does not provide individual peptide significance values. Thus, all data that were deemed consistent (i.e., without a SD greater than 1.96) were included. In addition, the fold change magnitudes and direction generated following transformation were improved by PIIKA. PIIKA generated more consistent data when looking for canonical pathways produced by known ligands. This is an important factor when hoping to discover novel biology in future experiments. **Figures 4.4** and **4.5** are pathway networks generated from the same data input into InnateDB using the Cerebral plugin to Cytoscape. These figures are not intended to be detailed depictions of the given pathways or canonical pathway representations; rather, they are intended to be simple visual illustrations of the increase in protein representation in the given pathways. Cytoscape uses a different method of generating pathway networds than InnateDB. The figures provide a contrast between QNorm and PIIKA in their ability to identify representative proteins in a given pathway. QNorm was used as the comparative method for these figures, as it was the best method at producing canonical pathways while allowing for a calculation of individual peptide p-values for input into InnateDB.

Table 4.4. Comparison of pathway results from each data analysis method.

Ligand	Pathway	Pep	PNorm + FC			QNorm + *limma*			VSN + *limma*			VSN + paired t-test (PIIKA)		
			↕	↑	↓	p	↑	↓	p	↑	↓	p	↑	↓	p
CpG	TLR	34	15	12	0.021	4	0	0.019	1	0	1.000	14	4	0.008
LPS	IL-2	25	8	10	0.587	1	2	0.600	1	2	0.405	9	0	0.002
IFN	JAK-STAT	25	18	2	0.122	1	1	0.700	1	0	1.000	12	0	0.003

Based on the differential phosphorylation data, InnateDB indicated the pathways which were consistent with published data. Each pathway was assigned a probability value (p) based on the number of proteins (corresponding to input peptides) present from that pathway. Output included the number of uploaded peptides associated with a particular pathway and the subset of those peptides which were differentially phosphorylated. Pep indicates the total number of peptides on the array relating to the pathway. ↑ and ↓ show the number of identified peptides from the pathway with significantly increased or decreased phosphorylation, respectively, relative to control.

IL-2 identified by QNorm + *limma*   **IL-2 identified by PIIKA (our pipeline)**
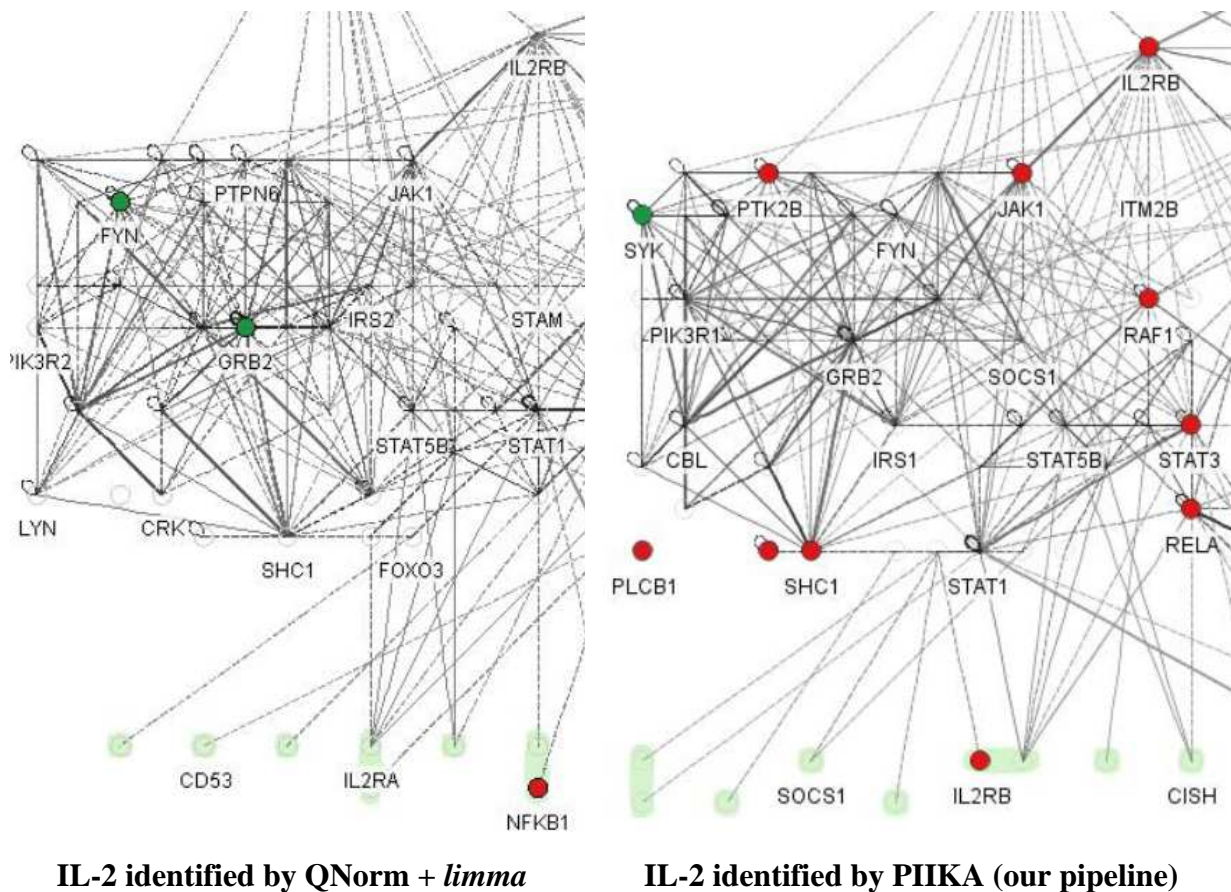
Figure 4.4. IL-2 signalling networks method comparison. Shown are pathway network representations of the identified IL-2 signalling pathway from LPS-treated monocyte data. Proteins were identified as belonging to the IL-2 pathway. The nodes in each network represent proteins corresponding to peptides identified as being significantly differentially phosphorylated. Red colouration of a node indicates an increase in phosphorylation, while green indicates a decrease. The non-coloured nodes were identified as either not significantly phosphorylated or not on the array. The networks were generated through the use of the Cerebral plugin of the interaction viewer Cytoscape. The lines connecting each node are putative interactions according to the Cytoscape database. The network on the left was derived from QNorm + *limma*, while the network on the right was from PIIKA. The green colouration at the bottom of the networks can be ignored for the purposes of this figure.
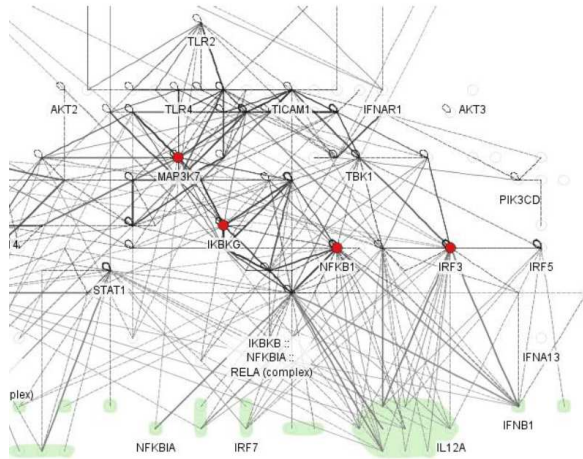
TLR identified by QNorm + *limma*   TLR identified by PIIKA (our pipeline)
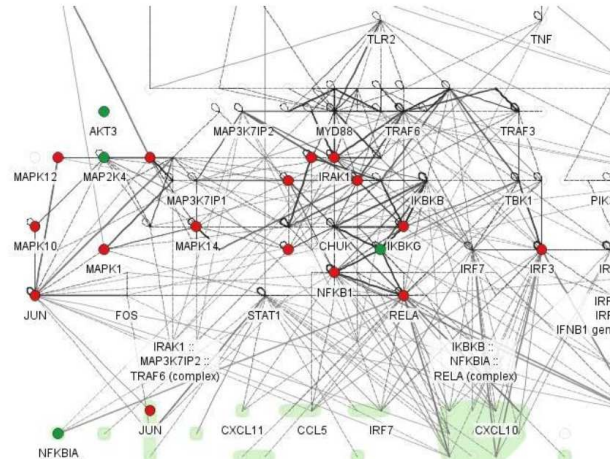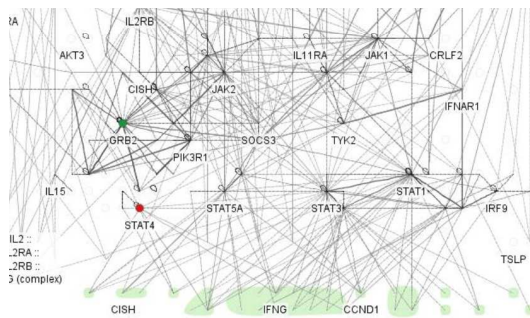
JAK-STAT identified by QNorm + *limma*   JAK-STAT identified by PIIKA (our pipeline)
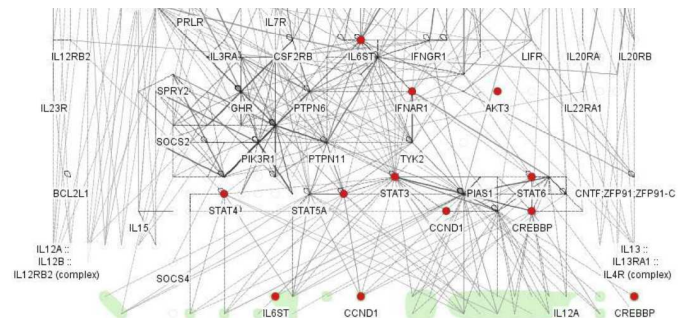
Figure 4.5. CpG and IFNγ signalling networks method comparison. Shown here are network representations of the identified TLR signalling pathway from CpG-treated monocyte data (top) and the JAK-STAT pathway identified from IFNγ-treated monocyte data (bottom). The nodes in each network represent proteins containing peptides that were identified as being significantly differentially phosphorylated. Red colouration of a node indicates an increase in phosphorylation, while green indicates a decrease. The non-coloured nodes were identified as either not significantly phosphorylated or not on the array. The networks were generated through the use of the Cerebral plugin of the interaction viewer Cytoscape. The lines connecting each node are putative interactions according to the Cytoscape database. The networks on the left were derived from QNorm + *limma*, while the networks on the right were from PIIKA. The green colouration at the bottom of the networks can be ignored for the purposes of this figure.

4.3 Prion Signalling Studies

4.3.1 Flow Cytometric Analysis of PrP^C Expression on BE(2)M17 Cells

To confirm that the human neuronal cell line BE(2)M17 was an appropriate cell line for PrP^C stimulation studies, the level of cell surface expression of PrP^C was determined. Flow cytometric analysis using the PrP^C-specific antibody 6H4 confirmed cell surface expression of PrP^C on the majority of the viable cultured cells (**Figure 4.6**). This indicated that these cells were appropriate for studying ligand interactions with PrP^C.
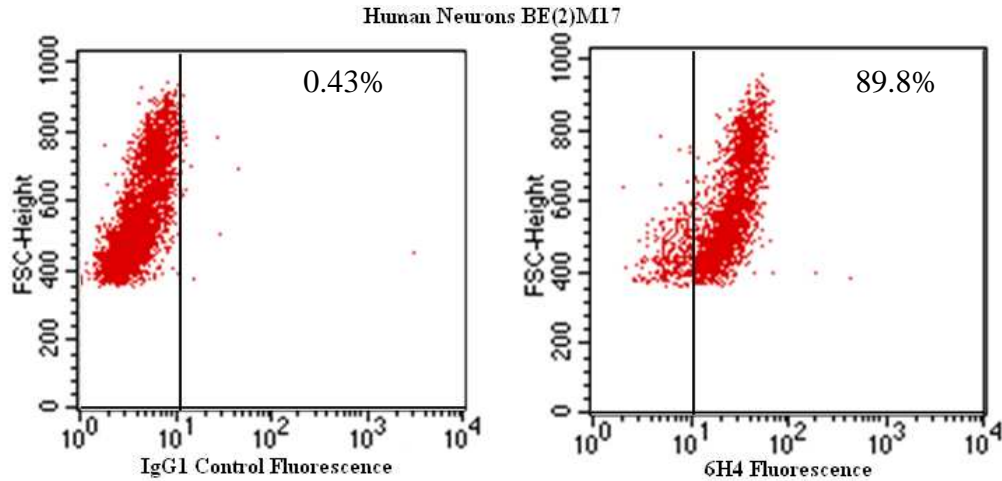
Figure 4.6. PrP surface expression. Shown above are flow cytometic analyses plots of neuronal cells labelled with antibody 6H4. A secondary antibody, GAM-FITC, was used to visualize the cells. The plots to the left shows non-specific GAM-FITC binding following incubation with an irrelevant isotype control IgG antibody. The plot to the right depicts cell fluorescence following incubation with the PrP^C-specific antibody 6H4 and the FITC-conjugated GAM. The % shows the percent of cells which have shifted, indicating fluorescence. Media control cell autofluorescence (no antibody added) resulted in 1.05% of cells indicating fluorescence (data not shown).

4.3.2 Peptide Array Experiment

Human neuronal cells were treated with two PrP-specific stimulants: a prion protein fragment of amino acids 106-126 and the PrP-specific antibody 6H4. The peptide response served as a model of prion disease-like signalling, while the response to antibody cross-linking of PrP^C modeled the endogenous signalling pathways of PrP^C. In addition, three controls were used: a peptide of identical amino acid composition to PrP 106-126 but with a scrambled sequence, an irrelevant isotype control IgG1 monoclonal antibody and a media control.

4.3.3 Cluster Analysis of Kinome Data

Heatmap clustering was done on data from all 300 peptides in each of the various prion stimulants and controls. In **Figure 4.7 A**, the individual stimulants are shown at the bottom of the heatmap. The lines above the heatmap indicate the relative similarity between the totalities of the signals for each of the stimulants. The plot was generated from the data post-normalization without subtracting the individual specificity controls. Without subtracting the control signal from the stimulant signal, clustering was first based on the type of stimulant. The 6H4 and isotype control antibody stimulants clustered together. The PrP 106-126 and scramble peptide control stimulants clustered together. The media control sample is in the centre between the two stimulant types. This clustering was important as it indicated that stimulant-related events were occurring which are not necessarily specific to PrP^C. Phosphorylation events were detected which were common to the addition of exogenous monoclonal antibody to cultured neuronal cells. Similarly, phosphorylation events were detected which occured when a peptide was added to cultured neurons. These observations underscored the importance of taking into account specificity controls before biological significance was assigned to any of the resulting patterns of peptide phosphorylation. In this case, comparing the PrP-specific stimulants to their individual controls eliminated non-specific signalling effects due to the type of stimulant. For example, removing scramble control signal from PrP 106-126 signal revealed the signal unique to PrP 106-126. If media control signal was removed from PrP 106-126 signal, the non-prion related peptide effects would have been observed in addition to the effects of PrP 106-126 interaction with PrP^C. In **Figure 4.7 A**, it can be seen that clustering was performed on the individual peptides, shown

by the lines on the left side of the heatmap which link the peptides. Though performed automatically by the software, this clustering was not considered in the analysis of our data. This individual peptide clustering may be a future consideration in the analysis of peptide array data. In addition, relative peptide signal intensities are shown on a colour scale from low (green) to high (red). This provides a visual indication of the similarities and differences between the stimulants. Colours that match across columns indicated peptides of greater similarity, while colours that do not match when looking across columns indicated peptides which were different.

The clustering results shown in **Figure 4.7 A** were supported by a different means of clustering based on PCA (**Figure 4.7 B**). PCA clustering is explained in detail in Section 1.2.4.4.2 and **Figure 1.5**. The data were broken down into principal components represented by the axes PC1, PC2 and PC3. PC1 incorporated the most variation between data points: 33.16%. PC2 incorporated 25.05% of the variation, and PC3 incorporated 22.35%. Thus, **Figure 4.7 B** displays 80.56% of the variation between the stimulants on the three axes. The PrP 106-126 and scramble control points are close together in the PCA plot. Similarly, the 6H4 and isotype control monoclonal antibody clustered together relative to the media control point. This alternate means of considering the data again indicated there are antibody-specific and peptide-specific effects which led to this close clustering. These effects had to be taken into account by comparing the stimulant signal with the relevant control. Factoring in relevant controls was done for all subsequent analyses.

The pseudo-image of the normalized, merged data from peptide- and antibody-stimulated neuronal cells revealed that distinct phosphorylation events occurred with each stimulus (**Figure 4.8**). The figure shows a graphic representation of an array block. The left side of each spot shows the normalized, specificity-control-corrected signal when peptide stimulated. The right side of each spot shows corresponding antibody signal. Signal is shown as a scale of significantly phosphorylated (red) to significantly dephosphorylated (green) relative to control. The spots can be organized into three groups: both stimulants causing phosphorylation (all red) on the left, both stimulants causing dephosphorylation (all green) in the middle and the largest group showing differential phosphorylation (one side green and one side red) on the right. While there were some peptides that showed conserved patterns of

phosphorylation, indicated by spots which are all red or all green, there was a substantial subset of peptides which shows distinct responses with each stimulant.

The level of differential phosphorylation between the peptide and antibody stimulation became even more apparent when considering both the unique and common peptides for each stimulant (**Figure 4.9**). Sixty-eight peptides were uniquely phosphorylated when cells were stimulated with peptide. Seventy-five peptides were uniquely phosphorylated when cells were stimulated with antibody. Forty-three peptides displayed significant phosphorylation when stimulated with either peptide or antibody. Following further inspection of these shared peptides, only 15 peptides were phosphorylated in the same direction relative to control. By contrast, 28 peptides were phosphorylated in opposite directions. Thus, of the 186 peptides that displayed differential phosphorylation relative to controls, only 15 were common and phosphorylated in the same direction. This is a noteworthy result, considering that the two stimulants targeted the same extracellular protein and the controls used should have eliminated as much signal noise as possible. This differential phosphorylation between stimulants indicated possibly significant variation in the signalling abilities of PrP^C.
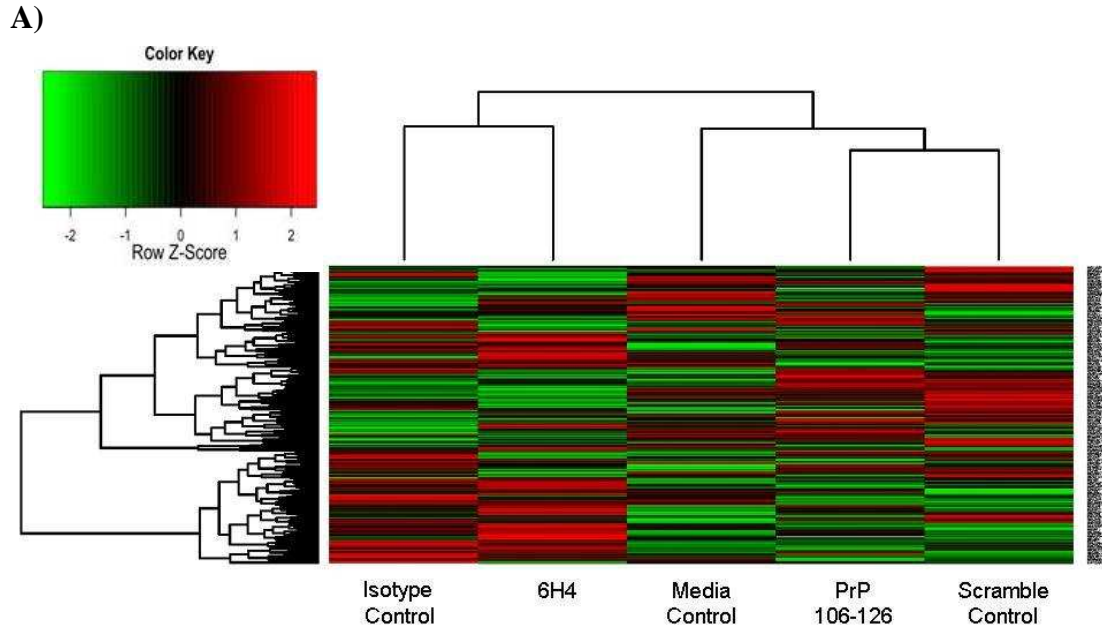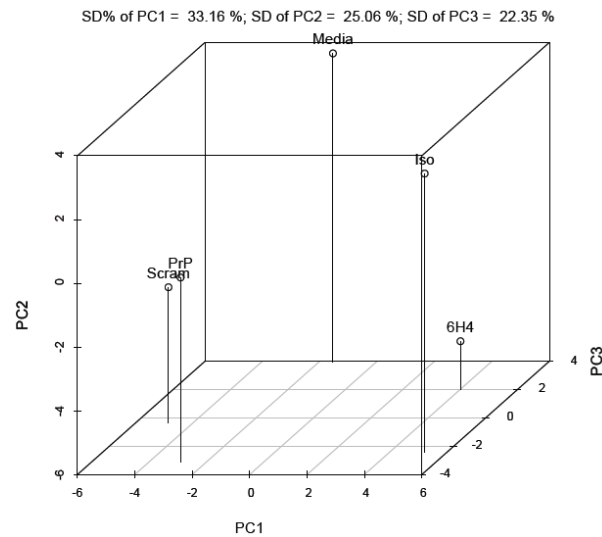
Figure 4.7. Phosphorylation heatmap and clustering. A) The background-corrected raw data collected from the peptide arrays were VSN-transformed, and a heatmap/clustering of the data was produced using the Complete Linkage + Euclidian Distance method. The lines at the top of the heatmap indicate the relative similarity between the stimulants indicated at the bottom of the heatmap. The shorter the lines, the more similar the two connected stimulants. The lines on the left side of the heatmap indicate the relative similarity in signal between the 300 individual peptides on the array. The coloured lines indicate the relative degree of phosphorylation of each peptide from strongly phosphorylated (red) to non-phosphorylated (green) as indicated by a Z-score. **B)** Shown here is the 3D Principal Component Analysis of the five treatments. Relative distance on the three axes indicates level of similarity or difference among the treatments. PrP refers to PrP 106-126 peptide. Scram refers to scramble control peptide. 6H4 refers to the PrP-specific antibody. Iso refers to the IgG1 isotype control antibody. Media refers to media control.
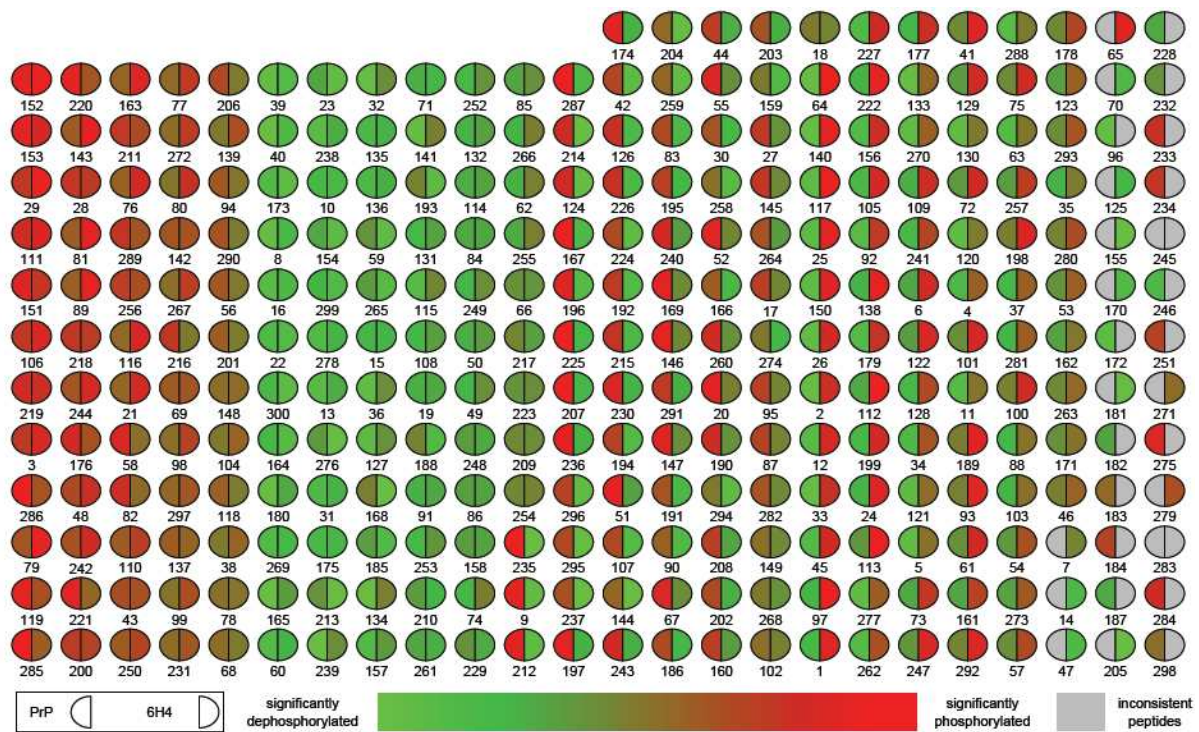
Figure 4.8. Peptide array pseudo-image. Shown is a pseudo-image of a peptide array block combining the prion stimulation data. Transformed data for PrP 106-126 was compared to scramble control peptide data, and a significance value was determined based on a significant increase or decrease in phosphorylation between the two. This process was also performed for 6H4 antibody stimulated and isotype control antibody. The relative intensity of each spot indicates the level of significance of the phosphorylation of that spot. The left side of each spot is the response to PrP 106-126 stimulation. The right side of each spot indicates 6H4 stimulation response. Grey spots represent inconsistent peptides between array peptide replicates as determine by X^2 test (Section 3.12.1.2).
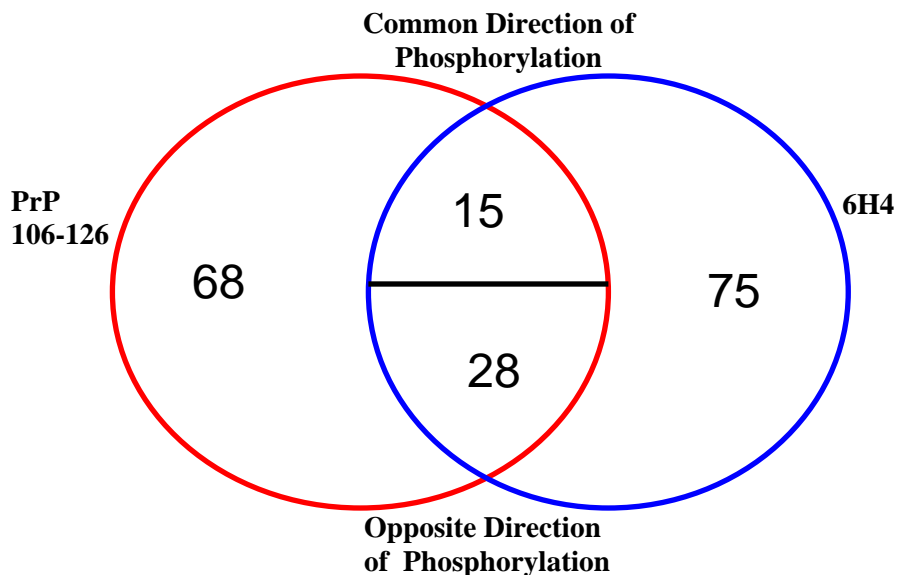
Figure 4.9. Comparison of peptide phosphorylation following PrP 106-126 and 6H4 stimulation. Peptides displaying differential phosphorylation following the two stimulations were compared. The majority of the significantly differentially phosphorylated peptides were unique to one stimulant or the other. A minority of the peptides were common to both PrP 106-126 and 6H4. Common Direction of Phosphorylation refers to peptides displaying either increased or decreased phosphorylation following both stimulations. Opposite Direction of Phosphorylation refers to one stimulation resulting in an increased phosphorylation, while the other stimulation results in a decrease.

4.3.4 Pathway Analysis

The processed kinome data were subject to pathway over-representation analysis using the InnateDB database. To ensure the identified pathways represented conserved and consistent biological responses, input data were limited to peptides with a consistent pattern of phosphorylation across the technical replicates and significant changes in phosphorylation levels relative to the relevant control treatment ($p < 0.20$). Significant pathways ($p < 0.05$) for each stimulation condition are shown (**Table 4.5**).

Table 4.5. InnateDB-generated pathway list.

	Pathway	Up/ Down	PrP 106-126		6H4	
			p-value	#	*p*-value	#
Growth Factor Signalling	VEGF signalling pathway	Up	**0.01**	22	0.83	14
	Class I PI3K signalling events	Up	**0.02**	5	0.77	3
	TGFBR	Down	**0.02**	10	0.97	3
	Phosphoinositides and their downstream targets	Up	**0.02**	5	0.99	1
	Regulation of nuclear SMAD2/3 signalling	Down	**0.04**	6	0.94	1
	EGF receptor (ErbB1) signalling pathway	Down	0.79	2	**0.05**	5
	Signalling by EGFR	Down	0.66	2	**0.05**	5
	Signalling by PDGF	Down	1	0	**0.05**	5
Integrin Signalling	Integrin alphaIIbbeta3 signalling	Up	**0.04**	4	0.68	2
	Integrin cell surface interactions	Up	**0.04**	4	0.68	2
Cytokine Signalling	IL-7 signalling pathway(JAK1 JAK3 STAT5)	Up	**0.04**	20	0.69	15
	IL12-mediated signalling events	Down	**0.02**	9	0.60	5
	IL12 and STAT4 dependent signalling pathway in Th1 development	Down	**0.02**	5	0.90	1
	IL23-mediated signalling events	Down	**0.04**	6	0.47	4
	JAK-STAT signalling pathway	Down	**0.03**	8	0.78	4
	Chemokine signalling pathway	Up	0.95	6	**0.01**	19
MAPK Signalling	Erk1/Erk2 mapk signalling pathway	Down	0.93	1	**0.01**	5
	Role of Erk5 in neuronal survival pathway	Down	1	0	**0.02**	6
	Signalling by insulin receptor	Down	1	0	**0.03**	4
	Signalling to RAS	Down	0.73	1	**0.03**	4
	Sprouty regulation of tyrosine kinase signals	Down	1	0	**0.03**	4
	Insulin receptor signalling cascade	Down	1	0	**0.03**	4
	IRS-mediated signalling	Down	1	0	**0.03**	4
	IRS-related events	Down	1	0	**0.03**	4
Cell Cycle	Cell cycle	Down	**0.04**	6	0.36	9
NFkB Signalling	NFkB signalling	Up	0.98	1	**0.03**	7
	IKK-NFkB cascade	Up	0.91	2	**0.05**	6
Other	Signalling pathway from G-protein families	Down	0.76	2	**0.03**	4
	Regulation of splicing through Sam68	Down	0.46	1	**0.03**	4
	Roles arrestin dependent recruitment of Src	Down	0.46	1	**0.03**	4
	Alpha-synuclein signaling	Down	0.93	1	**0.03**	4
	Axon guidance	Down	0.66	2	**0.03**	8
	TrkA signalling from the plasma membrane	Down	0.93	2	**0.04**	10
	NOTCH	Down	**0.002**	8	0.64	3
	Glucocorticoid receptor regulatory network	Down	**0.01**	8	0.78	4
	Akt (PKB) Bad signaling	Up	**0.04**	20	0.77	14
	EPHA forward signaling	Up	**0.04**	4	0.97	1
	Platelet aggregation (Plug Formation)	Up	**0.04**	4	0.68	2

Transformed phosphorylation data obtained from the peptide arrays were uploaded into InnateDB. This table lists all pathways indicated for both treatments with a *p*-value of ≤0.05. Up/Down describes whether InnateDB indicated an up regulation or down regulation of the pathway. *p*-value describes *p*-value of the pathway calculated by InnateDB. # indicates the number of significant peptides on the array which are in a given pathway.

4.3.4.1 PrP 106-126 Stimulation

In PrP 106-126 treated cells, VEGF, PI3K and additional growth factor related signalling pathways were identified by pathway over-representation analysis. The pathways shown in **Table 4.5** can be linked together in putative pathways collected from the peptide array data (**Figure 4.10**). VEGF has been linked to neuroplasticity and a variety of neurodegenerative diseases (Storkebaum, 2004), making it an interesting receptor to consider in the context of prion function. Cell viability assays carried out in the presence of the prion-specific stimulants, with and without recombinant VEGF, provided supporting evidence for this pathway's involvement in prion function (Section 4.3.6). While it is possible the VEGF receptor (VEGFR) is an interacting partner with PrP^C, it is also possible that PrP^C interacts with growth factor receptors more generally, considering that transforming growth factor beta receptor (TGFBR) was also implicated by the data (**Table 4.5**). It would also be possible to consider other specific receptors which showed significant phosphorylation, including fibroblast growth factor receptor (FGFR) (*p* 0.06), nerve growth factor receptor (NGFR) (*p* 0.13) and PDGFRB (*p* 0.06) (**Table A1**). The downstream-signalling of these growth-factor receptors was similar and may implicate any of them as potential candidates in prion function.

Cell survival and apoptosis have been strongly implicated as potential functions of PrP^C (Roucou and LeBlanc, 2005). There have been numerous studies that have attempted to describe the mechanism by which the prion protein induces an apoptotic response in cells (O'Donovan, *et al.*, 2001; Paitel, *et al.*, 2003). However, many of the studies that purport to explain apoptosis signalling in prion-stimulated cells have provided contradictory results (Roucou and LeBlanc, 2005). The peptide array data in this study indicated that cell death via apoptosis is carried out through signalling involving Caspase-3 (**Figure 4.10** and **Table A1**). Caspase-3 activation could occur due to the following phosphorylation events: Akt (Asselin, *et al.*, 2001) or calcium related signalling and nuclear factor of activated T-cells (NFAT).

As mentioned, calcium-related signalling appears to be a key aspect of PrP^C function. Calcium signalling and the prion protein have been linked for over a decade (Kristensson, *et al.*, 1993). The peptide array data indicated that the mechanism which initiated calcium release was phospholipase C gamma (PLCγ) activity. Analysis of peptide-stimulated cells revealed PLCγ1 phosphorylation at residue Y771 with a *p*-value of 0.02 and a fold change of 1.86. By contrast, antibody stimulation by 6H4 was associated with phosphorylation at

residue Y771 with a *p*-value of 0.16 and a fold change of -1.58 (**Table A1**). Downstream effects may subsequently affect calcineurin and NFAT (**Figure 4.10**) (Chow, *et al.*, 1997). Calcium release upon cell stimulation with PrP 106-126 was confirmed with a calcium release assay (Section 4.3.7).

The signalling induced by the PrP 106-126 peptide, taken together with the fact that it has been used extensively as a model of prion disease, provides possible insights into prion disease state signalling. The key pathways uncovered by pathway over-representation analysis of peptide array data were growth factor related signalling, calcium signalling and PI3K signalling. These pathways are all directly linked to cell death/survival functionality. Alteration of these signalling pathways can lead to cells undergoing apoptosis, and the possible subversion of these pathways when PrP^C is altered to become PrP^{Sc} could ultimately result in loss of neurons.

Pathway over-representation analysis strongly implicated integrin-related signaling. There is no literature to support a direct interaction between prion and integrin; however, there has long been a link between laminin and the prion protein (Graner, *et al.*, 2000), specifically the 37 kDa laminin (Rieger, *et al.*, 1997). Since integrin receptors are receptors for laminin, these results may provide supporting evidence for these previously reported results.

4.3.4.2 Antibody Stimulation

Following PrP^C cross-linking with antibody, a group of pathways was identified that can broadly be represented as MAPK-related signalling. MAPK signalling is central to many key cellular functions including cell proliferation, cell cycle, differentiation, immunity and apoptosis (Chang and Karin, 2001). Therefore, it could have been expected that MAPK-related signalling played a role in PrP^C biology, though interestingly it appears not in peptide-induced signalling.

Previous prion studies have linked MAPK involvement with apoptosis (Thellung, *et al.*, 2002) and iNOS (Fabrizi, *et al.*, 2001), both of which displayed significant differential phosphorylation on the peptide arrays. Interestingly, neuronal cells stimulated with PrP 106-126 also showed iNOS phosphorylation (at targets Y151, S909 and S739) at the highest statistical significance levels of any of peptides in this study (*p*-values of 1.6×10^{-3}, 1.6×10^{-3}

and $3.1x10^{-4}$, respectively). However, while both antibody and peptide induced iNOS differential phosphorylation, it was in opposite directions. Peptide significantly increased iNOS phosphorylation at all three sites; conversely, antibody cross-linking induced significantly decreased phosphorylation at S909 (**Table A1**).

If we consider growth factor receptors as possible interacting partners with peptide-stimulated PrP^C, then insulin receptor was a contender in antibody-stimulated PrP^C (**Table 4.5**). Altered insulin receptor function in neuronal cells has been linked to prion function in previous studies (Ostlund, *et al.*, 2001). Considerable work has recently focused on the insulin receptor of pancreatic β-cells as a possible link between blood sugar regulation and prions (Strom, *et al.*, 2007). Thus, the high significance assigned to insulin receptor signalling in neuronal cells may be a noteworthy result.

4.3.5 Phosphospecific Antibody Array
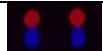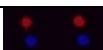
A commercial phosphospecific antibody array was used to validate the kinome results. While the peptide array contained target sites which were phosphorylated by active kinases, the antibody array contained phosphorylation-specific antibodies bound to the array. If a protein had been phosphorylated, and the array contained an antibody complementary to that phosphorylated site, the protein would be captured by the antibody and bound to the array. Before exposure to the array, the proteins within the cells were labelled with one of two colours: blue dye for control samples and red dye for treatment samples. This way, control and treatment could be visualized on a single array. This type of data provided information on the phosphoproteome of the cell; in effect, it was like doing nearly 1,000 individual western blots. These data were distinct from the peptide array data in that it provided information on the phosphorylated proteins, rather than the active kinases, within a sample. The antibody array technique was limited in a number of ways. The key limitation was the availability of phosphospecific antibodies such that only a small portion of the antibodies on the array were exact matches for target sites on the peptide array. Antibody array analysis was done on the neuronal cells stimulated with PrP 106-126, again using scramble peptide as a control. The cells were treated in an identical fashion to those used for peptide array analysis. In much the same way as with the peptide arrays, the PrP 106-126 signal was compared to the scramble signal for each antibody spot on the array. This provided a fold change value and a direction

of phosphorylation, increased or decreased relative to control. The signal confidence was indicated for the reported data in a yes/no format. All data presented were shown to have positive confidence; that is, the fold change presented was considered statistically significant. **Table 4.6**, which contains only the phosphorylation sites that were identical between peptide array and antibody array, indicates strong agreement between the two techniques, both in magnitude and direction of phosphorylation relative to control. This provided added confidence in the accuracy of the peptide array results.
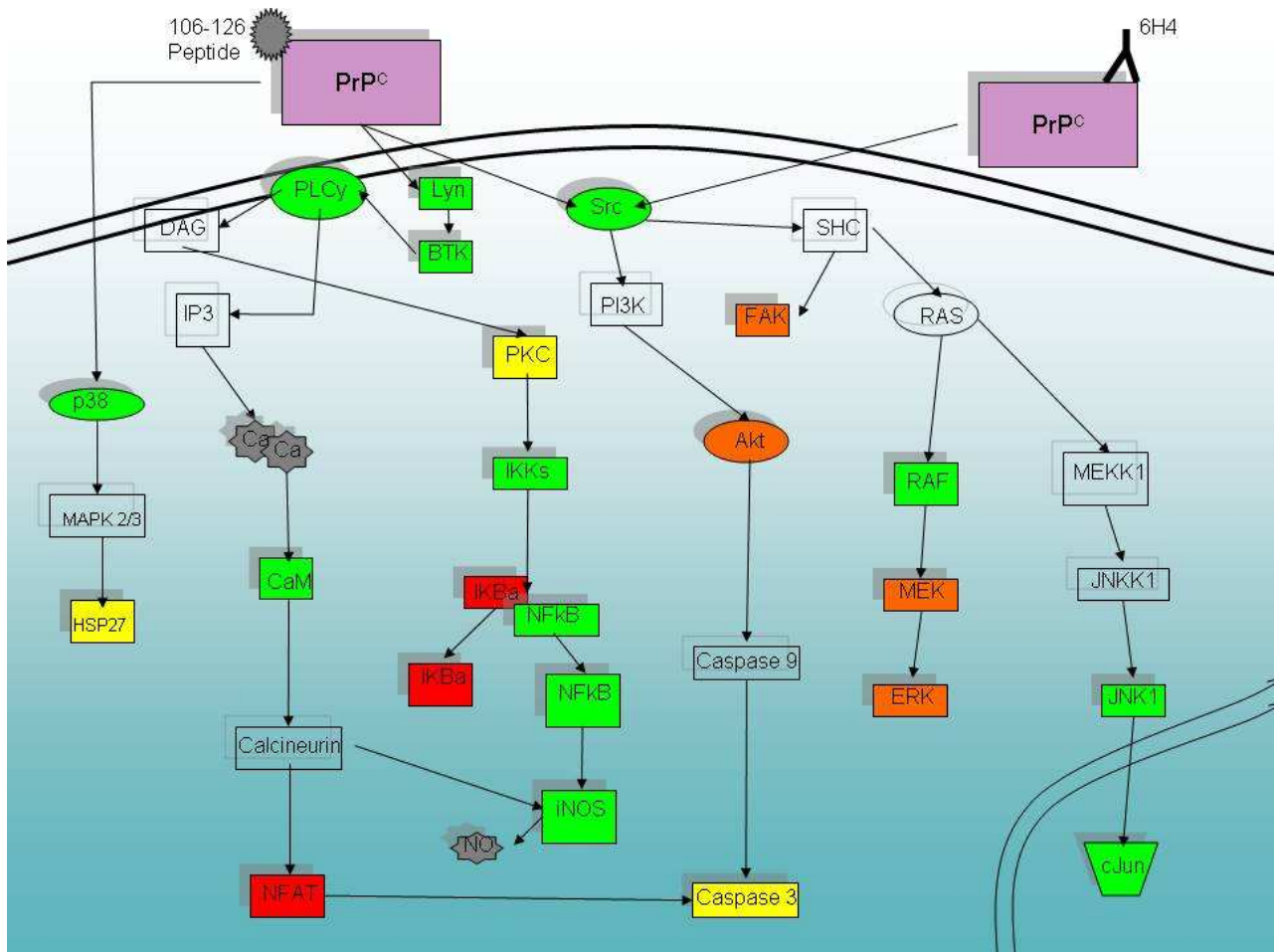
Figure 4.10. Signalling pathways linked to PrP^C stimulation. Shown is a selection of proteins implicated by peptide array data that were organized into interconnected pathways. Yellow indicates unique PrP 106-126-related phosphorylation. Orange indicates unique 6H4-related phosphorylation. Red indicates that both stimulants affect the peptide in the same direction of phosphorylation. Green indicates that both stimulants affect the peptide in opposite directions. Clear indicates insignificant signal or that the peptide is not present on the array.

Table 4.6. Phosphorylation of select signalling molecules indicated by peptide array and phosphospecific antibody array.

Name	Target Amino Acid	Fold Change Peptide Array	*p*-value	Fold Change Antibody Array	Antibody Array Spot
CaMK2-alpha	T286	-1.41	0.07	-1.27	
FAK	Y397	1.03	0.47	1.15	
Fos	T232	-1.10	0.38	-1.06	
HSP27	S78/82/3	-1.76	0.07	-1.87	
Jak2	Y1007/8	-1.08	0.42	-1.12	
Jun	S73	-1.62	0.02	-1.86	
NFkB-p65	S276	1.32	0.21	1.19	
p38-alpha	T180/2	-1.21	0.28	-2.12	
pRb	S780	1.23	0.22	1.28	
STAT3	Y705	-1.44	0.10	-1.52	
STAT3	S727	1.35	0.32	2.03	

Identical phosphorylation target sites on both the peptide array and the antibody array are listed. Fold change was calculated as a ratio of PrP 106-126 treated signal to scramble control signal. The fold change and *p*-value calculated from the peptide array data are indicated. Fold change *p*-value for the antibody array data was not assigned because the significance was reported as a binary yes/no. All listed fold changes for the antibody array data were indicated to be significant. Antibody Array Spot shows the treated (red) and control (blue) spots on the array.

4.3.6 Cell Viability Assay, Prion Stimulants and VEGF Treatment

Pathway analysis of the kinome data implicated the VEGF signalling pathway as being involved in peptide-induced PrP^C signalling. In addition, previous studies have indicated that VEGFR is an important receptor in neurodegeneration and neuronal cell viability (Storkebaum, 2004). The combination of the kinome data and the previous VEGF studies led to the consideration of VEGF's affect on cell viability when also stimulated with prion-specific ligands. Neuronal cells were stimulated with peptide, antibody or the respective controls and then exposed to recombinant VEGF. The apoptosis inducer camptothecin was used as a positive control for cell death. Cell viability results (**Figure 4.11**) indicated that the VEGF plus PrP 106-126-stimulated cells had increased viability compared to PrP 106-126-stimulated cells. Treating 6H4-stimulated cells with VEGF had no significant impact on cell viability. These data agreed with the kinome analysis in that VEGF signalling was implicated in the context of peptide stimulation but not antibody stimulation. This differential response confirmed the distinct phenotypes which emerged following the PrP-specific stimulations. The peptide- and antibody- stimulated neuronal cells showed a significant difference in cell viability, with the antibody displaying limited observable effect on viability. There was a significant drop in cell viability in the peptide-treated cells. These viability results were consistent with peptide-induced effects that model disease and antibody-induced effects that model endogenous signalling. A key characteristic of TSEs is neuronal death (O'Donovan, *et al.*, 2001; Paitel, *et al.*, 2003). Comparing peptide-stimulated cells, with or without VEGF, showed a significant difference in viability. This result confirmed the involvement of VEGFR in peptide induced cell death. Taken together, these results were in agreement with the conclusion that PrP^C is capable of distinct effects, depending on the stimulation given. **Figure 4.11** shows the stimulant/treatment viability compared to respective control.
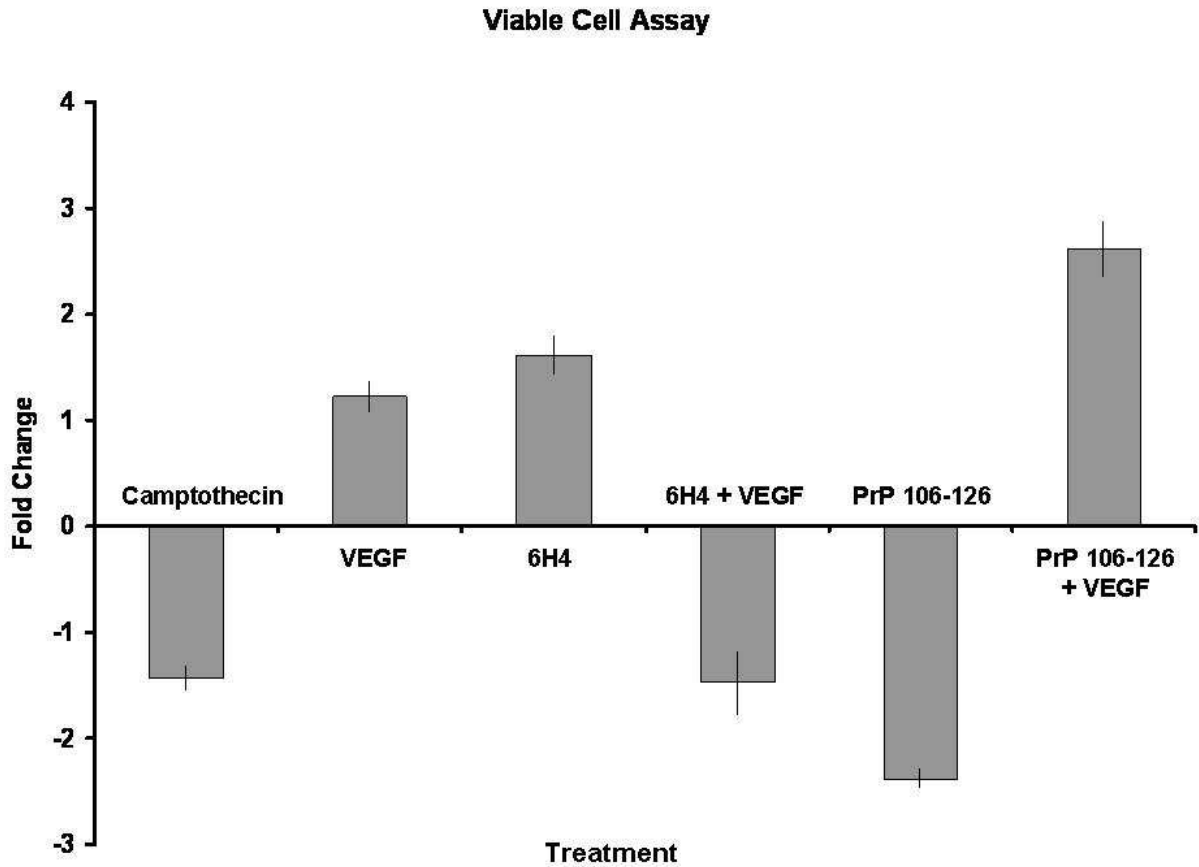
Figure 4.11. Cell viability. Stimulated human neuronal cells were assayed for viability using trypan blue dye exclusion and a hemocytometer. Camptothecin refers to the inducer of apoptosis. PrP 106-126 refers to the prion peptide fragment. 6H4 refers to the 6H4 antibody. PrP 106-126 + VEGF refers to PrP 106-126 peptide plus the addition of recombinant VEGF. 6H4 + VEGF refers to 6H4 antibody plus recombinant VEGF. To calculate fold change each stimulated sample was compared to its respective control sample to keep analyses as similar to peptide array analyses as possible. Camptothecin and VEGF counts were compared to unstimulated control counts. 6H4 counts were compared to IgG1 isotype control counts. 6H4 + VEGF counts were compared to 6H4-stimulated counts. PrP 106-126 counts were compared to scramble peptide control counts. PrP 106-126 + VEGF counts were compared to PrP 106-126-stimulated counts. Assays were performed in triplicate with fold change and standard error presented.

4.3.7 Calcium Release

Numerous studies indicate that calcium-related signalling is involved in prion function (Kristensson, *et al.*, 1993; Whatley, *et al.*, 1995; Ferreiro, *et al.*, 2008). The importance of calcium had also been supported by the peptide arrays in that several calcium-related signalling molecules, including calmodulin (CaM), NFAT2 and PLCγ, showed significantly altered phosphorylation in PrP 106-126-stimulated cells relative to control. **Figure 4.10** shows where calcium signalling fits into the pathways as indicated by the peptide array data. Calcium release induced by PLCγ leads to down stream effects on CaM and NFAT. A calcium release assay was conducted following the PrP stimulations. Results indicated a significant induction of calcium release when cells were stimulated with PrP 106-126 peptide but not antibody (**Figure 4.12**). In fact, there was a significant increase in calcium release relative to both media control and peptide control in PrP 106-126-stimulated cells, while there was no statistically significant effect in antibody-stimulated cells. These results confirmed that distinct cellular responses were elicited depending on which PrP^C ligand was used. This result supported the conclusion that PrP^C is capable of engaging in multiple distinct responses.
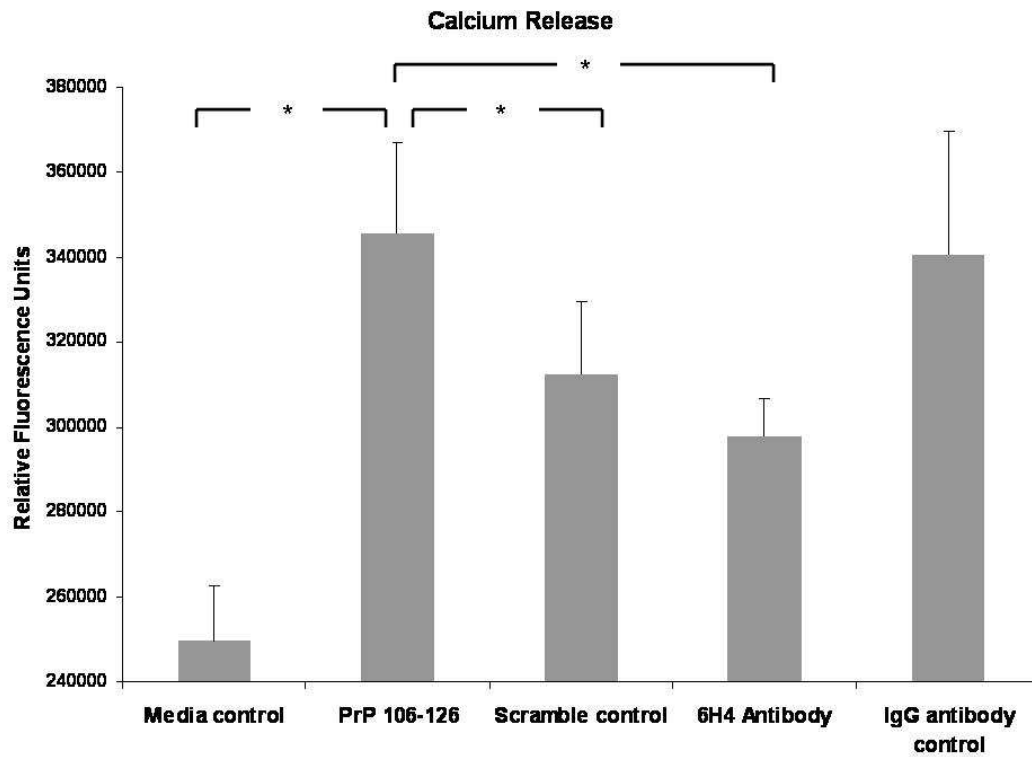
Figure 4.12. Intracellular calcium release. Stimulated human neuronal cells were assayed for release of intracellular calcium as measured by fluorescence. The assay was performed in triplicate. The means of the replicates are presented along with standard error of the means. Analysis of variance indicated a *p*-value of 0.032 between groups. The greater the fluorescence signal, the more calcium released. Pairs which showed a statistically significant difference in signal of at least $p \leq 0.05$ are indicated.

4.4 MAP Signalling Studies

4.4.1 MAP Infection of Bovine Monocytes

Following *in vitro* MAP infection of purified bovine monocytes, bacteria cytospins and acid fast staining were conducted to confirm infection (**Figure 4.13**). Over three repeated infections using a multiplicity of infection of 10:1, an infection efficiency of 93 +/- 4% was obtained. This level of infection and the consistency among experiments was well within the range required for performing kinome analysis. To optimize sensitivity in detecting changes in kinomic signal, a homogenous target cell population and a consistent level of infection or treatment was desirable. This way, potential kinase activity was avoided from uninfected/untreated cells or from cell types not of interest.

Uninfected **MAP Infected**
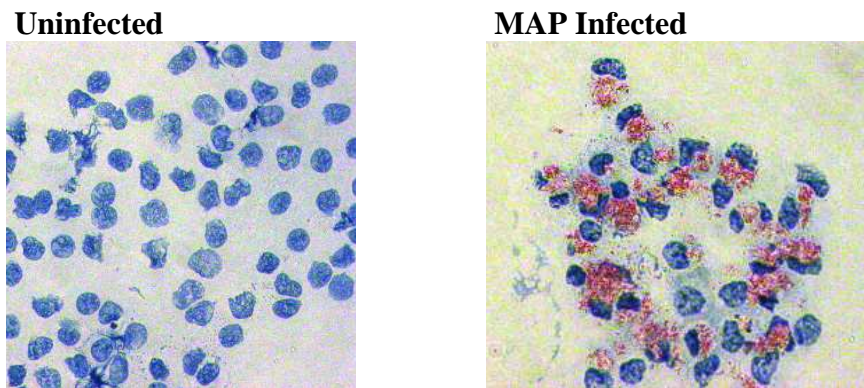
Figure 4.13. Acid-fast staining of bovine monocytes. Figures show monocytes both infected and uninfected following the acid-fast staining technique. Blue indicates bovine monocytes and red indicates MAP. Cells were observed under a light microscope using oil immersion (100X). An estimate of infection efficiency was obtained based on the co-localization of MAP and cells.

4.4.2 Peptide Array Experiment

To minimize the possibility of technical variation among peptide arrays, the raw data were collected, and were subsequently normalized and analyzed as a single experiment. The experiment consisted of monocytes isolated from the blood of three cattle. Uninfected or MAP-infected monocyte samples were treated with IFNγ and subjected to kinome analysis.

4.4.2.1 Animal-Animal Variability

With outbred populations such as cattle, variability in biological responses to infection was anticipated. To ensure that the core conserved biological responses across animals were being obtained and to determine the animal-dependent and animal-independent phosphorylation events, an animal-to-animal variability analysis was conducted. Under the same treatment condition, peptides with p-values of less than 0.01 were considered animal-dependent. Recall that this was a test of animal-animal variation and not phosphorylation significance. In other words, when studying the response of two identically treated animals, if a given peptide showed a 99% or greater likelihood of being different, it was discarded. By this criterion, only eight peptides appeared to have a response dependent on animal, rather than treatment, across all samples. Two-hundred peptides elicited responses that were similar across animals within a specific treatment. Ninety-two peptides were inconclusive: under some treatment conditions they appeared animal-dependent, while under other treatment conditions, the various animals displayed a similar response.

Within the three treatment/infection conditions, relative to control, the results showed that significant animal-dependent responses were observed in 52 peptides following IFNγ treatment, 43 peptides following MAP infection, and 37 peptides following MAP infection and IFNγ treatment. Interestingly, this indicated that there was more variation in the animals' responses to IFNγ stimulation than to MAP infection. This may be due to the proportion of phosphorylation events represented on the peptide array being affected by treatment with IFNγ as compared to MAP infection. An infection with MAP will likely induce more changes in a wider variety of kinases than treatment with IFNγ, which acts on a smaller, specific subset of pathways. Thus, the remaining kinases that were peripherally affected by treatment with IFNγ or infection with MAP will be active at a more variable level, possibly due to the natural biological background activity of the animal. For example, IFNγ treatment of cells will induce specific phosphorylation events related to the IFNγ receptor. These phosphorylation events induced by IFNγ will represent a limited subset of the peptides found on the array. Other phosphorylation events, represented by peptides on the array, that are part of pathways connected to the IFNγ response may be affected in a more animal-dependent manner. MAP infection will induce immune responses and general stress reponses which represent a larger subset of the peptides on the array. There are then fewer peptides on the

array that are peripheral to these pathways that may be affected in a more animal dependent way. It would be expected that MAP-infected-IFNγ-treated samples would affect the largest proportion of peptides on the array due to the numerous phosphorylation events involved. The more phosphorylation events specifically affected by the treatment/infection, the less peripheral phosphorylation events which may respond in an animal-dependent manner.

4.4.2.2 Cluster Analysis

The kinome datasets from each treatment were subjected to cluster analysis to visualize the difference between animals and treatment conditions. PCA was conducted before and after subtraction of the control untreated animal-matched datasets. PCA clustering is explained in detail in Section 1.2.4.4.2 and in **Figure 1.5**. The data were broken into principal components, as represented by the axes. This enabled comparison of the general kinome profiles under the various treatment conditions.

PCA clustering without biological control subtraction showed random arrangement of animals and treatments (**Figure 4.14 A**). This random arrangement was expected for the complete kinome profile with outbred animals. It was expected because small variations in the kinase activity of individual animals, multiplied by the 300 peptides on the array, result in substantial variation in total response. Numerous factors can affect the baseline cellular kinase activity including genetic, developmental and environmental factors. These factors can also affect the dynamic kinase response to stimuli, especially a response as complex as an intracellular bacterial infection.

Following the subtraction of the animal-matched control data, the kinome changes that were induced by the treatment/infection were more apparent in the PCA plot. These data represent the dynamic response of the monocytes from each animal to given treatment conditions: IFNγ-, MAP-, or MAP and IFNγ-treated (**Figure 4.14 B**). Clustering based predominantly on animal-to-animal variation was still apparent. The animals separated into different areas of the plot: animal 89 to the top middle, animal 136 to the bottom left and animal 148 to the bottom right. While this animal-based clustering seems contradictory given that the animal-to-animal analysis indicated 200 of the 300 peptides were animal-independent, this combined dataset is still relatively large. Subtle variations in the phosphorylation levels of

individual peptides across animals following subtraction still combined to result in the individual animal clustering distinctly.

The clustering by animal was confirmed by hierarchical clustering (**Figure 4.15**). This clustering highlights the similarities between animals and treatments by how closely they group together. The lines above the heatmap indicate the relative similarity between the biological control subtracted treatments. By observing how close together the groups are, a hierarchy of difference is presented. In **Figure 4.15**, it can be seen that clustering was performed on the individual peptides, as shown by the lines on the left side of the heat map linking the peptides. The clustering of the peptides was performed automatically by the software, and was not considered in the analysis of our data. This may be a future consideration in the analysis of peptide array data. In addition, relative peptide signal intensities are shown on a colour scale from low (green) to high (red). This provides a visual indication of the similarities and differences between the stimulants. Colours that match across the columns indicate peptides of greater similarity, while colours that do not match when looking across the columns indicate peptide differences.

While animal-based clustering was clearly observed, there was also clustering corresponding to individual treatment conditions, as observed in **Figure 4.14 B**. The monocytes treated with IFNγ cluster near the centre of the plot as a separate group. A box was drawn around these points to illustrate the relative proximity of the IFNγ-treated monocytes following biological control subtraction. This indicated that, despite the cumulative baseline differences among animals, there was a conserved and consistent response to IFNγ across the biological replicates. Similarly, in the hierarchical clustering, there was a pattern to the treatments within the animal clusters (**Figure 4.15**). In two of the three animals, MAP-infected monocytes and MAP-infected monocytes treated with IFNγ cluster together. The close clustering within animals indicated that there were limited differences in response to these two treatments. MAP had inhibited the IFNγ response from taking place in the infected cells.
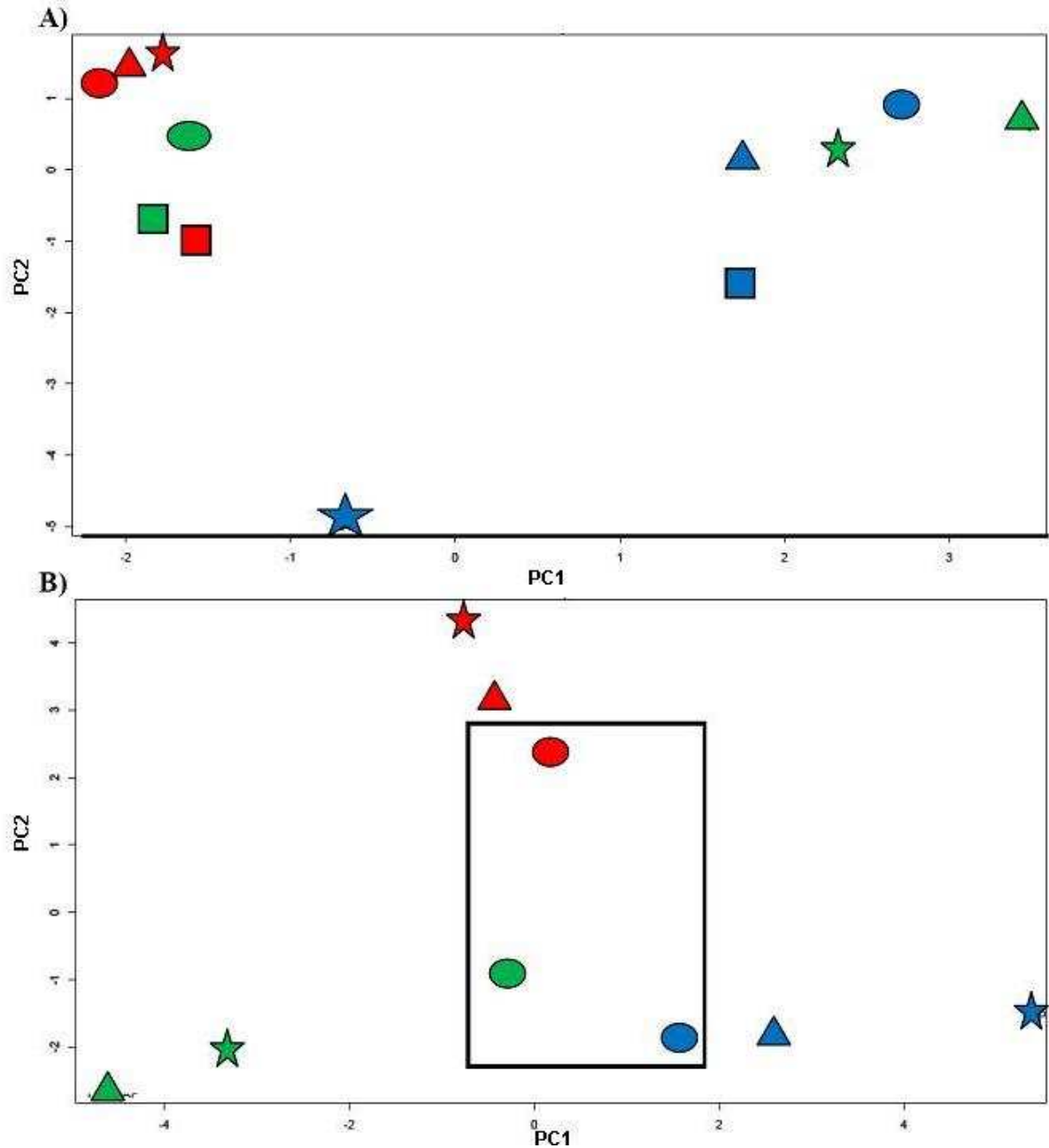
Figure 4.14. PCA of kinome data. Kinome datasets were subjected to 2D PCA cluster analysis. The data were broken into principal components, as represented by the axes. The X-axis represents principle component 1, and the Y-axis represents principal component 2. Datasets for each animal are colour coded: Animal 89 (red), Animal 136 (green) and Animal 148 (blue). Treatment/infection conditions are coded by shape: monocyte control (squares), MAP (triangles), IFNγ (circles) and MAP-infected-IFNγ-treated (stars). The black box indicates a conserved clustering of responses of uninfected monocytes to IFNγ stimulation following biological control subtraction. **A)** This plot shows treatments/animals prior to subtraction of biological control. **B)** This plot shows treatments/animals with subtraction of biological control.
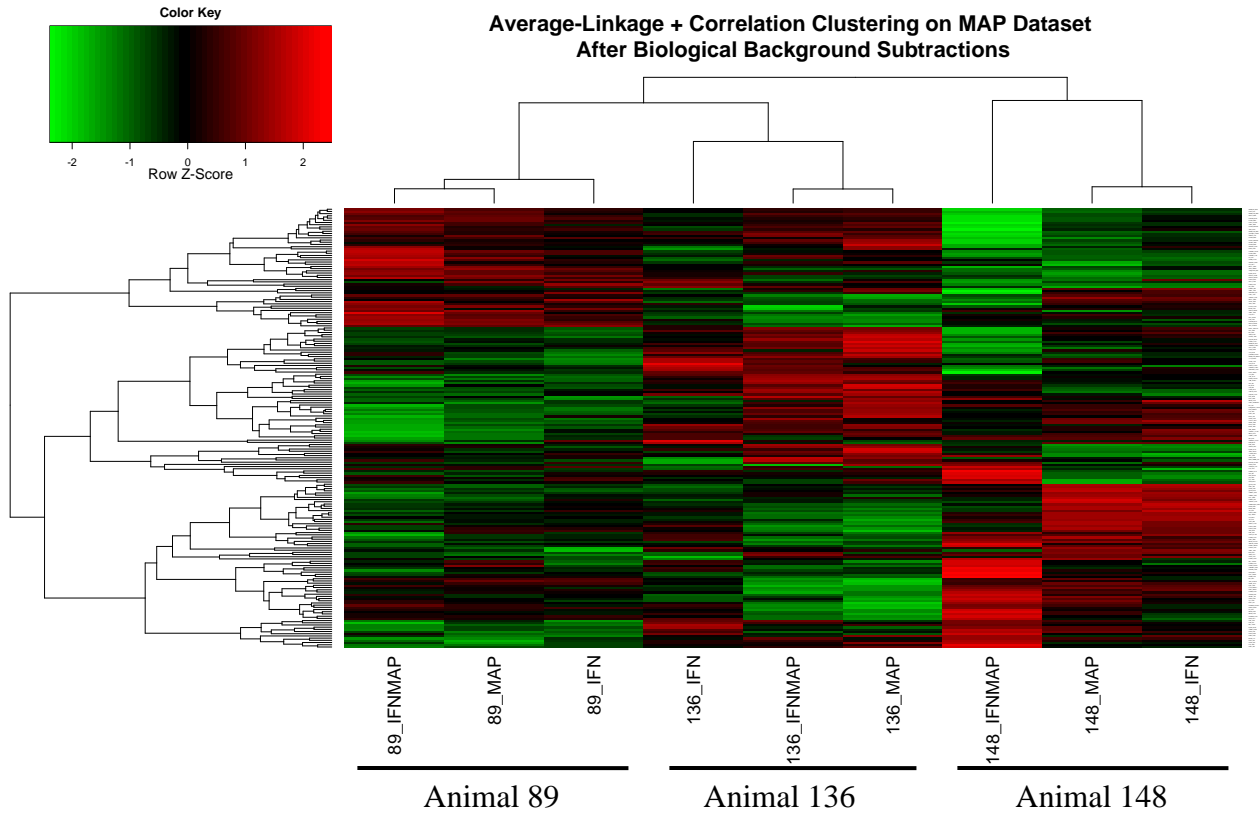
Figure 4.15. Clustering and heatmap of MAP kinome data. The background-corrected raw data collected from the peptide arrays were VSN-transformed, and respective control signal was subtracted. The heatmap/clustering of the data was produced using the Average Linkage + (1 - Pearson Correlation) method. The lines at the top of the heatmap indicate the relative similarity between the treatment conditions indicated at the bottom of the heatmap. The shorter the lines, the more similar the two connected columns. The animal codes are indicated below the treatment conditions. The lines on the left side of the heatmap indicate the relative similarity in signal between the 300 individual peptides on the array. The coloured lines indicate the relative degree of phosphorylation of each peptide from strongly phosphorylated (red) to non-phosphorylated (green) as indicated by a Z-score.

4.4.2.3 Pathways Implicated

To determine which peptides displayed significant changes in phosphorylation state under the various treatment conditions, the peptide signals were subjected to paired treatment-treatment variability *t*-tests. IFNγ-treated monocytes and MAP-infected monocytes treated with IFNγ were both compared to monocytes alone. IFNγ-treated monocytes were used as the

103

baseline because an induction of IFNγ response was required in order to see any subsequent lack of response in MAP-infected-IFNγ-treated cells.

Pathway over-representation analysis was carried out to determine the cellular pathways/processes that were activated/inactivated by the treatments. To ensure that the pathways identified were of conserved and consistent biological relevance, only those peptides which were identified as consistent (p >0.01) across the three biological replicates in one of the treatment conditions were considered. In addition, only those peptides which displayed a certain level of statistical significance (p <0.2) were input into the database. The data from the three animals were merged to produce a single representative bovine dataset before input into InnateDB.

When the monocytes treated with IFNγ were compared to control monocytes, several pathways were up-regulated with a high degree of statistical confidence (p <0.05). Notably, five of these pathways were related to JAK-STAT signalling (**Table 4.7**). According to InnateDB, the peptide arrays used in this experiment contained 25 peptides that could be directly attributed to the canonical JAK-STAT signalling pathway. Of these 25 peptides, 16 were significantly (p <0.20) differentially phosphorylated relative to control untreated cells. Fifteen peptides showed increased phosphorylation, and one showed decreased phosphorylation (**Table 4.7**).

JAK-STAT is a well-defined pathway involved in the cellular response to IFNγ stimulation (Bach, *et al.*, 1997; Darnell, 1997). Because this pathway was so strongly implicated by InnateDB, it provided a level of confidence that the peptide arrays were detecting real biological responses. The confidence level for the JAK-STAT pathway indicated by InnateDB (p 0.002) was the highest significance level obtained in the experiment (**Table 4.7**). By contrast, when MAP-infected monocytes treated with IFNγ were compared to the monocyte control, only four peptides indicated increased differential phosphorylation, and the pathway confidence level was negligible (p 0.83). This indicated that the treatment of MAP-infected monocytes with IFNγ did not induce the JAK-STAT signalling cascade.

In addition to JAK-STAT, a number of secondary signalling pathways were activated following IFNγ treatment of monocytes. These pathways included cytokine/chemokine signalling and activation of the pro-inflammatory TLR pathway. Many of these pathways share signalling intermediates with JAK-STAT, and they overlap downstream function. The

activation of these secondary IFNγ responses were not observed in MAP-infected monocytes treated with IFNγ. MAP appeared to block IFNγ responsiveness in monocytes. This blocking must occur upstream in the IFNγ response pathway; otherwise, a certain portion of the signalling cascade observed in IFNγ-treated cells would also be observed in MAP-infected-IFNγ-treated cells. Repression of these signalling responses may facilitate intracellular survival and immune evasion by MAP.

As numerous points along the JAK-STAT pathway were represented on the array, it was possible to investigate the specific point at which MAP influenced the ability of the monocytes to respond to IFNγ. IFNγ treatment of uninfected monocytes resulted in the differential phosphorylation of numerous isoforms of JAK, STAT and other signalling intermediates (**Table 4.8**). In general, it can be stated that there was an increased differential phosphorylation of key signalling peptides in the IFNγ-treated monocytes, while there was decreased phosphorylation of these important peptides in the MAP-infected-IFNγ-treated monocytes (**Table 4.8**). This decreased phosphorylation was also observed for IFNγ receptor 1 (IFNGR1), indicating that this repression of the JAK-STAT pathway appears to be occurring at the level of the receptor. A representation of the signalling network highlights the differences in response between IFNγ-treated monocytes (**Figure 4.16 A**) and the reduced signalling in the MAP-infected-IFNγ-treated samples (**Figure 4.16 B**).

Interestingly, the suppression of cytokine signalling (SOCS) expression pathway was also implicated in the pathway analysis of IFNγ-treated cells. SOCS is a natural repressor of JAK-STAT signalling, which modulates the activity of that pathway. An increase in the expression of SOCS would inhibit JAK-STAT signaling (Pauli, *et al.*, 2008). This may be the detection of the compensatory activation of SOCS to modulate JAK-STAT, thus, keeping the system in balance by inhibiting excess JAK-STAT signalling.

Table 4.7. Pathway analysis of bovine monocytes and MAP-infected bovine monocytes in response to IFNγ stimulation.

			Monocytes				MAP-Infected Monocytes			
			Up Regulated		Down Regulated		Up Regulated		Down Regulated	
	Pathway	$\updownarrow$	$\uparrow$	p	$\downarrow$	p	$\uparrow$	p	$\downarrow$	p
JAK-STAT Signalling	JAK-STAT signalling pathway	16	15	0.002	1	0.999	4	0.831	7	0.309
	JAK-STAT pathway/ regulation	12	11	0.006	1	0.998	1	0.840	2	0.532
	Gene expression of SOCS	6	6	0.025	0	1	1	0.915	3	0.340
	Gene expression of SOCS1	6	6	0.025	0	1	1	0.915	3	0.340
	Gene expression of SOCS3	6	6	0.025	0	1	1	0.915	3	0.340
Cytokine/ Chemokine Signalling	IL27-mediated signalling events	6	6	0.025	0	1	1	0.915	3	0.340
	IL12-mediated signalling events	14	12	0.013	2	0.990	2	0.910	5	0.251
	IL22 soluble receptor signalling	5	5	0.047	0	1	1	0.915	3	0.340
	AndrogenReceptor	11	10	0.081	1	0.999	4	0.247	2	0.919
	IFN beta enhancer information processing	6	6	0.025	0	1	0	1	0	1
TGFB Signalling	TGF-beta (canonical)	8	7	0.139	1	0.990	3	0.236	1	0.952
	TGF-beta signalling pathway	5	5	0.045	0	1	2	0.425	1	0.895
	TGFBR	15	11	0.273	4	0.957	5	0.061	0	1
NFkB Signalling	Nfkb activation	10	9	0.012	2	0.994	2	0.425	1	0.895
Other	Toll-like receptor signalling pathway	25	18	0.044	3	0.999	5	0.373	4	0.802

InnateDB assigned pathways from input transformed peptide array data. Pathways were assigned a probability value (p) based on the number of proteins present for a particular pathway. Output included the number of peptides associated with a particular pathway and the subset of those which are differentially phosphorylated. For our investigation, peptide significance cut-offs were set at $p <0.2$. $\updownarrow$ indicates the number of peptides on the array relating to the pathway. $\uparrow$ and $\downarrow$ indicate the number of peptides with increased or decreased phosphorylation, respectively, as compared to the control condition.

Table 4.8 Differential phosphorylation of peptides of the JAK-STAT pathway following IFNγ stimulation of monocytes and MAP-infected monocytes.

Phosphoprotein	Monocytes		MAP-Infected Monocytes	
	Fold Change	*p*-value	Fold Change	*p*-value
IFNAR1	1.14	0.04	-1.17	0.23
IFNGR1	1.09	0.26	-1.07	0.27
IL10RA	1.11	0.19	-1.14	0.15
IL16	1.20	0.10	1.17	0.16
IL2RB	1.10	0.24	-1.09	0.27
IL4R	1.16	0.14	1.08	0.31
IL6ST	1.14	0.14	1.04	0.33
IL7R	1.56	0.07	1.16	0.18
JAK1	1.03	0.42	-1.16	0.12
JAK2	-1.01	0.44	-1.08	0.22
JAK3	-1.02	0.36	-1.27	0.02
STAT1	1.22	0.08	1.20	0.14
STAT2	1.13	0.06	-1.15	0.08
STAT3	1.16	0.05	-1.12	0.16
STAT4	1.17	0.09	-1.06	0.34
STAT5B	1.14	0.05	1.00	0.49
STAT6	1.22	0.01	-1.40	0.14
Tyk2	1.04	0.16	-1.03	0.43

Phosphoprotein indicates the name of the protein which corresponds to the peptide phosphorylation target site on the array. Fold Change is the relative change calculated by comparing the background-corrected and normalized signal values of these IFNγ-treated cells to the media control cells. *p*-values correspond to the level of significant difference between these IFNγ-treated cells and media control cells.
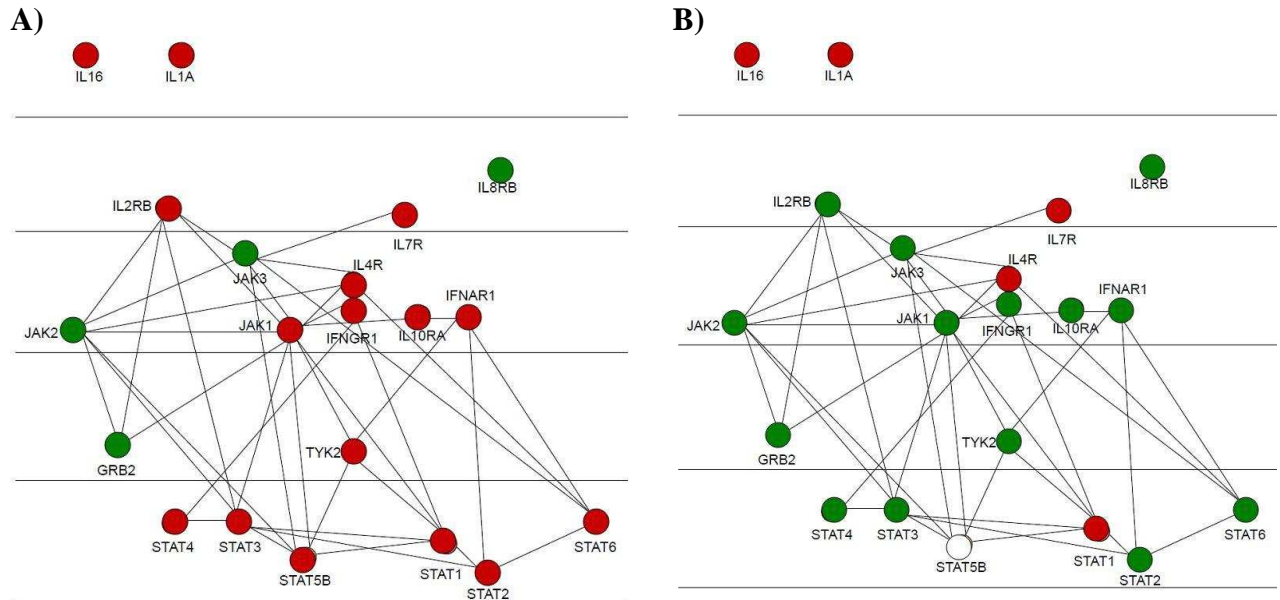
Figure 4.16. Signalling within the JAK-STAT pathway in bovine monocytes and MAP-infected bovine monocytes in response to IFNγ stimulation. Shown are proteins identified as belonging to the JAK-STAT pathway. The lines connecting each node are putative interactions according to the Cytoscape database. Protein members of the JAK-STAT pathway are colour coded with respect to direction of fold change using IFNγ treated monocytes as control. Red indicates increased phosphorylation, green indicates decreased phosphorylation and white indicates no change. **A)** Differential phosphorylation of JAK-STAT intermediates following IFNγ treatment of bovine monocytes is shown. **B)** Differential phosphorylation of MAP-infected monocytes treated with IFNγ is shown.

4.4.3 TNFα ELISA

The pathway analysis and signalling data indicated that MAP inhibited the ability of cells to respond to IFNγ stimulation. This appeared to occur at the level of the receptor as phosphorylation was decreased in MAP-infected cells from the level of the INFGR down through the pathway (**Table 4.8**). IFNγ-induced expression of TNFα is a well established response in macrophages (Collart, *et al.*, 1986). Treatment of bovine monocytes with 10 ng/mL recombinant bovine IFNγ induced significant release of TNFα (**Figure 4.17**). However, when MAP-infected monocytes were treated in the identical way, there was minimal release of TNFα. These results provided a functional confirmation that MAP infection could block signalling through the IFNGR, as observed in the kinome data.
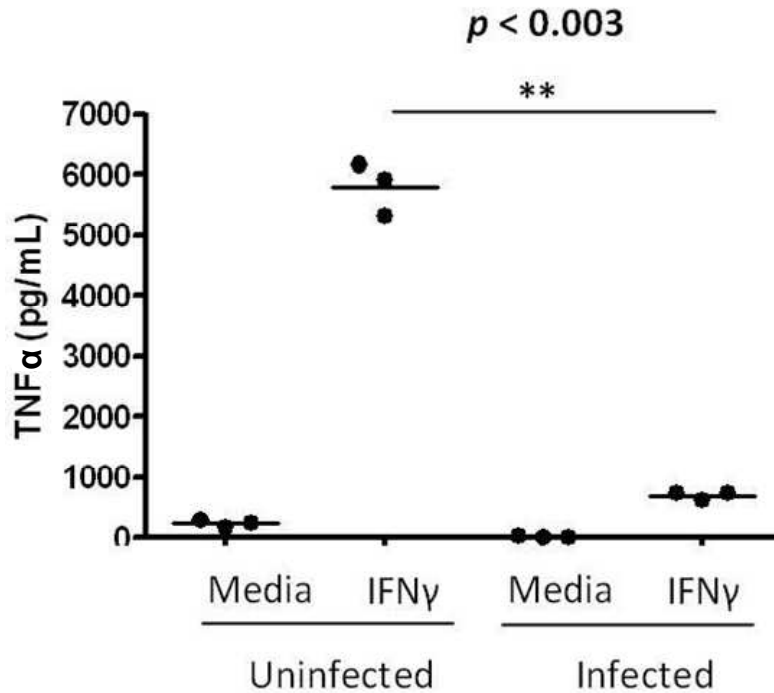
Figure 4.17. IFNγ-stimulated production of TNFα in MAP-infected and non-infected bovine monocytes. Monocytes, IFNγ-treated and untreated, and MAP-infected monocytes, IFNγ-treated and untreated, were cultured in growth media. This media was then collected, and the level of TNFα in culture supernatant was quantified with a capture ELISA. Cell samples were taken from a single representative animal. Statistical analysis was through a paired *t*-test of signal from the ELISA replicates. A standard curve of known TNFα concentrations was used to determine sample TNFα concentrations.

4.4.4 INFGR and SOCS Gene Expression

The absence of early JAK-STAT signalling in MAP-infected monocytes in response to IFNγ stimulation indicated that suppression of the signalling cascade was occurring at or near the IFNγ receptor. This could reflect suppression of receptor auto-phosphorylation, suppression of IFNγ receptor expression, suppression of JAK or STAT phosphorylation, suppression of JAK or STAT expression, or an increase in inhibitory factors silencing the JAK-STAT phosphorylation/activation at the level of the receptor. Both receptor-expression inhibition and increased expression of signalling inhibitors have been observed for other mycobacteria (Hussain, *et al.*, 1999). qRT-PCR results indicated that MAP reduced expression of IFNGR1 and INFGR2, while it increased the expression of the JAK-STAT

suppressor SOCS (**Figure 4.18**). An approximately four-fold decrease in both IFNGRs' expression was observed at the 18-hour time point, while no appreciable decrease in either IFNGRs' expression was seen at the 1-hour time point. In **Figure 4.18**, it is apparent that soon after infection, at the 1-hour time point, there was a significant increase in both SOCS1 and SOCS3 expression, and SOCS expression was further elevated at the 18-hour time point post-infection.
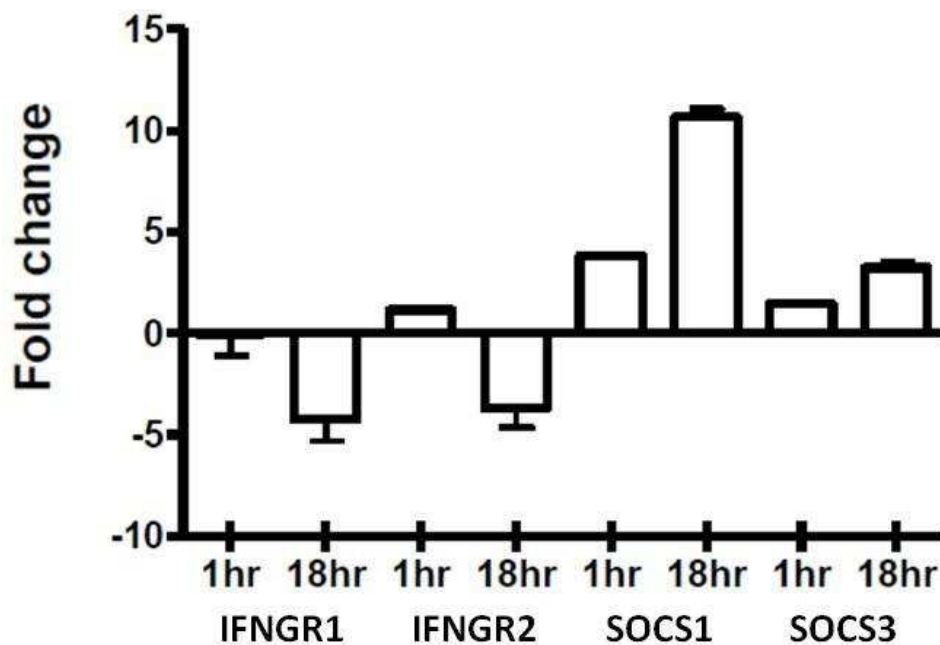
Figure 4.18. Altered expression of SOCS1, SOCS3, IFNGR1 and 2 in response to MAP infection. MAP-infected bovine monocytes were assayed in triplicate for relative expression of select genes as determined through qRT-PCR. Cultured bovine monocytes taken from a single representative animal were infected. RNA was extracted from cells collected at 1-hour and 18-hour time points. Cells were taken from three separate culture wells. The control sample was time-matched uninfected monocytes. The graph indicates fold change which was determined compared to control, as calculated by the $2^{-\Delta\Delta CT}$ method, along with standard deviation.

5.0 DISCUSSION

5.1 Cell Signalling, Disease and Kinome Analysis

To date, a large portion of the work done on peptide arrays, kinome analysis and kinase-based treatment has focused on cancer. This is understandable as cancer is recognized as a disease with altered cell signalling and is of great importance to human health, especially in the western world. The techniques developed and refined through the study of cancer are now being applied in other areas of biology and health. These techniques include high-throughput kinomic techniques such as peptide arrays. The development of genus-specific peptide arrays and computer techniques to mine the data will enable further expansion of this area of research. Disorders of protein function, such as TSEs, are diseases for which kinomics may provide a unique perspective. In these diseases, there is no pathogen to target, only internal cellular-level processes that become disordered. The disease may be treated by targeting the correct site of disorder. In the same vein, infectious diseases that effectively evade the immune system, such as MAP, and can hide from or adapt to current treatment regimes are problematic to treat. These infections need to be treated in a more elegant way, by either reactivating the suppressed immune responses or eliminating the pathogen effectors which cause the suppression. This project incorporates all of the aspects mentioned above: to enhance the utility of a kinome technology, to study an endogenous protein-based disorder involved in extracellular signal transduction and to study an intracellular pathogen that disrupts host signalling. These are diverse topics that all relate to kinomics.

5.2 Genus-Specific Peptide Arrays

The degree of genus difference in the sequences shown in **Table 4.2** highlights the importance of developing genus-specific arrays rather than relying on potential kinase cross reactivity between diverse genera. Even genera which display significant evolutionary proximity to humans, such as other mammals, can have significant differences in kinase target recognition sequences. Genus-specific peptide arrays should allow for a better match between kinase and peptide target sequence, allowing a greater likelihood of successful kinase recognition. It appears that the differences between genera are multiplied at the level of peptide sequence as compared to the genetic level. Humans and cattle share approximately 95% genetic similarity (Zimin, *et al.*, 2009); however, in the scope our peptide array design,

111

22% of peptides compared between human and bovine displayed no sequence homology as they corresponded to entirely different proteins (**Table 1.3**)

While some groups have taken the extreme step of using human peptide arrays to study genera as evolutionarily distinct as *Arabidopsis* plants (Ritsema, *et al.*, 2007), the results shown in **Table 4.2** provide a vivid illustration of why this may be inappropriate. For example, 99.69% of human phosphorylation target sites have no sequence homology in the rice plant. It is not a case of a cross-genus peptide array generating incorrect data but rather less significant data. For example, Ritsema *et al.* (2007) studied the plant *Arabidopsis* using a human peptide array. They generated 15 significant peptide phosphorylation events out of 184. These 15 peptides may have been the only human peptides with enough similarity to plant kinases to be phosphorylated. Meanwhile, in the prion study described here, use of human cells and a bovine-specific array showed that well over 100 peptides out of 300 were significantly phosphorylated. With a human array, perhaps even more peptides may have been considered significant. One of the benefits of PIIKA was the additional data points considered significant; this same benefit may result from genus-specific arrays. In addition, the method described of using human sequences as a basis for finding the equivalent sequence in the genus of interest works well in an evolutionarily proximal genus. Complications arise when the differences are greater, such as between humans and insects. A linear approach from human peptide sequence with assigned function to honey bee or wheat plant may not be possible. For these cases, it may be necessary to find a well-characterized genus of less evolutionary distance and then use these data as a starting point to develop an array for the genus of interest. Since using well-characterized human kinome data to develop bovine arrays was a successful approach, it may be a more straight forward bioinformatics process to take the well-characterized rice plant database, Rice Kinome Database (phylomics.ucdavis.edu/kinase/), to develop a wheat array, or a *Drosophila* database, such as www.phosphopep.org, to develop a bee array.

5.3 PIIKA Advances in the Peptide Array Technique
5.3.1 Data Normalization and Statistical Analysis

As an early adopter of high throughput microarray technology, genomics has been the dominant force in the development of mathematical and computational methods for data

analysis. When peptide arrays were developed, and specifically peptide arrays for kinome analysis, it was assumed that the data analysis methods developed for nucleotide-based arrays could be applied directly to this new technology. As the use of peptide arrays has become more wide-spread, it is becoming apparent that these approaches are not allowing the full potential of the peptide arrays to be realized, perhaps due to fundamental differences between the nature of the nucleotide and peptide arrays. In part, this relates to the distinct nature of the signals which are generated. Nucleotide-based arrays produce an output signal based on nucleotide hybridization reactions; however, peptide arrays are phosphorylated by transferring a phosphate group from ATP (or GTP) to the target sequence printed on the array. This creates two difficulties: the question of where to set a cut-off threshold and the issue of variance in signal increasing with phosphorylation. Since many statistical tests are based on the assumption of constant variance, data normalization is required before these tests can be conducted. The normalization method used to analyze the data needs to reflect the unique characteristics of peptide array data. Another difference between the two techniques is that the typical nucleotide array contains many more targets than the typical peptide array, possibly up to 100 times more. This requires a relatively less-stringent cut-off for the discarding of targets based on statistical significance. Too many discarded data points will limit the ability to identify clusters based on functional associations.

The data analysis pipeline that was developed, PIIKA, deals with the above-mentioned issues and unique characteristics of the peptide array data. Following a comprehensive comparison, PIIKA was found to be superior to the standard nucleotide array techniques that are commonly used. The key factors to consider when choosing an analysis method are that the data transformation does not alter the data in any way that may affect biological relevance (**Figure 4.3**) and that it enhances the amount of data that are considered statistically significant (**Table 4.3**). The increase in significant data is probably the greatest asset of PIIKA. Between the three treatments tested (CpG, LPS and IFNγ), PIIKA produced 273 significant peptides compared to 20 for VSN + *limma* and 44 for QNorm + *limma* (**Table 4.3**). This larger dataset allows more data mining and greater significance in the pathway analysis (**Table 4.4**). A large peptide array experiment containing multiple treatments that produces 20 significant peptides is not a large improvement over traditional methods such as phosphospecific antibodies and western blot, considering the time and cost. However, a

technique that generates significant signal from 273 peptides in the same experiment is a large advantage over traditional methods. Without this advancement, much of the high throughput nature of the peptide arrays would be lost. Additional data points allow effective use of PIIKA's higher-order data clustering, as well as pathway association using databases like InnateDB.

In determining which peptides are to be considered for further analysis, PIIKA uses the t-statistic generated p-value. It has been left up to the individual researcher to consider either fold change or p-value as the criterion for whether a gene, in the case of nucleotide arrays, or a peptide, in the case of peptide arrays, is distinct from control. Witten and Tibshirani (2007) made several observations contributing to this discussion. They compared the use of fold change and t-statistic in the generation of differential gene lists from microarray data. They concluded that the use of either fold change or t-statistic should be based on biological rather than mathematical considerations. However, they found that the use of fold change artificially enhances the perceived importance of noisy genes over those with true differential expression. This elimination of noisy genes is an important feature of the t-statistic, though the t-statistic does enhance the perceived importance of replicate consistency over magnitude of signal difference between treatment and control. With our experience analyzing peptide array data, we found that the t-statistic is the best means of peptide selection considering both the noise associated with replicate peptide phosphorylation and the negative phosphorylation values generated.

If considering the t-statistic as a cut-off, it is important to decide the confidence level that will be applied to the data. Peptide array data have a number of unique characteristics that distinguish it from nucleotide array data and make assigning a t-statistic cut-off difficult. A major characteristic of peptide array data is that there is substantially less data generated, potentially up to 100 times fewer data points per array than nucleotide array data. For this reason alone, a less stringent p-value cut-off is desirable for peptide array data. In a nucleotide array containing 30,000 oligos, a p-value cut-off of 0.05 would produce 1,500 significant data points by random chance. A peptide array of 300 peptides with a similar cut-off would produce 15 significant data points by random chance. For the reason above, a strict significance cut-off is a necessity in nucleotide array data. Another characteristic of peptide array data is the potentially large variation in signal between intra-array replicates due to

variations in staining and peptide phosphorylation level across the array. This variation could result in many more data points being eliminated when using a stringent t-statistic cut-off. In addition, the MicroArray Quality Control project conducted a large study on numerous microarray datasets and recommended using a less stringent p-value cut-off to enhance the reproducibility of gene lists generated from array data (Shi, *et al.*, 2008). Considering these characteristics, we have chosen a relatively liberal cut-off for peptide significance: p-value < 0.2.

5.3.2 Clustering and Pathway Analysis

As with any high throughput experimental methodology, a large amount of data are generated; thus, there is the problem of mining the data for biologically relevant information. Taking a systemic approach and applying higher-order analyses, such as clustering and functional associations, has become common in nucleotide-array studies. These types of analyses have not been a part of most kinome studies in the past. Many groups have simply used the kinome arrays as a means to find specific phosphorylation events, which are then further characterized by more classical methods. This approach, however, disregards the potential to do higher order analysis from such a large pool of data.

In this project, it has been shown that clustering of treatments and pathway analysis have added value to peptide array data analysis. It has been shown that some treatments are more similar than others and indicated which pathways are activated or deactivated under given conditions. For instance, in the prion study, clustering occurred based on the type of stimulant. This stimulant-type-dependent response had to be controlled so prion-specific effects could be observed. Subsequently, pathway analysis showed that the two prion ligands displayed unique pathway (de)activation, implicating multiple-pathway interactions between the cell-surface prion protein and the intracellular signalling environment. The MAP study showed the importance of biological controls, especially in outbred animal populations. Once biological variability was taken into account, clear treatment- and infection-specific patterns emerged. Following pathway analysis, a lack of JAK-STAT and secondary-pathway signalling was observed in MAP-infected cells treated with IFNγ. This was a clear indication that MAP inhibits the JAK-STAT pathway to suppress immune responses. These conclusions were later confirmed by additional experimental methods.

The results shown in this project clearly illustrate the utility of applying these higher order methods to peptide array kinome analysis.

5.4 Prion Signalling
5.4.1 The PrP Protein's Distinct Signalling Potential

While numerous studies have looked at signalling events associated with PrP^C, this study is the first to take a broad approach at the level of the kinome. The results confirm many of the individual results from previous studies and also point to a unique aspect of PrP^C that, until now, had not been fully considered: its multifarious signalling potential.

When treated with two PrP-specific ligands, distinct pathways and distinct (de)activation dichotomies are observed. The distinct pathways which are activated by the two stimulations may lead to different functions of the PrP protein based on conformation. PrP 106-126-induced cellular responses are a model of disease, and this peptide has been used in various *in vivo* prion disease studies (Tagliavini, *et al*., 1993; Fabrizi, *et al*., 2001; O'Donovan, *et al*., 2001; Thellung, *et al*., 2002; Carimalo, *et al*., 2005; Pietri, *et al*., 2006). PrP antibody-based stimulation has been used to model signalling and results in a milder cell phenotypic response (Mouillet-Richard, *et al.*, 2000; Schneider, *et al*., 2003; Solforosi, *et al.*, 2004). **Figure 4.10** shows how the various pathways that were implicated by the kinome data can be linked, revealing how several diverse functions may have been assigned to the prion protein previously. When only a small part of the prion signalling pathway is considered, it is understandable why different investigators assigned different functions to the prion protein.

The priority of the kinome investigation of PrP function was to take a more global perspective when analyzing PrP^C signalling. Many of the signalling events observed had been reported previously by other groups in various individual studies. The peptide array data indicated calcium response, growth factor signalling, and PI3K, all of which have been shown previously (Kristensson, *et al.*, 1993; Thellung, *et al.*, 2002; Vassallo, *et al.*, 2005). In addition, Thellung, *et al.*, (2002) showed PrP 106-126-dependent activation of Caspase 3 in human neuroblastoma cells, a response also identified in our study (**Figure 4.10** and **Table A1**). By analyzing multiple protein phosphorylation events within a single experiment, the combined dataset was able to implicate possible upstream cell-surface interacting partners for PrP^C. The most significant of these cell-surface receptor pathways, based on InnateDB

pathway-significance values, were VEGFR and TGFBR (**Table 4.5**). Previous studies have also implicated laminin receptors as possible PrP^C interactors (Rieger, *et al.*, 1997; Graner *et al.*, 2000), and the array data indicated that integrin receptors, a type of laminin receptor, may be linked to peptide-stimulated PrP^C.

Signalling events induced by antibody stimulation agreed with many of the previously published reports and demonstrated a signalling response that was distinct from the peptide. MAPK-related signalling was evident from pathway analysis, and this had been shown previously in antibody-treated neuronal cells (Mouillet-Richard, *et al.*, 2000). MAPK also appeared in peptide-treated cells, but the direction of phosphorylation was opposite, depending on treatment. This indicated an activation/deactivation response between the two stimulations. Based on pathway analysis and moving upstream of the pathway, insulin receptor was implicated as a possible cell-surface interactor, again, a previously reported result (Ostlund, *et al.*, 2001).

Confirmation of signalling implicated by the peptide array data analysis was obtained with a number of independent validation assays. Antibodies on the phosphospecific antibody array, which were exact matches to the printed array peptides, agreed in terms of direction of phosphorylation and magnitude of fold change (**Figure 4.6**). This result provided evidence that the phosphorylation of peptides on the array were correlated to phosphorylation of substrate proteins within the cells. Calcium release was indicated by the array data upon stimulation with PrP 106-126 but not antibody. This result was confirmed with a calcium-release assay (**Figure 4.2**). Previously published data had shown a strong apoptosis induction and cell death caused by PrP 106-126 (O'Donovan, *et al.*, 2001; Paitel, *et al.*, 2003). This study produced results showing that cell-viability was significantly decreased upon stimulation with the peptide (**Figure 4.11**). Peptide array data indicated a role for VEGFR signalling in peptide-stimulated but not antibody-stimulated cells. Both of these results were confirmed by viable cell counts with and without the addition of recombinant VEGF. A significant reduction in cell viability was observed following stimulation with peptide while no reduction was observed due to the antibody. Moreover, the addition of VEGF restored cell viability in PrP 106-126-stimulated cells but had no significant effect on antibody-treated cells (**Figure 4.11**). Considering the validation assays and that many results from the peptide

array study were confirmed by others using low throughput methods, there can be confidence in the array results.

PrP^C has the ability to differentially affect multiple signalling pathways based on the stimulation given, possibly as a result of different interacting partners on the cell surface. These differences are readily observed; for example, when stimulated with peptide, the PI3K and calcium responses were significant but were not apparent when the neuronal cells were treated with antibody. Antibody stimulation revealed MAPK signalling responses distinct from those in peptide-stimulated cells. In addition, Erk is significantly differentially phosphorylated when treated with antibody but not peptide. The NFκB pathway is another example where antibody affects a pathway, while peptide does not (**Table 4.5**).

Within the literature, it is rare to find examples of receptors that have the ability to elicit unique and unrelated phenotypes depending on the ligand bound. However, there are examples of receptor-modulating proteins that can alter receptor phenotype; these are referred to as receptor activity modifying proteins (RAMPs) (Sexton, *et al.*, 2001). Originally discovered in interaction with calcitonin receptor and the calcitonin receptor-like receptor, RAMPs interact with a much wider cross-section of receptors (Christopoulos, *et al.*, 2002). These proteins can bind at various sites on the receptor, affecting receptor trafficking, glycosylation and direct receptor activity through the interaction with the ligand binding domain (Sexton, *et al.*, 2001). Perhaps due to misfolding, PrP appears to share a similar ability to interact with more than one receptor on the cell surface. Multi-receptor interaction may explain prion's ability to elicit distinct signalling events within a given cell.

A reason the function of PrP^C has been so difficult to determine may be its multifarious signalling ability. Variable signalling pathway activation, resulting from the different experimental techniques and models that have been employed, activate different potential functions of the protein. This may be a reason that various studies have shown different PrP^C functions. It may be necessary to take a more global approach to elucidate a more complete interaction network for PrP^C in order to understand its variable cell signalling characteristics.

5.5 MAP Related Signalling

The host response to infection is often based on phosphorylation-mediated changes in normal cell function. A lack of activation of an immune response can lead to chronic infection; however, an aggressive immune response can lead to damaging inflammation or autoimmunity. Mycobacteria species display a pathogenic mechanism involving the production of bacterially encoded, eukaryotic-like protein phosphatases which play a role in virulence (Alber, 2009). The presence of these phosphatases underscores the importance of phosphorylation to these bacteria. Given this importance, the understanding of host-pathogen interaction related to cell signalling in MAP infections may be central to understanding the disease pathogenesis. Considering the widespread availability and success of kinase inhibitors to fight disease (Schreiber, *et al.*, 2009), MAP may be a natural fit for this treatment paradigm.

5.5.1 IFNγ Receptor and Immune Response

When comparing monocytes treated with IFNγ to MAP-infected monocytes treated with IFNγ, pathway analysis clearly revealed MAP's ability to block IFNγ-induced JAK-STAT signalling. In monocytes treated with IFNγ, activation of the JAK-STAT pathway, cytokine/chemokine pathways and TLR signalling were all observed. In MAP-infected monocytes, none of these pathways displayed any level of activation. Observing a number of JAK-STAT pathway intermediates, phosphorylation status indicated that this lack of signalling was occurring throughout the pathway up to the level of the receptor. As IFNγ is an important immune modulating molecule, the suppression of this pathway would give an intracellular pathogen, such as MAP, an advantage in establishing a chronic infection.

Gene expression experiments showed that the expression of IFNGR1 and IFNGR2 decreased, and expression of SOCS1 and SOCS3 increased in a time-dependent manner following MAP infection. SOCS are inhibitors of JAK-STAT signalling, so their induced expression by MAP would result in a loss of IFNγ response. A number of viruses have been shown to reduce IFNγ responsiveness through the action of SOCS, including Influenza A (Pauli, *et al.*, 2008), Herpes Simplex Virus 1 (Yokota, *et al.*, 2005), Hepatitis C Virus (Bode, *et al.*, 2003), Severe Acute Respiratory Syndrome coronavirus (Okabayashi, *et al.*, 2006) and Respiratory Syncytial Virus (Zhao, *et al.*, 2007). While a detectable increase in the expression

of SOCS1 and 3 was observed as early as 1 hour post infection, a significant decrease in IFNGR1 and 2 expressions required up to 18 hours to be observed. By contrast, SOCS expression was substantially increased at a very early time-point post infection. SOCS1 expression eventually increased approximately 10-fold and SOCS3 increased approximately 3-fold relative to uninfected cells (**Figure 4.18**). These results indicated that MAP suppresses the JAK-STAT pathway by inducing SOCS expression early in infection, which may provide a rapid way to suppress IFNγ responses prior to down-regulating IFNGR protein levels. Subsequently, for long-term immune suppression, MAP inhibits the expression of the IFNγ receptors. Other pathogens have been known to have a similar affect on IFNGR1 and 2 (Kierszenbaum, *et al.*, 1995; Ray, *et al.*, 2000) including *Mycobacterium avium*, a bacterium closely related to MAP (Hussain, *et al.*, 1999). However, in *Mycobacterium tuberculosis,* the inhibition of IFNγ signalling is not based on the suppression of STAT signalling (Ting, *et al.*, 1999).

This MAP study has offered insight into the pathogenic mechanisms of MAP. It also characterizes the nature of MAP's blockage of IFNγ signalling, specifically the redundant nature of the blockage both by signalling suppression via decreased receptor expression and pathway suppressor activation.

5.6 Future Directions

5.6.1 The Kinome

In the future, the characterization of the complex interplay between pathogen and host for the discovery of novel and specific therapeutic targets of treatment will be a growing field of research. The importance of phosphorylation in cellular activity and the growing body of evidence implicating signalling in varied diseases show how key disruptions of signalling are critical. This means that kinome analysis will be important as a means of developing treatments. An increasing number of "endogenous" diseases such as cancer, Alzheimer's disease, genetic disorders and protein misfolding diseases are becoming increasingly relevant to human health. In addition, high throughput technology and data analysis techniques are constantly improving while more targeted therapies are being demanded. Considering all of the above, kinomic research should receive much attention.

5.6.2 Prion

5.6.2.1 The Multifarious Prion Function

Despite the huge amount of work that has already gone into understanding PrP^C, the function of this prion protein is still a mystery. Putative functions seem to fall into and out of favour within the research community, with no clear consensus emerging. A more global analysis or meta-analysis may be in order. This prion study indicates that taking a broader approach to understanding prion function may be a critical step to finally assigning a function to this protein. It is possible that PrP^C is able to interact with multiple partners, thus affecting multiple signalling pathways with varied functions. Adding further complexity to the understanding of PrP^C is that its function may be subverted or altered upon misfolding. Since the search for a single interactor or pathway has yet to be successful, the source of this variability should be studied.

A first step in the study of PrP functional variability is the prion study described here, which takes a more global approach to prion activities in the context of the kinome. With the advent of multiple high-throughput techniques involving various "omes" (genomes, transcriptomes, proteomes, kinomes, metabolomes and interactomes), perhaps the prion protein exemplifies the need for a systems biology approach to certain biological questions. Systems biology could incorporate and integrate the individual omics approaches. The prion protein is a protein without a clear function. PrP may have the potential for multiple interactions which alter its function. A linear approach, considering a single protein-protein interaction or looking at genetic answers to protein function, has failed to provide the answer. The variation encountered in the study of PrP function may describe a problem which a systems approach could more effectively address.

5.6.2.2 Misfolding Diseases

With the success of science in curing infectious disease since the advent of antibiotics and vaccination, new diseases of concern appear increasingly to be diseases without an obvious infectious trigger. Genetic disorders, degenerative disorders and now misfolding diseases are becoming increasingly prevalent as more infectious diseases are cured or successfully treated. The first protein misfolding disease to be characterized as such was the prion disease scrapie (Pruisner, 1982). This expanded to other prion diseases such as Kuru,

Creutzfeldt-Jakob disease, bovine spongiform encephalopathy and chronic wasting disease. There is now more evidence that other diseases such as Alzheimer's disease, Huntington's disease and Parkinson's disease are caused by the misfolding of key proteins (Aguzzi, 2009). The ability to treat these diseases may not come from the classical methods applied to infectious disease, or the hope of effective gene therapy; rather, treatment may involve targeting misfolding or correcting the physiological disorder resulting from misfolding. This "protein only" paradigm is relatively new. In many of the cases of these misfolding diseases, no genetic component has been determined; in fact, the protein misfolding appears independent of the genome. The current misfolding disease field is dominated by Alzheimer's disease and prion diseases; however, it may become a much broader field in the future. Diseases that result from protein misfolding could become even more important as we realize there are limits to what genes can tell us.

5.6.3 MAP

5.6.3.1 Treatment of MAP's Effects on the Immune System

MAP's ability to not only evade the immune system but also survive and grow inside immune cells meant to destroy it makes it a model bacterium for kinome studies. It is clear that MAP survives and is able to cause chronic infection, at least in part, due to its specific targeting of immune signalling. Thus, it is possible that an effective treatment of MAP infection can come from a signalling approach. For the first time, this study points to events affecting the IFNγ receptor that leads to the loss of JAK-STAT signalling and downstream immune response. Possible treatments may include reactivation of a key phosphorylation event in the JAK-STAT pathway, use of an inhibitor designed to stop the activation of SOCS or a combination of the two. Alternatively, if the bacteria-produced molecular effector which carries out this JAK-STAT suppression were identified, then this molecule may be a target for vaccination. If effective, such treatments are of great interest to the cattle industry as they could lead to a substantial increase in production and improved animal health.

While MAP has been inconclusively linked to human disease, other mycobacteria, like *M. tuberculosis*, are important causes of human disease. MAP and *M. tuberculosis* share many common immune-evasion characteristics. It is possible that effective treatment for MAP infections could be helpful in advancing the research for *M. tuberculosis* treatments.

5.6.3.2 MAP and its Tyrosine Phosphatases

MAP, like other *Mycobacterium* species, produce two tyrosine phosphatases: PtpA and PtpB. Since, 1) MAP contains no tyrosine kinases, 2) its internal signalling is based on serine/threonine phosphorylation and 3) these phosphatases are secreted, it is believed that these phosphatases are designed to interfere with host cell signalling. Given the importance of phosphorylation-mediated signalling and the amount of time bacteria have co-evolved with host animals, it is not surprising that they would develop means of affecting cell signalling. However, this is a relatively new area of infectious disease research and an opportunity for disease treatment. If this pathogen-specific signalling disruption is a widespread strategy of infectious disease, the kinase- and phosphatase-based treatments used for cancer may be more widely applicable. Diseases which affect signalling by the production of phosphatases or kinases to alter host signalling will be among the first to be treated by this signalling modulation approach.

5.6.4 Peptide Arrays

Peptide arrays, and specifically peptide arrays for kinome analysis, have been around for a number of years. The technology has now advanced to a point where more is expected of it, and new tools need to be developed for the technology to truly achieve its full potential. In the past, the peptide arrays were used as a hypothesis-generating technique. These hypotheses could then be tested and validated by other more classical techniques. Increasingly, peptide-array kinome analysis is standing on its own, much the way nucleotide-array based work is. Two key aspects of the future of peptide arrays are described below: mining as much data out of the arrays as possible and producing arrays for more evolutionarily diverse genera.

5.6.4.1 Analysis Techniques and Enhanced Data Mining

When peptide arrays were first used for kinome analysis, a limited amount of data were produced and used. An array of 300 or more peptides would be used to observe a few phosphorylation events. These results were then validated by western blot or other classical methods (Diks, *et al.*, 2004; Lowenberg, *et al.*, 2006). The remaining data were discarded as characterizing a single protein phosphorylation event in the context of a disease or treatment was an adequate goal. Now, much like nucleotide arrays, a more integrated approach is being

adopted. It was clear that looking at a limited number of genes on an array containing 30,000 potential hybridization events was a waste of potentially important data. Databases such as KEGG and InnateDB were first developed to organize gene expression data into pathways and functional associations. The same is occurring for peptide arrays. Analysis pipelines such as PIIKA and the adaptation of InnateDB for use with phosphorylation data is only the start of this trend.

The data mining that we achieved is better than what was done previously, but much more can be done. One example of possible additional data mining is that peptide arrays could generate two potential data points per spot. One data point is the phosphorylation of the protein phosphorylation target sites modeled by the peptides on the array, which can be matched to proteins found in the cell. This phosphorylation site analysis is what was done in this project. The second potential data point is the identity of the kinases, which are active within a cell under the experimental conditions. To date, only a peptide which represents a protein has been studied, but it is equally valid to consider the kinase recognizing and phosphorylating the target site. Considering the fact that there are now thought to be 518 kinases in the human genome (Manning, *et al.*, 2002), it is theoretically possible to design a universal kinase array containing 518 spots corresponding to the consensus sequence of each kinase. This array could then be used for any human kinome experiment. The problems of kinase specificity, multiple kinases phosphorylating the same spot and varying kinase activity would need to be addressed. In addition, peptide arrays that include a larger number of target peptides would enhance kinome coverage. With improved printing and experimental techniques, it may be possible to have thousands of kinase target peptides on an array. This would enhance the high-throughput, global nature of the technology.

Another potential direction for kinomics is the profiling of groups or individuals. As we observed in the MAP study, individual outbred animals display unique kinome profiles which can be used to separate and organize them. Using kinome profiles, it may be possible to screen for disease susceptibility or resistance and environmental effects based on the profile generated. This has begun with our work on cancer profiles (Van den Brooke, *et al.*, 2011). For example, if a cancer cell line is more like a normal cell than a tumour cell growing in an animal, it may be inappropriate to use cell lines such as these for signalling studies that purport to model cancer.

Kinome profiles can be incorporated into a wider systems biology approach. It may be invaluable to incorporate kinomics with the other "omics", such as genomics, transcriptomics, proteomics and metabolomics, to obtain a more comprehensive view of biology. Again, this will require data-analysis techniques and data-mining approaches of increased sophistication. It will be the work of biologists and bioinformaticians to combine their skills and produce biologically relevant, mathematically sound analysis methods.

5.6.4.2 Novel Genera

The interest in performing peptide array kinome analysis on genera other than human and mouse has become clear. Some groups have already attempted to profile plants with human peptide arrays (Ritsema, *et al.*, 2007). Our group has taken a more exact approach by designing arrays which are customized and genus-specific, based on bioinformatic techniques (Jalal*, et al.*, 2009). The desire to use this approach has been shown by groups which have approached us to design arrays. To date, bovine, chicken, pig, bee and soy bean arrays are in development. The challenge of designing arrays for genera that are evolutionarily distant from humans, such as bee and soy bean, is significant. Computer-based techniques which automate the process are able to run through tens of thousands of proteins and link them to known phosphorylation events. This will be a key advancement in the genus-specific array technique.

6.0 CONCLUSIONS

Phosphorylation-mediated cellular signalling represents the central mechanism for regulation of cell function. Kinases are a class of enzyme which phosphorylates protein through the transfer of a phosphate group, usually from the donor ATP, to the target protein. The study of kinases has led to the development of peptide-array technology which exploits the kinase recognition site sequences on proteins. These sequences are printed onto array surfaces and are recognized and phosphorylated by active kinases. Our development of custom-designed genus-specific peptide arrays has allowed for kinomic studies of genera besides human and mouse. Specifically, the study of bovine response to various pathogens and ligands has been the main focus thus far.

The limitations of the mathematical analysis and mining of peptide array data have impeded further development of this technology. Historically, peptide array data were analyzed in much the same way that nucleotide-based array data were. However, due to the numerous differences between the two types of data, sharing analysis methods was not ideal. Therefore, a data-analysis pipeline called PIIKA was developed to both analyze and mine peptide array data more effectively and efficiently. A comparison with other standard microarray analysis techniques confirmed the increased efficacy of PIIKA. PIIKA enables analysis of data by a method purpose-adapted to peptide arrays. It also allows for a higher-order analysis of peptide array data, organizing it into clusters based on similarity and the output can be used to query pathway databases based on the phosphorylation signal generated.

Peptide arrays and PIIKA were applied to the biological question of prion function. The properly folded form of the prion protein known as PrP^C is highly conserved in various cell types and species. Upon misfolding to the scrapie-like form (PrP^{Sc}), the protein causes neurodegenerative disease. There is little known about the function of prion, but there is ample evidence that it is a cell-surface signalling molecule. The prion protein's GPI anchor, location within lipid rafts and required linkage to the cell surface for disease pathogenesis all point to a role as a signalling molecule. Two PrP-specific stimulants were used to induce signalling in neuronal cells. One stimulant was a fragment of the prion protein containing amino acids 106-126, considered to be an inducer of responses modelling prion disease. The second PrP stimulant was the prion-specific antibody 6H4, considered to be an inducer of responses modelling endogenous signalling. Kinome results showed a distinct set of

signalling events based on the two treatments, displaying a variable signalling ability. Prion function may be difficult to determine, as it may be ligand-dependent or interacting partner dependent.

The host-pathogen interaction and immune-evasion abilities of MAP were another cell signalling problem studied in this project. MAP has the ability to evade immune responses and grow inside of the phagosome of macrophages, a place where bacteria are normally destroyed. Kinome analysis indicated that MAP is able to inhibit the IFNγ-induced JAK-STAT signalling pathway, thus, eliminating the activation of downstream effectors. The MAP-induced pathway inhibition occurred at the level of the IFNγ receptor. MAP also caused the activation of JAK-STAT suppressor molecules known as SOCS. Both receptor-level inhibition and SOCS activation are novel findings in the study of MAP pathogenesis. In addition, long-term MAP immune suppression may occur due to the suppression of IFNγ receptor gene expression. While SOCS expression is upregulated in as little as 1 hour, a significant decrease in the expression of IFNγ receptor is observed at 18 hours. This suppression is another indication that MAP targets the receptor to eliminate IFNγ immune signalling.

This project has increased the efficacy of peptide array experimental techniques, data analysis and data mining. Comprehensive comparisons of other array analysis methods show a clear benefit over these previously used methods. These advances have allowed the study of prion signalling and the description of prion's multifarious signalling ability. The project has advanced the characterization and understanding of IFNγ-based immune suppression by MAP infection. These results prove custom-designed genus-specific peptide arrays, in conjunction with customized data analysis methods, represent a valuable strategy to determine host signalling responses induced by a variety of stimuli, including infection.

7.0 REFERENCES

Abendroth, A., Slobedman, B., Lee, E., Mellins, E., Wallace, M., and Arvin, A.M. (2000). Modulation of major histocompatibility class II protein expression by *varicella-zoster* virus. J. Virol. *74*, 1900–1907.

Adams, L.B., Fukutomi, Y., and Krahenbuhl, J.L. (1993). Regulation of murine macrophage effector functions by lipoarabinomannan from mycobacterial strains with different degrees of virulence. Infect. Immun. 61, 4173–4181.

Aguzzi, A. (2005). Prion toxicity: all sail and no anchor. Science *308*, 1420-1421.

Aguzzi, A. (2009). Cell biology: beyond the prion principle. Nature *459*, 924-925.

Aguzzi, A., Baumann, F., and Bremer, J. (2008). The prion's elusive reason for being. Annu. Rev. Neurosci. *31*, 439-477.

Alber, T. (2009). Signaling mechanisms of the *Mycobacterium tuberculosis* receptor ser/thr protein kinases. Curr. Opin. Struct. Biol. *6*, 650-657.

Alonso, A., Sasin, J., Bottini, N., Friedberg, I., Friedberg, I., Osterman, A., Godzik, A., Hunter, T., Dixon, T., and Mustelin, T. (2004). Protein tyrosine phosphatases in the human genome. Cell *117*, 699-711.

Arsenault, R.J., Jalal, S., Babiuk, L.A., Potter, A., Griebel, P.J., and Napper, S. (2009) Kinome analysis of Toll-like receptor signaling in bovine monocytes. J. Recept. Sig. Transd. *29*, 299-311.

Asselin, E., Mills, G.B., and Tsang, B.K. (2001). XIAP regulates Akt activity and caspase 3 dependent cleavage during cisplatin-induced apoptosis in human ovarian epithelial cancer cells. Cancer Res. *61*, 1862.

Bach, E.A., Aguet, M., and Schreiber, R.D. (1997). The IFN gamma receptor: a paradigm for cytokine receptor signaling. Annu. Rev. Immunol. *15*, 563–591.

Bach, E.A., Tanner, J.W., Marsters, S., Ashkenazi, A., Aguet, M., Shaw, A.S., and Schreiber, R.D. (1996). Ligand-induced assembly and activation of the gamma interferon receptor in intact cells. Mol. Cell. Biol. *16*, 3214–3221.

Bach, H., Sun, J., Hmama, Z., and Av-Gay, Y. (2006). *Mycobacterium avium* subsp. *paratuberculosis* PtpA is an endogenous tyrosine phosphatase secreted during infection. Infect. Immun. *74*, 6540-6546.

Barsky A., Gardy J.L.,Hancock R.E.W., and Munzner, T. (2007). Cerebral: a Cytoscape plugin for layout of and interaction with biological networks using subcellular localization annotation. Bioinformatics *23*, 1040-1042.

Blanchette, J., Racette, N., Faure, R., Siminovitch, K.A., and Olivier, M. (1999). *Leishmania*-induced increases in activation of macrophage SHP-1 tyrosine phosphatase are associated with impaired IFN-gamma-triggered JAK2 activation. Eur. J. Immunol. *29*, 3737–3744.

Bode, J.G., Ludwig, S., Ehrhardt, C., Albrecht, U., Erhardt, Schaper, F., Heinrich, P.C. and Haussinger, D. (2003). IFN-alpha antagonistic activity of HCV core protein involves induction of suppressor of cytokine signaling-3. Fed. Am. Soc. Exp. Biol. J. *17*, 488–490.

Bonecini-Almeida, M.G., Chitale, S., Boutsikakis, I., Geng, J., Doo, H., He, S., and Ho, J.L. (1998). Induction of in vitro human macrophage anti-*Mycobacterium tuberculosis* activity: requirement for IFN-gamma and primed lymphocytes. J. Immunol. *160*, 4490-4499.

Booth, J.S., Arsenault, R., Napper, S., Griebel, P.J., Potter, A.A., Babiuk, L.A., and Mutwiri, G.K. (2010). TLR9 signaling failure renders Peyer's patch regulatory B cells unresponsive to stimulation with CpG oligodeoxynucleotides. Innate Immun. *2*, 483-494.

Bostrom, S.L., Dore, J., and Griffith, L.C. (2009). CaMKII used GTP as a phosphate donor for both substrate and autophosphorylation. Biochem. Bioph. Res. Co. *390*, 1154-1159.

Brown, D.R., Qin, K., Herms, J.W., Madlung, A., Manson, J., Strome, R., Fraser, P.E., Kruck, T., von Bohlen, A., Schulz-Schaeffer, W., Giese, A., Westaway, D., and Kretzschmar, H. (1997). The cellular prion protein binds copper in vivo. Nature *390*, 684.

Bueler, H., Fischer, M., Lang, Y., Bluethmann, H., Lipp, H., Dearmond, S.J., Prusiner, S.B., Aguet, M., and Weissmann, C. (1992). Normal development and behaviour of mice lacking the neuronal cell-surface PrP protein. Nature *356*, 577-582.

Camps, M., Nichols, A., and Arkinstall, S. (2000). Dual specificity phosphatases: a gene family for control of MAP kinase function. FASEB J. *14*, 6-16.

Carimalo, J., Cronier, S., Petit, G., Peyrin, J.M., Boukhtouche, F., Arbez, N., Lemaigre-Dubreuil, Y., Brugg, B., and Miquel, M.C. (2005). Activation of the JNK-c-Jun pathway during the early phase of neuronal apoptosis induced by PrP 106-126 and prion infection. Eur. J. Neurosci. *21*, 2311.

Chang, L., and Karin, M. (2001). Mammalian MAP kinase signaling cascades. Nature *410*, 37-40.

Chesebro, B., Trifilo, M., Race, R., Meade-White, K., Teng, C., LaCasse, R., Raymond, L., Favara, C., Baron, G., Priola, S., Caughey, B., Masliah, E., and Oldstone, M. (2005). Anchorless prion protein results in infectious amyloid disease without clinical scrapie. Science *308*, 1435.

Chi, J., Van Leeuwen, J.A., Weersink, A., and Keefe, G.P. (2002). Direct production losses and treatment costs from bovine viral diarrhoea virus, bovine leukosis virus, *Mycobacterium avium* subspecies *paratuberculosis*, and *Neospora caninum*. Prev. Vet. Med. *55*, 137-153.

Chiarini L.B., Freitas A.R., Zanata S.M., Brentani R.R., Martins V.R., and Linden R. (2002). Cellular prion protein transduces neuroprotective signals. EMBO J. *21*, 3317–26.

Chiodini, R.J., Kruiningen, H.J., and Merkal, R.S. (1984). Ruminant paratuberculosis (Johne's disease): The current status and future prospects. Cornell Vet. *74*, 218-262.

Chow, C.W., Rincon, M., Cavanagh, J., Dickens, M., and Davis, R.J. (1997). Nuclear accumulation of NFAT4 opposed by the JNK signal transduction pathway. Science *278*, 1638-1641.

Christopoulos, A., Christopoulos, G., Morfis, M., Udawela, M., Laburthe, M., Couvineau, A., Kuwasako, K., Tilakaratne, N, and Sexton, P.M. (2002). Novel receptor partners and function of receptor activity-modifying proteins. J. Biol. Chem. *278*, 3293-3297.

Cohen, P. (2002). Protein kinases–the major drug targets of the twenty-first century? Nat. Rev. Drug Discov. *1*, 309–315.

Collart, M.A., Belin, D., Vassalli, J.D., de Kossodo, S., and Vassalli, P. (1986). Gamma interferon enhances macrophage transcription of the tumor necrosis factor/cachectin, interleukin 1, and urokinase genes, which are controlled by short-lived repressors. J. Exp. Med. *164*, 2113-2118.

Collins, F.S., and McKusick, V.A. (2001). Implications of the human genome project for medical science. J. Am. Med. Assoc. *305*, 2257-2368.

Cooper, A.M., Dalton, D.K., Stewart, T.A., Griffin J.P., Russell, D.G., and Orme, I.M. (1993). Disseminated tuberculosis in interferon gamma gene disrupted mice. J. Exp. Med. *178*, 2243-2247.

Cori, G.T. and Green, A.A. (1943). Crystalline muscle phosphorylase I preparation, properties, and molecular weight. J. Biol. Chem. *151*, 21-29.

Coussens, P.M., Verman, N., Coussens, M.A., Elftman, M.D., and McNulty, A.M. (2004). Cytokine gene expression in peripheral blood mononuclear cells and tissues of cattle infected with *Mycobacterium avium* subsp. *paratuberculosis*: evidence for an inherent proinflammatory gene expression pattern. Infect. Immun. *72*, 1409-1422.

Dalton, D.K., Pitts-Meek, S., Keshav, S., Figari, I.S., Bradley, A., and Stewart, T.A. (1993). Multiple defects of immune cell function in mice with disrupted interferon-gamma genes. Science *259*, 1739-1742.

Darnell, J.E. (1997). STATS and gene regulation. Science *277*, 1630–1635.

Darnell, J.E., Kerr, I.M., and Stark, G.R. (1994) Jak-STAT pathways and transcription activation is response to IFNs and other extracellular signaling proteins. Science *264*, 1415-1421.

Denis, M., Gregg, E.O., and Ghandirian, E. (1990). Cytokine modulation of *Mycobacterium tuberculosis* growth in human macrophages. Int. J. Immunopharmacol. *12*, 721-727.

Diks, S. H., Kok, K., O'Toole, T., Hommes, D. W., van Dijken, P., Joore, J., and Peppelenbosch, M. P. (2004). Kinome profiling for studying lipopolysaccharide signal transduction in human peripheral blood mononuclear cells. J. Biol. Chem. *279*, 49206-49213.

Doffinger, R., Jouanguy, E., Dupuis, S., Fondane`che, M., Stephan, K., Emile, J., Lamhamedi-Cherradi, S., Altare, F., Pallier, A., Barcenas-Morales, G., Meinl, E., Krause, C., Pestka, S., Schreiber, R.D., Novelli, F., and Casanova, J.L. (2000). Partial interferon-gamma receptor signaling chain deficiency in a patient with bacilli Calmette-Guerin *Mycobacterium* abscesses infection. J. Infect. Dis. *181*, 379-384.

Dorman, S.E., and Holland, S.M. (1998). Mutation in the signal-transducing chain of the interferon-gamma receptor and suseptibility to mycobacterial infection. J. Clin. Invest. *101*, 2364–2369.

Draghici, S. (2003). Elements of statistics. Data analysis tools for DNA microarrays, Etheridge, A.M., *et al.*, eds. (Boca Raton, Fla: Chapman & Hall/CRC), pp. 61-107.

Druker, B., Talpaz, M., Resta, D., Peng, B., Buchdunger, E., Ford, J.M., Lydon, N.B., Kantarjian, H., Capdeville, R., Ohno-Jones, S., and Sawyers, C.L. (2001). Efficacy and safety of a specific inhibitor of the BCR-ABL tyrosine kinase in chronic myeloid leukemia. N. Engl. J. Med. *2*, 561-566.

Druker, B., Tamura, S., Buchdunger, E., Ohno, S., Segal, G.M., Fanning, S., Zimmermann, J., and Lydon, N.B. (1996). Effects of a selective inhibitor of the Abl tyrosine kinase on the growth of Bcr-Abl positive cells. Nat. Med. *2*, 561-566.

Dupuis, S., Doffinger, R., Picard, C., Fieschi, C., Altare, F., Jouanguy, E., Abel, L. and Casanova, J.L. (2000). Human interferon-gamma-mediated immunity is a genetically controlled continuous trait that determines the outcome of mycobacterial invasion. Immunol. Rev. *178*, 129-137.

Eckner, R., Ewen, M.E., Newsome, D., Gerdes, M., DeCaprio, J.A., Lawrence, J.B., and Livingston, D.M. (1994). Molecular cloning and functional analysis of the adenovirus E1A-associated 300-kD protein (p300) reveals a protein with properties of a transcriptional adaptor. Genes. Dev. *8*, 869–884.

Edenhofer F., Rieger R., Famulok M., Wendler W., Weiss S., and Winnacker E.L. (1996). Prion protein PrP^C interacts with molecular chaperones of the Hsp60 family. J. Virol. *70*, 4724–28.

Eglen, R. M. and Reisine, T. (2009). The current status of drug discovery against the human kinome. Assay Drug Dev. Techn. *7*, 22-43.

Eisen M.B., Spellman P.T., Brown P.O., and Botstein D. (1998). Cluster analysis and display of genome-wide expression patterns. Proc. Natl. Acad. Sci. USA. *95*, 14863-8.

Elchebly, M., Payette, P., Michaliszyn, E., Cromlish, W., Collins, S., Loy, A.L., Normandin, D., Cheng, A., Himms-Hagen, J., Chan C.C., Ramachandran, C., Gresser, M., Tremlay, M.L., and Kennedy, B.P. (1999). Increased insulin sensitivity and obesity resistance in mice lacking the protein tyrosine phosphatase-1B gene. Science *283*, 1544-1548.

Ellis, J.A., Godson, D., Campos, M., Sileghem, M., and Babiuk, L.A. (1993). Capture immunoassay for ruminant tumor necrosis factor-α: comparison with bioassay. Vet Imm. Immunopath. *35*, 289-300.

Eltholth, M.M., Marsh, V.R., Van Winden, S., Guitian, F.J. (2009). Contamination of food products with *Mycobacterium avium paratuberculosis*: a systematic review. J. Appl. Microbiol. *107*, 1061-1071.

Everitt B. (1974). Cluster Analysis. (London: Heinemann Education).

Fabrizi, C., Silei, V., Menegazzi, M., Salmona, M., Bugiani, O., Tagliavini, F., Suzuki, H., and Lauro, G.M. (2001). The stimulation of inducible nitric-oxide synthase by the prion protein fragment 106-126 in human microglia is tumor necrosis factor-α-dependent and involves p38 mitogen-activated protein kinase. J. Biol. Chem. *276*, 25692.

Falsey, J. R., Renil, M., Park, S., Li, S., and Lam, K. S. (2001). Peptide and small molecule microarray for high throughput cell adhesion and functional assays. Bioconjug. Chem. *12*, 346- 353.

Ferrari, G., Langen, H., Naito, M., and Pieters, J. (1999). A coat protein on phagosomes involved in the intracellular survival of mycobacteria. Cell *97*, 435-447.

Ferreiro, E., Oliveira, C.R., and Pereira, C.M.F. (2008). The release of calcium from the endoplasmic reticulum induced by amyloid-beta and prion peptides activates the mitochondrial apoptotic pathway. Neurobiol. Dis. *30*, 331-342.

Fischer, E. H. and Krebs, E. G. (1955). Conversion of phosphorylase b to phosphorylase a in muscle extracts. J. Biol. Chem. *216*, 121-132.

Fletcher H.A., Keyser A., Bowmaker M., Sayles P.C., Kaplan G., Greg, H., Adrian, H., and Willem, H. (2009). Transcriptional profiling of mycobacterial antigen-induced responses in infants vaccinated with BCG at birth. BMC Med. Genomics. *2*, 10.

Flynn, J.L., Chan, J., Triebold, K.J., Dalton, D.K., Stewart, T.A., and Bloom, B.R. (1993). An essential role for interferon gamma in resistance to *Mycobacterium tuberculosis* infection. J. Exp. Med. *178*, 2249-2254.

Frank, R. (1992). SPOT synthesis: an easy technique for the positionally addressable, parallel chemical synthesis on a membrane support. Tetrahedron. *48*, 9217-9232.

Fratti, R.A., Backer, J.M., Gruenberg, J., Corvera, S., and Deretic, V. (2001). Role of phosphatidylinositol 3-kinase and Rab5 effectors in phagosomal biogenesis and mycobacterial phagosome maturation arrest. J. Cell Biol. *154*, 631.

Fujii, N., Yokosawa, N., and Shirakawa, S. (1999). Suppression of interferon response gene expression in cells persistently infected with mumps virus, and restoration from its suppression by treatment with ribavirin. Virus Res. *65*, 175–185.

Gehring, A.J., Rojas, R.E., Canaday, D.H., Lakey, D.L., Harding, C.V., and Boom, W.H. (2003). The *Mycobacterium tuberculosis* 19-kilodalton lipoprotein inhibits gamma interferon-regulated HLA-DR and FcgammaR1 on human macrophages through toll-like receptor 2. Infect. Immun. *71*, 4487–4497.

Gelderblom, H., Hogendoorn, Dijkstra, S.D., van Rikswijk, C.S., Krol, A.D., Taminiau, A.H.M., and Bovee, J.V.M.G. (2007) The clinical approach towards chondrosarcoma. Oncologist *13*, 320-329.

Goren, M.B., Vatter, A.E., and Fiscus, J. (1987). Polyanionic agents do not inhibit phagosome-lysosome fusion in cultured macrophages. J. Leukoc. Biol. *41*, 122–129.

Gorg, A., Weiss, W., and Dunn, M.J. (2004). Current two-dimensional electrophoresis technology for proteomics. Proteomics *4*, 3665-3685.

Graner E., Mercadante A.F., Zanata S.M., Forlenza O.V., Cabral A.L., Veiga, S.S., Juliana, M.A., Roesler, R., Walz, R., Minetti, A., Izquierdo, I., Martins, V.R. and Brentani, R.R. (2000). Cellular prion protein binds laminin and mediates neuritogenesis. Mol. Brain Res. *76*, 85–92.

Greenlund, A.C., Morales, M.O., Viviano, B.L., Yan, H., Krolewski, J., and Schreiber, R.D. (1995). Stat recruitment by tyrosine-phosphorylated cytokine receptors: an ordered reversible affinity-driven process. Immunity *2*, 677–687.

Hanks, S.K., and Hunter, T. (1995). The eukaryotic protein kinase superfamily: kinase (catalytic) domain structure and classification. FASEB J. *9*, 576-596.

Hartigan J.A. (1975). Clustering algorithms. (New York: Wiley).

Heitman, J., Movva, N.R. and Hall, M.N. (1991). Targets for cell cycle arrest by the immunosuppressant rapamycin in yeast. Science *253*, 905–909.

Hemmi, H., Takeuchi, O., Kawai, T., Kaisho, T., Sato, S., Sanjo, H., Matsumoto, M., Hoshino, K., Wagner, H., Takeda, K., and Akira, S. (2000). A Toll-like receptor recognizes bacterial DNA. Nature *408*, 740-745.

Hines, M.E., Stiver, S., Giri, D., Whittington, L., Watson, C., Johnson, J., Musgrove, J., Pence, M., Hurley, D., Baldwin, C., Gardner, I.A., and Aly, S. (2007). Efficacy of sphereoplastic and cell-wall competent vaccines for *Mycobacterium avium* subsp. *paratuberculosis* in experimentally-challenged baby goats. Vet. Microbiol. *120*, 261-283.

Holter, W., Goldman, C.K., Casabo, L., Nelson, L., Greene, W.C., and Waldmann, T.A. (1987). Expression of functional IL 2 recpetors by lipopolysaccharide and interferon-gamma stimulated human monocytes. J. Immunol. *138*, 2917-2922.

Hopkins, A.L. and Groom, C.R. (2002). The druggable genome. Nat. Rev. Drug Discov. *1*, 727–730.

Houseman, B.T., Huh, J.H., Kron, S.J., and Mrksich, M. (2002). Peptide chips for the quantitative evaluation of protein kinase activity. Nature Biotech. *20*, 270-274.

Huber W., von Heydebreck A., Sueltmann H., Poustka A., and Vingron M. (2003). Parameter estimation for the calibration and variance stabilization of microarray data. Stat. Appl. Genet. Mol. Biol. *2*, Article 3.

Hunter, T. (1995). Protein kinases and phosphatases: the yin and yang of protein phsophorylation and signaling. Cell *80*, 225-236.

Hussain, S., Zwilling, B.S., and Lafuse, W.P. (1999). *Mycobacterium avium* infection of mouse macrophages inhibits IFN-gamma Janus kinase-STAT signaling and gene induction by down-regulation of the IFN-gamma receptor. J. Immunol. *163*, 2041–2048.

Igarashi, K., Garotta, G., Ozmen, L., Ziemiecki, A., Wilks, A.F., Harpur, A.G., Larner, A.C., and Finbloom, D.S. (1994). Interferon-gamma induces tyrosine phosphorylation of interferon-gamma receptor and regulated association of protein tyrosine kinases, Jak1 and Jak2, with its receptor. J. Biol. Chem. *269*, 14333–14336.

Indrigo, J., Hunter, R.L., Jr, and Actor, J.K. (2002). Influence of trehalose 6,6′-dimycolate (TDM) during mycobacterial infection of bone marrow macrophages. Microbiology *148*, 1991–1998.

Jalal, S., Arsenault, R., Potter, A.A., Babiuk, L.A., Griebel, P., and Napper, S. (2009). Genome to kinome: species-specific peptide arrays for kinome analysis. Science Sig. *2*, l1.

Jalal, S., Kindrachuk, J. and Napper, S. (2007). Phosphoproteome and kinome analysis: unique perspectives on the same problem. Curr. Anal. Chem. *3*, 1-15.

Joseph, T.D., and Look, D.C. (2001). Specific inhibition of interferon signal transduction pathways by adenoviral infection. J. Biol. Chem. *276*, 47136-47142.

Jouanguy, E., Lamhamedi-Cherradi, S., Lammas, D., Dorman, S.E., Fondaneche, M.C., Dupuis, S., Doffinger, R., Altare, F., Girdlestone, J., Emile, J.F., Ducoulombier, H., Edgar, D., Clarke, J., Oxelius, V.A., Brai, M., Novelli, V., Heyne, K., Fischer, A., Holland, S.M., Kumararatne, D.S., Schreiber, R.D., and Casanova, J.L. (1999). A human IFNGR1 small deletion hotspot associated with dominant susceptibility to mycobacterial infection. Nat. Genet. *21*, 370-378.

Kalume, D. E., Molina, H. and Pandey, A. (2004). Tackling the phosphoproteome: tools and strategies. Curr. Opin. Chem. Biol. *7*, 64-69.

Kanehisa, M., and Goto, S. (2000). KEGG: Kyoto encyclopedia of genes and genomes. Nucleic Acids Res. *28*, 37-30.

Karakousis, P.C., Bishai, W.R., and Dorman, S.E. (2004). *Mycobacterium tuberculosis* cell envelope lipids and the host immune response. Cell Microbiol. *6*, 105-116.

Keri, G., Orfi, L., Eros, D., Hegymegi-Barakonyi, B., Szantai-Kis, C., Horvath, Z., Waczek, F., Marosfalvi, J., Szabadkai, I., Pato, Janos, Greff, Z., Hafenbradl, D., Daub, H., Muller, G., Klebl, B., and Ullrich, A. (2006). Signal transduction therapy with rationally designed kinase inhibitors. Curr. Signal Transd. T. *1*, 67-95.

Khosravani, H., Zhang, Y., Tsutsui, S., Hameed, S., Altier, C., Hamid, J., Chen, L., Villemaire, M., Ali. Z., Kirik, F.R., and Zamponi, G.W. (2008). Prion protein excitotoxicity by inhibiting NMDA receptors. J. Cell. Biol. *181*, 551-565.

Kierszenbaum, F., Lopez, H.M., Tanner, M.K., Sztein, M.B. (1995). *Trypanosoma cruzi*-induced decrease in the level of interferon-gamma receptor expression by resting and activated human blood lymphocytes. Parasite Immunol. *17*, 207–214.

Kim, Y., Huang, J., Cohen, P., and Matthews, H.R. (1993). Protein phosphatases 1, 2A and 2C are protein histidine phosphatases. J. Biol. Chem. *268*, 18513-18518.

Kinoshita, E., Takahashi, M., Takeda, H., Shira, M., and Koike, T. (2004). Recognition of phosphate monoester dianion by alkoxide-bridged dinuclear zinc(II) complex. Dalton T. *8*, 1189-1193.

Knight, Z.A., Lin, H., and Shokat, K.M. (2010). Targeting the cancer kinome through polypharmacology. Nat. Rev. Cancer *10*, 130-137.

Knutson, K.L., Hmama, Z., Herrera-Velit, P., Rochford, R., and Reiner, N.E. (1998). Lipoarabinomannan of *Mycobacterium tuberculosis* promotes protein tyrosine dephosphorylation and inhibition of mitogen-activated protein kinase in human mononuclear phagocytes. Role of the Src homology 2 containing tyrosine phosphatase 1. J. Biol. Chem. *273*, 645–652.

Knuutila, S., Bjorkqvist, A. M., Autio, K., Tarkkaqnen, M., Wolf, M., Monni, O., Szymanska, J., Larramendy, M.L., Tapper, J., Pere, H., El-Rifai, W., Hemmer, S., Wasenius, V.M., Vidgren, V., and Zhu, Y. (1998). DNA copy number amplifications in human neoplasms: review of comparative genomic hybridization studies. Am. J. Pathol. *152*, 1107-1123.

Koul, A., Choidas, A., Treder, M., Tyagi, A.K., Drlica, K., Singh, Y., and Ullrich, A. (2000). Cloning and characterization of secretory tyrosine phosphatases of *Mycobacterium tuberculosis*. J. Bacteriol. *182*, 5425-5432.

Koul, A., Herget, T., Klebl, B., and Ullrich, A. (2004). Interplay between mycobacteria and host signaling pathways. Nat. Rev. Microbiol. *2*, 189-202.

Krebs, E. G. and Fischer, E. H. (1955). Phosphorylase activity of skeletal muscle extracts. J. Biol. Chem. *216*, 113-120.

Krebs, E. G. and Fischer, E. H. (1956). The phosphorylase b to a converting enzyme of rabbit skeletal muscle. Biochim. Biophys. Acta. *20*, 150-157.

Kreegipuu, A., Blom, N., Brunak, S. and Jarv, J. (1998). Statistical analysis of protein kinase specificity determinants. FEBS Letters *430*, 45-50.

Kristensson, K., Feuerstein, B., Taraboulos, A., Hyun, W.C., Prusiner, S.B., and DeArmond, S.J. (1993). Scrapie prions alter receptor-mediated calcium responses in cultured cells. Neurology *43*, 2335.

Lee, H.P., Jun, Y.C., Choi, J.K., Kim, J.L., Carp, R.I., and Kim, Y.S. (2005). Activation of mitogen-activated protein kinases in hamster brains infected with 263K scrapie agent. J. Neurochem. *95*, 584.

Lee, J. C., Laydon, J. T., McDonnell, P. C., Gallagher, T. F., Kumar, S., Green, D., Mcnulty, D., Blumenthal, M.J., Keys, J.R., Vatter, S.W.L., Strickler, J.E., McLaughlin, M.M., Siemens, I.R., Fisher, S.M., Livi, G.P., White, J.R., Adams, J.L., and Young, P.R. (1994). A protein kinase involved in the regulation of inflammatory cytokine biosynthesis. Nature *372*, 739–746.

Lesaicherre, M. L., Uttamchandani, M., Chen, G. Y., and Yao, S. Q. (2002). Antibody-based fluorescence detection of kinase activity on a peptide array. Bioorg. Med. Chem. Lett. *12*, 2085- 2088.

Liu, J., Farmer J. D., Lane, W. S., Friedman, J., Weissman, I., and Schreiber, S.L. (1991). Calcineurin is a common target of cyclophilin–cyclosporin A and FKBP–FK506 complexes. Cell. *166*, 807–815.

Look, D.C., Roswit, W.T., Frick, A.G., Gris-Alevy, Y., Dickhaus, D.M., Walter, M.J., and Holtzman, M.J. (1998). Direct suppression of Stat1 function during adenoviral infection. Immunity. *9*, 871–880.

Lowenberg M., Tuynman J., Scheffer M., Verhaar A., Vermeulen L., van Deventer, S., Hommes, D., and Peppelenbosch, M. (2006). Kinome analysis reveals nongenomic glucocorticoid receptor-dependent inhibition of insulin signaling. Endocrinology *147*, 3555-3562.

Lynn, D. J., Winsor, G. L., Chan, C., Richard, N., Laird, M. R., Barsky A., Gardy, J.L., Roche, F.M., Chan, T.H.W., Shah, N., Lo, R., Naseer, M., Que, J., Yau, M., Acad, M., Tulpan, D., Whiteside, M.D., Chikatamarla, A., Mah, B., Munzner, T., Hokamp, K., Hancock, R.E.W., and Brinkman, F.S.L. (2008) InnateDB: facilitating systems-level analysis of the mammalian innate immune response. Mol. Syst. Biol.. *4*, 1-11.

MacBeath, G., and Schreiber, S. L. (2000). Printing proteins as microarrays for high-throughput function determination. Science *289*, 1760-1763.

Maehama, T., Okahara, F., and Kanaho, Y. (2004). The tumor supressor PTEN: involvement of a tumour supressor candidate proteína in PTEN turnover. Biochem. Soc. T. *32*, 343-347.

Maness, P.F., and Schachner, M. (2007). Neural recognition molecules of the immunoglobulin superfamily: signaling transducers of axon guidance and neuronal migration. Nat. Neurosci. *10*, 19–26.

Mann, M., Ong, S. E., Gronborg, M., Steen, H., Jensen, O.N., and Pandey, A. (2002). Analysis of protein phosphorylation using mass spectrometry: deciphering the phosphoproteome. Trends Biotechnol. *20*, 261.

Manning, G. and Caenepeel, S. (2005). Encyclopedia of protein kinases in human diseases. Catalog Reference Manual. (Beverly, MA: Cell Signaling Technology).

Manning, G., Whyte, D.B., Martinez, R., Hunter, T. and Sudarsanam, S. (2002). The protein kinase complement of the human genome. Science *298*, 1912-1934.

Mardia, K.V., Kent, J.T., and Bibby, J.M. (1979). Multivariate analysis. (London: Academic Press).

Marella, M., Gaggioli, C., Batoz, M., Deckert, M., Tartare-Deckert, S., and Chabry, J. (2005). Pathological prion protein exposure switches on neuronal mitogen-activated protein kinase pathway resulting in microglia recruitment. J. Biol. Chem. *280*, 1529-34.

Martin, K., Steinberg, T.H., Cooley, L.A., Gee, K.R., Beechem, J.M., and Patton, W.F. (2003a). Quantitative analysis of protein phosphorylation status and protein kinase activity on microarrays using a novel fluorescent phosphorylation sensor dye. Proteomics *3*, 1244-1255.

Martin, K., Steinberg, T.H., Goodman, T., Schulenberg, B., Kilgore, J.A., Gee, K.R., Beechem, J.M., and Patton, W.F. (2003b). Strategies and solid-phase formats for the analysis of protein and peptide phosphorylation employing a novel fluorescent phosphorylation sensor dye. Comb. Chem. High T. Scr. *6*, 331-339.

Mastro, A.M., and Sniezek, M.J. (1982). Utilization of $\gamma\text{-}^{32}$P-GTP by ectoprotein kinase of 3T3 and SV40 3T3 cells. Cell Biol. Int. Rep. *6*, 385-392.

Mattei, V., Garofalo, T., Misasi, R., Circella, A., Manganelli, V., Lucania, G., Pavan, A., and Sorice, M. (2004). Prion protein is a component of the multimolecular signaling complex involved in T cell activation. FEBS Lett. *560*, 14–18.

McGuire, K., Jones, M., Werling, D., Williams, J.L., Glass, E.J., and Jann, O. (2006) Radiation hybrid mapping of all 10 characterized bovine Toll-like receptors. Anim. Genet. *37*, 47-50.

McQuitty, L.L. (1966). Similarity analysis by reciprocal pairs for discrete and continuous data. Educ. Psychol. Meas. *26*, 825-831.

Miller, D.M., Rahill, B.M., Boss, J.M., Lairmore, M.D., Durbin, J.E., Waldman, W.J., and Sedmak, D.D. (1998). Human cytomegalovirus inhibits major histocompatibility complex II expression by disruption of the Jak/Stat pathway. J. Exp. Med. *187*, 675–683.

Momotani, E., Whipple, D.L., Thiermann, A.B., and Cheville, N.F. (1988). Role of M cells and macrophages in the entrance of *Mycobacterium paratuberculosis* into domes of ileal Peyer's patches in calves. Vet. Pathol. *25*, 131-137.

Monnet, C., Gavard, J., Mege, R.M., and Sobel, A. (2004). Clustering of cellular prion protein induces ERK1/2 and stathmin phosphorylation in GT1-7 neuronal cells. FEBS letters, *576*, 114.

Mouillet-Richard, S., Ermonval, M., Chebassier, C., Laplanche, J.L., Lehmann, S., Launay, J.M., and Kellermann, O. (2000). Signal transduction through prion protein. Science *289*, 1925-1928.

Niefind, K., Putter, M., Guerra, B., Issinger, O.G., and Schomburg, D. (1999). GTP plus water mimic ATP in the active site of protein kinase CK2. Nat. Struct. Biol. *6*, 1100-1103.

Nigou, J., Zelle-Rieser, C., Gilleron, M., Thurnher, M., and Puzo, G. (2001). Mannosylated lipoarabinomannans inhibit IL-12 production by human dendritic cells: evidence for a negative signal delivered through the mannose receptor. J. Immunol. *166*, 7477–7485.

Nixon, R.R. (2005). Prion-associated increases in Src-family kinases. J. Biol. Chem. *280*, 2455.

Noble, M., Endicott, J., and Johnson, L. (2004). Protein kiase inhibitors: insights into drug design from structure. Science *303*, 1800-1805.

Noss, E.H., Pai, R.K., Sellati, T.J., Radolf, J.D., Belisle, J., Golenbock, D.T., Boom, W.H., and Harding, C. (2001). Toll-like receptor 2-dependent inhibition of macrophage class II

MHC expression and antigen processing by 19-kDa lipoprotein of *Mycobacterium tuberculosis*. J. Immunol. *167*, 910–918.

O'Donovan, C.N., Tobin, D., and Cotter, T.G. (2001). Prion protein fragment PrP-(106-126) induces apoptosis via mitochondrial disruption in human neuronal SH-SY5Y cells. J. Biol. Chem. *276*, 43516.

Ojida, A., Mito-oka, Y., Inoue, M., and Hamachi, I. (2002). First artificial receptors and chemosensors toward phosphorylated peptide in aqueous solution. J. Am. Chem. Soc. *124*, 6256-6258.

Okabayashi, T., Kariwa, H., Yokota, S., Iki, S., Indoh, T., Yokosawa, N., Takashima, I., Tsutsumi, H., and Fujii, N. (2006). Cytokine regulation in SARS *coronavirus* infection compared to other respiratory virus infections. J. Med. Virol. *78*, 417–424.

Olsen, I., Tollefsen, S., Aagaard, C., Reitan, L.J., Bannantine, J.P., Andersen, P., Sollid, L.M., Lundin, K.E. (2009). Isolation of *Mycobacterium avium* subspecies *paratuberculosis* reactive CD4 T cells from intestinal biopsies of Crohn's disease patients. PLoS One *4*, e5641.

Ostlund, P., Lindegren, H., Pettersson, C., and Bedecs, K. (2001). Altered insulin receptor processing and function in scrapie-infected neuroblastoma cell lines. Mol. Brain Res. *97*, 161-170.

Ouyang, Z., Takats, Z., Blake, T. A., Gologan, B., Guymon, A.J., Wiseman, J.M., Oliver, J.C., Davisson, V.J., and Cooks, R.G. (2003). Preparing protein microarrays by soft-landing of mass-selected ions. Science *301*, 1351-1354.

Pabst, M.J., Gross, J.M., Brozna, J.P., and Goren, M.B. (1988). Inhibition of macrophage priming by sulfatide from *Mycobacterium tuberculosis*. J. Immunol. *140*, 634–640.

Paitel, E., Fahraeus, R., and Checler, F. (2003). Cellular prion protein sensitizes neurons to apoptotic stimuli through Mdm2-regulated and p53-dependent caspase 3-like activation. J. Biol. Chem. *278*, 10061-10066.

Panse, S., Dong, L., Burian, A., Carus, R., Schutkowski, M., Reimer, U., and Schneider-Mergener, J. (2004). Profiling of generic anti-phosphopeptide antibodies and kinases with peptide microarrays using radioactive and fluorescence-based assays. Mol. Divers *8*, 291-299.

Pauli, E.K., Schmolke, M., Wolff, T., Viemann, D., Roth, J., Bode, J.G., and Ludwig, S. (2008). *Influenza A* virus inhibits type I IFN signaling via NF-kB dependent induction of SOCS-3 expression. PLoS Pathog. *4*, e1000196.

Pearson, K. (1896). Mathematical contributions to the theory of evolution. III. Regression, heredity and panmixia. Philos. T. R. Soc. Lond. *187*, 253-318.

Pelech, S., and Zhang, H. (2008). Antibody-based proteomics analysis of tumor cell signaling pathways. Principles of Molecular Oncology, Third Edition, M.G. Bronchud *et al.*, eds. (Totowa, NJ: Humana Press Inc.), pp. 117-134.

Pertea, M., and Salzberg, S.L. (2010). Between a chicken and a grape: estimating the number of human genes. Genome Biol. *11*, 206.

Pierce, E.S (2010). Ulcerative colitis and Crohn's disease: is *Mycobacterium avium* suspecies *paratuberculosis* the common villain? Gut. Pathog. *2*, 21.

Pietri, M., Caprini, A., Mouillet-Richard, S., Pradines, E., Ermonval, M., Grassi, J., Kellermann, O., and Schneider, B. (2006). Overstimulation of PrP[C] signaling pathways by prion peptide 106-126 causes oxidative injury of bioaminergic neuronal cells. J. Biol. Chem. *281*, 28470.

Pike, L.J., (2005). Growth factor receptors, lipid rafts and caveolae: an evolving story. Biochim. Biophys. Acta. Mol. Cell Res. *1746*, 260.

Post, F.A., Manca, C., Neyrolles, O., Ryffel, B., Young, D.B., and Kaplan, G. (2001). *Mycobacterium tuberculosis* 19-kilodalton lipoprotein inhibits *Mycobacterium smegmatis*-induced cytokine production by human macrophages in vitro. Infect. Immun. *69*, 1433–1439.

Povey, A.C. and Cooper, D.P. (1995) The development, validation and application of a 32P-postlabelling assay to quantify O6-methylguanine in human DNA. Carcinogenesis. *16*, 1665-1669.

Prusiner, S.B. (1982). Novel proteinaceous infectious particles cause scrapie. Science *216*, 136.

Rani, P.S., Sechi, L.A., and Ahmed, N. (2010). *Mycobacterium avium* subsp. *paratuberculosis* is a trigger of type-1 diabetes: destination Sardinia, or beyond. Gut Pathog. *2*, 1.

Ray, M., Gam, A.A., Boykins, R.A., and Kenney, R.T. (2000). Inhibition of interferon-gamma signaling by *Leishmania donovani*. J. Infect. Dis. *181*, 1121–1128.

Rieger, R., Edenhofer, F., Lasmezas, C.I., and Weiss, S. (1997). The human 37-kDa laminin receptor precursor interacts with the prion protein in eukaryotic cells. Nat. Med. *3*, 1383-1388.

Ritsema, T., Joore, J., van Workum, W., and Pieterse, C.J.M. (2007). Kinome profiling of *Arabidopsis* using arrays of kinase consensus substrates. Plant Methods *3*, 3.

Robertson, A.K., and Andrew, P.W. (1991) Interferon gamma fails to activate human monocyte-derived macrophages to kill or inhibit the replication of a non-pathogenic mycobacterial species. Microb. Pathog. *11*, 283-288.

Rosenshine, R., Duronio, V., and Finlay, B.B. (1992). Tyrosine protein kinase inhibitors block invasion-promoted bacterial uptake by epithelial cells. Infect. Immun. *60*, 2211-2217.

Roucou, X., and LeBlanc, A.C. (2005). Cellular prion protein neuroprotective function: implications in prion diseases. J. Mol. Med. *83*, 3.

Rubin, C.S., and Rosen, O.M. (1975) Protein phosphorylation. Annu. Rev. Biochem. *44*, 831-887.

Sasaki, Y., Suzuki, M., and Hidaka, H. (2002). The novel and specific Rho-kinase inhibitor (S)-(+)-2-methyl-1-[(4-methyl-5-isoquinoline)sulfonyl]-homopiperazine as a probing molecule for Rho-kinase-involved pathway. Pharmacol. Ther. *93*, 225–232.

Schmitt-Ulms, G., Legname, G., Baldwin, M.A., Ball, H.L., Bradon, N., Bosque, P.J., Crossin, K.L., Edelman, G.M., DeArmond, S.J., Cohen, F.E., and Prusiner, S.B. (2001). Binding of neural cell adhesion molecules (N-CAMs) to the cellular prion protein. J. Mol. Biol. *314*, 1209–25.

Schneider, B., Mutel, V., Pietri, M., Ermonval, M., Mouillet-Richard, S., and Kellermann, O. (2003). NADPH oxidase and extracellular regulated kinases 1/2 are targets of prion protein signaling in neuronal and nonneuronal cells. P. Natl. Acad. Sci. USA. *100*, 13326.

Schrage, Y.M., de-Bruijn, I.H.B, de Miranda, N.F.C.C., van Oosterwijk, J., Taminiau, A.H.M., van Wezel, T., Hogendoorn, P.C.W., and Bovee, J.V.M.G. (2009). Kinome profiling of chondrosarcoma reveals Src pathway activity and dasatinib as option for treatment. Cancer Res. *69*, 6216-6222.

Schreiber, M., Res, I., and Matter, A. (2009). Protein kinases as antibacterial targets. Curr. Opin. Cell Biol. *2*, 325-330.

Schulenberg, B., Goodman, T.N., Aggeler, R., Capaldi, R.A., and Patton, W.F. (2004). Characterization of dynamic and steady-state protein phosphorylation using fluorescent phosphoprotein gel stain and mass spectrometry. Electrophoresis *25*, 2526-2532.

Schutkowski, M., Reineke, U., and Reimer, U. (2005). Peptide arrays for kinase profiling. Chem. Bio. Chem. *6*, 513-521.

Secott, T.E., Lin, T.L., and Wu, C.C. (2004). *Mycobacterium avium* subsp. *paratuberculosis* fibronectin attachment protein facilies M-cell targeting and invasion through a fibronectin bridge with host integrins. Am. Soc. Microbiol. *72*, 3724-3732.

Sexton, P.M., Albiston, A., Morfis, M., and Tilakaratne, N. (2001). Receptor activity modifying proteins. Cellular Sig. *13*, 73-83.

Shannon P., Markiel A., Ozier O., Baliga N.S., Wang J.T., Ramage, D., Amin, N., Schwikowski, B., and Ideker, T. (2003). Cytoscape: a software environment for integrated models of biomolecular interaction networks. Genome Res. *13*, 2498-2504.

Shi, Y. (2009). Serine/threonine phosphatases: mechanism through structure. Cell. *139*, 468-484.

Shi, L., Jones, W.D., Jensen, R.V., Harris, S.C., Perkins, R.G., Goodsaid, F.M., Guo, L., Croner, L.J., Boysen, C., Fang, H., Qian, F., Amur, S., Bao, W., Barbacioru, C.C., Bertholet, V., Cao, X.M., Chu, T.M., Collins, P.J., Fan, X.H., Frueh, F.W., Fuscoe, J.C., Guo, X., Han, J., Herman, D., Hong, H., Kawasaki, E.S., Li, Q.Z., Luo, Y., Ma, Y., Mei, N., Peterson, R.L., Puri, R.K., Shippy, R., Su, Z., Sun, Y.A., Sun, H., Thorn, B., Turpaz, Y., Wang, C., Wang, S.J., Warrington, J.A., Willey, J.C., Wu, J., Xie, Q., Zhang, L., Zhang, L., Zhong, S., Wolfinger, R.D., and Tong, W. (2008) The balance of reproducibility, sensitivity, and specificity of lists of differentially expressed genes in microarray studies. BMC Bioinformatics *9*, S10.

Shin, A.R., Kim, H.J., Cho, S.N., Collins, M.T., Manning, E.J., Naser, S.A., and Shin, S.J. (2010). Identification of seroreactive proteins in the culture filtrate antigen of *Mycobacterium avium* ssp. *paratuberculosis* human isolates to sera from Crohn's disease patients. FEMS Immunol. Med. Microbiol. *58*, 128-137.

Shorter, J., and Lindquist, S. (2005). Prions as adaptive conduits of memory and inheritance. Nat. Rev. Genet. *6*, 435.

Singh, R., Rao, V., Shakila, H., Gupta, R., Khera, A., Dhar, N., Singh, A., Koul, A., Singh, Y., Naseema, M., Narayanan, P.R., Paramasivan, C.N., Ramanathan, V.D., and Tyagi, A.K. (2003). Disruption of mptpB impairs the ability of *Mycobacterium tuberculosis* to survive in guinea pigs. Mol. Microbiol. *50*, 751-762.

Siguroardottir, O.G., Bakke-McKellep, A.M., Djonne, B., and Evensen, O. (2005). *Mycobacterium avium* subsp. *paratuberculosis* enters the small intestinal mucosa of goat kids in areas with and without Peyer's patches as demonstrated with the everted sleeve method. Coll. Immu. Microbiol. Infec. Dis. *28*, 223-230.

Simons, K. and D. Toomre. (2000). Lipid rafts and signal transduction. Nat. Rev. Mol. Cell Biol. *1*, 31-39.

Smith, H., Peggie, M., Campbell, D.G., Vandermoere, F., Carrick, E., and Cohen, P. (2009) Identification of the phosphorylation sites of the E3 ubiquitin ligase Pellino that are critical for the activation by IRAK1 and IRAK4. P. Natl. Acad. Sci. USA. *106*, 4584-4590.

Smyth, G.K., Michaud, J., and Scott, H.S. (2005). Use of within-array replicate spots for assessing differential expression in microarray experiments. Bioinformatics *21*, 2067-75.

Solforosi, L., Criado, J.R., McGavern, D.B., Wirz, S., Sanchez-Alavez, M., Sugama, S., DeGiorgio, L.A., Volpe, B.T., Wiseman, E., Ablos, G., Masliah, E., Gilden, D., Oldstone, M.B., Conti, B., and Williamson, R.A. (2004). Cross-linking cellular prion protein triggers neuronal apoptosis *in vivo*. Science *303*, 1514-1516.

Sridevi, G., Rao, N.L., and Fung-Leung, W.P. (2007) IRAK1: a critical signaling mediator of innate immunity. Cell. Signal. *20*, 269-276.

Stabel, J.R. (1998). Johne's disease: A hidden threat. J. Dairy Sci. *81*, 283-288.

Steinberg, T.H., Agnew, B.J., Gee, K.R., Leung, W.Y., Goodman, T., Schulenberg, B., Hendrickson, J., Beechem, J.M., Haugland, R.P., and Patton, W.F. (2003). Global quantitative phosphoprotein analysis using multiplexed proteomics technology. Proteomics *3*, 1128-1144.

Storkebaum, E. (2004). VEGF: a critical player in neurodegeneration. J. Clin. Invest. *113*, 14.

Strom, A., Wang, G.S., Reimer, R., Finegood, D.T., and Scott, F.W. (2007). Pronounced cytosolic aggregation of cellular prion protein in pancreatic β -cells in response to hyperglycemia. Lab. Invest. *87*, 139-149.

Strumbo, B., Ronchi, S., Bolis, L.C., and Simonic, T. (2001). Molecular coloning of the cDNA coding for *Xenopus laevis* prion protein. FEBS Lett. *508*, 170-174.

Sweeney, R.W., Jones, D.E., Habecker, P., and Scott, P. (1998). Interferon-gamma and interleukin 4 gene expression in cows infected with *Mycobacterium paratuberculosis*. Am. J. Vet. Res. *59*, 842-847.

Tagliavini, F., Prelli, F., Verga, L., Giaccone, G., Sarma, R., Gorevic, P., Ghetti, B., Passerini, F., Ghibaudi, E., and Forloni, G. (1993). Synthetic peptides homologous to prion protein residues 106-147 form amyloid-like fibrils in vitro. P. Natl. Acad. Sci. USA. *90*, 9678-9682.

Takeuchi, M., Alard, P., and Streilein, J.W. (1998). TGF-beta promotes immune deviation by altering accessory signals of antigen-presenting cells. J. Immunol. *160*, 1589–1597.

Thellung, S., Villa, V., Corsaro, A., Arena, S., Millo, E., Damonte, G., Benatti, U., Tagliavini, F., Florio, T., and Schettini, G. (2002) p38 MAP kinase mediates the cell death induced by PrP106–126 in the SH-SY5Y neuroblastoma cells. Neurobiol. Dis. *9*, 69.

Ting, L., Kim, A.C., Cattamanchi, A., Ernst, J.D. (1999). *Mycobacterium tuberculosis* inhibits IFN-gamma transcriptional responses without inhibiting activation of STAT1. J. Immunol. *163*, 3898–3906.

Turner-Brannen, E., Choi, K.Y.G., Arsenault, R., El-Gabalawy, H., Napper, S., and Mookherjee, N. (2011). Inflammatory cytokines IL-31 and IL-17 have common signaling intermediates despite differential dependence on TNF-Receptor 1. J. Immunol. *186*, 7127-7135.

van Baal, J.W.P.M., Diks, S.H., Wanders, R.J.A., Rygiel, A.M., Milano, F., Joore, J., Bergman, J.J.G.H.M., Peppelenbosch, M.P., and Krishnadath, K.K. (2006). Comparison of kinome profiles of Barrett's esophagus with normal squamous esophagus and normal gastric cardia. Cancer Res. *66*, 11605-11612.

Van den Broeke, A., Arsenault, R., Cleuter, Y., Dehouck, C., Martiat, P., Burny, A., Napper, S., and Griebel, P. (2011). Kinome profiling of bovine leukemia virus-induced ovine leukemia: an approach for identifying altered signaling pathways and drugable targets in cancer. JAIDS. *56*, 98.

Vassallo, N., Herms, J., Behrens, C., Krebs, B., Saeki, K., Onodera, T., Windl. O., and Kretzschmar, H.A. (2005). Activation of phosphatidylinositol 3 kinase by cellular prion protein and its role in cell survival. Biochem. Bioph. Res. Co. *332*, 75-82.

Vergne, I., Chua, J., Lee, H.H., Lucas, M., Belisle, J., and Deretic, V. (2005). Mechanism of phagolysosome biogenesis block by viable *Mycobacterium tuberculosis*. P. Natl. Acad. Sci. USA *102*, 4033-4038.

Weiss, D.J., and Souza, C.D. (2008). Review paper: modulation of mononuclear phagocyte function by *Mycobacterium avium* subsp. *paratuberculosis*. Vet. Pathol. *45*, 829-841.

Wenschuh, H., Volkmer-Engert, R., Schmidt, M., Schulz, M., Schneider-Mergener, J., and Reineke, U. (2000). Coherent membrane supports for parallel microsynthesis and screening of bioactive peptides. Biopolymers *55*, 188-206.

Whatley, S.A., Powell, J.F., Politopoulou, G., Campbell, I.C., Brammer, M.J., and Percy, N.S. (1995). Regulation of intracellular free calcium levels by the cellular prion protein. Neuroreport *6*, 2333.

Witten, D., and Tibshirani, R. (2007). A comparison of fold-change and the t-statistic for microarray data analysis. Stanford University.

Wolanin, P.M., Thomason, P.A., and Stock, J.B. (2002) Histidine protein kinases: key signal transducers outside the animal kingdom. Genome Biol. *3*, 3013.1-3013.8.

Woo, S.R., Heintz, J.A., Albrecht, R., Barletta, R.G., and Czuprynski, C.J. (2007). Life and death in bovine monocytes: the fate of *Mycobacterium avium* subsp. *paratuberculosis*. Microb. Pathog. *43*, 106-113.

Ying, H., Biroc, S.L., Li, W.W., Alicke, B., Xuan, J.A., Pagila, R., Ohashi, Y., Okada, T., Kamata, Y., and Dinter, H., (2006). The Rho kinase inhibitor fasudil inhibits tumor progression in human and rat tumor models. Mol. Cancer Ther. *5*, 2158.

Yokota, S., Yokosawa, N., Okabayashi, T., Suzutani, T., and Fujii, N. (2005). Induction of suppressor of cytokine signaling-3 by herpes simplex virus type 1 confers efficient viral replication. Virology *338*, 173–181.

Zachos, G., Koffa, M., Preston, C.M., Clements, J.B., and Conner, J. (2001). Herpes simplex virus type 1 blocks the apoptotics host cell defense mechanisms that target Bcl-2 and manipulates activation of p38 mitogen-activated protein kinase to improve viral replication. J. Virol. *75*, 2710-2728.

Zanata, S.M., Lopes, M.H., Mercadante, A.F., Hajj, G.N., Chiarini, L.B., Nomizo, R., Freitas, A.R.O., Cabral, A.L.B., Lee, K.S., Juliano, M.A., de Oliveria, E., Jachieri, S.G., Burlingame, A., Huang, L., Linden, R., Brentani, R.R., and Martins, V.R. (2002). Stress-inducible protein 1 is a cell surface ligand for cellular prion that triggers neuroprotection. EMBO J. *21*, 3307–3316.

Zhang, C.C., Steele, A.D., Lindquist, S., and Lodish, H.F. (2006). Prion protein is expressed on long-term repopulating hematopoietic stem cells and is important for their self-renewal. P. Natl. Acad. Sci. USA. *103*, 2184.

Zhang, H., Zha, X., Tan, Y., Hornbeck, P. V., Mastrangelo, A. J., Alessi, D. R., Polakiewicz, R. D., and Comb, M. J. (2002). Phosphoprotein analysis using antibodies broadly reactive against phosphorylated motifs. J Biol Chem *277*, 39379-39387.

Zhang, L., Goren, M.B., Holzer, T.J., and Andersen, B.R. (1988). Effect of *Mycobacterium tuberculosis*-derived sulfolipid I on human phagocytic cells. Infect. Immun. *56*, 2876–2883.

Zhao, D.C., Yan, T., Li, L., You, S., and Zhang, C. (2007). Respiratory syncytial virus inhibits interferon-alpha-inducible signaling in macrophage-like U937 cells. J. Infect. *54*, 393–398.

Zhu, H., Klemic, J. F., Chang, S., Bertone, P., Casamayor, A., Klemic, K.G., Smith, D., Gerstein, M., Reed, M.A., and Snyder, M. (2000). Analysis of yeast protein kinases using protein chips. Nat. Genet. *26*, 283-289.

Zimin, A.V., Delcher, A.L., Florea, L., Kelley, D.R., Schatz, M.C., Puiu, D., Hanrahan, F., Pertea, G., Van Tassell, C.P., Sonstegard, S., Marcais, G., Roberts, M., Subramanian, P., Yorke, J.A., and Salzberg, S.L. (2009). A whole-genome assembly of the domestic cow, *Bos taurus*. Genome Biol. *10*, R42.

8.0 APPENDIX

Table A1. Transformed peptide array data: prion project.

Name	ID	Target	PrP vs Scram		6H4 vs IgG1	
			p-value	Fold Change	*p*-value	Fold change
4E-BP1	Q13541	T46	0.295	1.214	0.233	-1.491
4E-BP1	Q13541	T37	0.359	-1.124	0.132	-1.543
Akt1	P31749	T308	0.438	-1.031	0.327	1.240
Akt1	P31749	S473	0.491	1.007	0.076	-1.709
Akt1	P31749	S124/9	0.386	-1.148	0.149	1.344
Akt1	P31749	Y326	0.319	-1.196	0.195	1.453
Akt3	Q9Y243	T447	0.451	-1.053	0.139	1.588
Akt3	Q9Y243	S120	0.223	-1.401	0.496	-1.004
APE1	P27695	S289	0.197	1.266	0.102	1.492
A-Raf	P10398	Y301	0.062	1.658	0.404	1.116
ASK1	Q99683	S1033	0.429	1.068	0.222	1.241
ASK1	Q99683	S83	0.355	1.216	0.422	1.050
ASK1	Q99683	S966	0.102	1.504	0.272	-1.338
ATF-2	P15336	T51/3/5	0.200	1.314	0.015	2.156
ATF-2	P15336	S44	0.190	1.321	0.207	1.311
ATF-4	P18848	S245	0.333	1.206	0.202	-1.505
axin-1	O15169	S486	0.422	-1.074	0.148	1.492
Bad	Q92934	S118	0.343	-1.155	0.175	-1.693
BATF	Q16520	T48	0.271	1.223	0.067	-1.501
BCAP	Q6ZUJ8	Y17	0.154	1.495	0.409	-1.062
BCAP	Q6ZUJ8	Y281	0.333	1.104	0.173	-1.283
Bid	P55957	T59	0.446	-1.035	0.414	1.106
BLNK	Q8WV28	Y72	0.290	-1.169	0.164	1.544
BLNK	Q8WV28	Y96	0.364	1.099	0.240	1.306
B-Raf	P15056	T598	0.263	-1.191	0.034	2.142
Btk	Q06187	Y223	0.164	1.208	0.418	1.091
Btk	Q06187	Y551	0.291	1.121	0.167	-1.449
Calmodulin	P62158	Y99	0.468	-1.021	0.359	-1.193
CaMK2-alpha	Q9UQM7	T286	0.074	-1.406	0.011	2.384
Casp3	P42574	S150	0.078	1.306	0.461	-1.039
Casp8	Q14790	S347	0.408	-1.063	0.372	1.102
CBP	Q92793	S2063	0.260	1.250	0.469	-1.036
CCR2	P41597	Y139	0.436	-1.079	0.118	1.456
CCR5	P51681	S336/7	0.439	1.065	0.488	-1.012

CCR7	P32248	S356/7	0.240	-1.420	0.361	1.127
CCR7	P32248	T372/3/4/5/7	0.326	1.144	0.448	-1.047
CD28	P10747	Y206/9	0.378	-1.109	0.147	1.404
CD45	P08575	S999/02/03	0.416	1.066	0.372	-1.221
CD45	P08575	Y1216	0.258	1.176	0.097	-1.978
Cdc25A	P30304	S82	0.205	1.424	0.295	1.235
Cdc25A	P30304	S88	0.067	1.904	0.063	-2.058
Cdc42	P60953	Y64	0.092	-1.437	0.490	1.012
CDK2	P24941	T160	0.166	-1.320	0.287	-1.272
CDK2	P24941	T14/5	0.181	-1.241	0.271	-1.227
CDK7	P50613	T170	0.027	-1.452	0.409	1.083
Cot	P41279	S400	0.375	1.101	0.500	1.000
CREB	P16220	S110/1	0.453	1.031	0.087	-1.844
CREB	P16220	S129	0.407	1.103	0.047	-2.207
Crk	P46108	Y221	0.255	-1.212	0.173	1.477
CSFR	P07333	Y561	0.437	1.061	0.425	1.062
CSFR	P07333	Y809	0.437	1.051	0.446	-1.050
CSK	P41240	Y184	0.457	-1.040	0.277	1.258
CTLA-4	P16410	Y201	0.017	-1.822	0.320	-1.185
CTNNB1	P35222	T41/45	0.405	1.087	0.131	1.404
CTNNB1	P35222	S33/37	0.066	1.998	0.489	-1.010
CTNNB1	P35222	Y142	0.147	-1.330	0.126	-1.264
CTNNB1	P35222	S675	0.333	-1.098	0.050	-1.522
CXCR4	P61073	Y157	0.258	-1.155	0.438	1.067
cyclin D1	P24385	T286/8	0.276	-1.193	0.351	-1.153
cyclin E1	P24864	T395	0.410	-1.071	0.012	-2.052
DAPK1	P53355	S308	0.323	1.187	0.370	-1.118
DAPK1	P53355	S735	0.372	-1.161	0.100	-1.487
DAPK3	O43293	T225	0.139	-1.243	0.147	1.419
DAPK3	O43293	T180	0.176	1.415	0.167	-1.519
DAPP1	Q9UHF2	Y139	0.230	-1.164	0.361	-1.127
Daxx	Q9UER7	S668/71	0.057	-1.305	0.385	1.157
DNA-PK	P78527	T2609	0.333	-1.095	0.423	-1.061
DNA-PK	P78527	T2638	0.364	-1.108	0.341	-1.116
DOCK2	Q5XG91	Y221/4	0.227	-1.216	0.451	1.039
Elk-1	P19419	T417	0.343	1.201	0.476	1.020
Elk-1	P19419	S389	0.101	1.656	0.429	-1.082
eNOS	P29474	S1176	0.403	1.056	0.013	-1.398
EphA1	P21709	Y781	0.356	-1.120	0.385	1.081

EphA2	P29317	Y594	0.398	1.107	0.231	-1.288
EphA2	P29317	Y772	0.176	1.572	0.163	-1.412
EphA2	P29317	Y588	0.146	1.372	0.035	-1.718
ERK1	P27361	T202/4	0.356	1.140	0.334	1.119
ERK2	P28482	Y205	0.434	-1.103	0.145	-1.222
ERK3	Q16659	S189	0.292	-1.119	0.234	-1.287
Etk	P51813	Y40	0.376	-1.159	0.019	-3.704
Ezrin	P15311	T566	0.146	1.313	0.167	1.334
FADD	Q13158	S194	0.489	-1.008	0.393	1.111
FADD	Q13158	S196	0.203	-1.332	0.079	-2.115
FAK	Q05397	Y397	0.470	1.029	0.182	1.473
Fas	P25445	Y232	0.479	1.016	0.414	-1.092
Fas	P25445	Y291	0.139	-1.481	0.201	-1.482
Fes	P07332	Y713	0.230	-1.283	0.434	-1.105
FGFR1	P11362	Y653/4	0.495	-1.003	0.099	1.559
FGFR1	P11362	Y154	0.211	-1.216	0.127	1.346
FGFR1	P11362	Y463	0.055	1.859	0.280	-1.186
FGFR3	P22607	Y724	0.364	1.110	0.496	1.004
FGFR3	P22607	Y760	0.292	1.221	0.283	-1.352
FGFR4	P22455	Y754	0.224	1.296	0.255	1.199
FLT3	P36888	Y589/91	0.397	1.093	0.096	1.486
FLT3	P36888	Y597/9	0.192	-1.435	0.109	-1.494
Fos	P01100	T232	0.382	-1.102	0.319	1.239
FRS2	Q8WU20	Y196	0.329	1.148	0.288	-1.409
FRS2	Q8WU20	Y436	0.412	1.029	0.029	-2.826
FRS3	Q8WU20	Y416	0.196	-1.302	0.220	-1.516
gp130	P40189	S782	0.325	-1.196	0.247	1.299
gp130	P40189	Y814	0.345	-1.104	0.474	1.035
gp130	P40189	Y767	0.240	1.236	0.371	-1.091
Grb10	Q13322	S150	0.354	1.090	0.029	2.310
GSK3-beta	P49840	S9	0.431	-1.048	0.290	1.223
GSK3-beta	P49840	Y216	0.102	1.471	0.435	1.069
HIF1A	Q16665	T796	0.234	1.279	0.294	-1.212
HIF2A	Q99814	T840	0.120	-1.572	0.123	1.369
HMGA1	P17096	T52	0.291	-1.226	0.327	-1.118
H-Ras-1	P01112	T35	0.253	1.413	0.256	1.433
HSP27	P04792	S78/82/3	0.067	-1.765	0.413	-1.075
HSP70	P08107	Y525/6	0.197	-1.335	0.285	1.241
IFNAR1	P17181	S535	0.408	1.096	0.340	1.080

IFNAR1	P17181	Y466	0.254	1.161	0.059	-2.249
IFNGR1	P15260	Y479	0.338	1.125	0.322	1.162
IFNGR1	P15260	Y457	0.034	-1.922	0.493	-1.004
IGF1R	P08069	Y1166	0.323	1.269	0.007	-3.497
IkB-alpha	P25963	S32/36	0.318	1.184	0.136	1.915
IkB-alpha	P25963	Y42	0.134	1.794	0.285	-1.337
IkB-beta	Q15653	S313/15	0.321	1.160	0.109	1.748
IkB-beta	Q15653	T19/23	0.430	1.083	0.435	-1.106
IkB-epsilon	O00221	S18/22	0.168	-1.483	0.353	1.196
IKK-alpha	O15111	T23	0.047	1.486	0.117	1.502
IKK-alpha	O15111	S180	0.215	1.431	0.286	-1.168
IKK-beta	O14920	Y199	0.489	-1.011	0.077	1.879
IKK-beta	O14920	Y188	0.084	-1.436	0.219	1.501
IKK-gamma	Q9Y6K9	S31	0.021	-1.551	0.216	-1.222
IKK-gamma	Q9Y6K9	S43	0.043	1.280	0.038	-1.466
IL-10R-A	Q13651	Y496	0.346	1.173	0.467	1.040
IL-16	Q14005	S143/4	0.438	1.066	0.257	1.158
IL1A	P01583	S87	0.463	1.045	0.298	1.283
IL2RB	P14784	Y364	0.248	1.228	0.466	-1.041
IL2RB	P14784	Y536	0.031	-1.920	0.321	-1.231
IL4R	P24394	Y713	0.253	-1.340	0.001	2.635
IL7R	P16871	Y449	0.486	-1.013	0.139	1.415
IL-8R B	P25025	S351/2/3	0.143	1.615	0.052	2.795
IL-8R B	P25025	S347	0.180	1.460	0.447	-1.089
iNOS	P35228	S739	0.001	2.844	0.326	1.201
iNOS	P35228	Y151	0.002	3.450	0.370	1.146
iNOS	P35228	S909	0.002	1.305	0.151	-1.515
IRAK1	P51617	T209	0.282	1.383	0.172	1.482
IRAK1	P51617	S376	0.253	-1.320	0.427	-1.058
IRAK1	P51617	T387	0.300	-1.178	0.377	-1.146
IRAK1	P51617	S568	0.027	1.486	0.349	-1.264
IRAK1	P51617	T100	0.427	1.080	0.153	-1.630
IRF-3	Q14653	S396/8	0.078	-1.979	0.050	1.636
IRF-3	Q14653	S385/6	0.269	-1.173	0.105	1.258
IRF-3	Q14653	S402/5	0.043	-2.020	0.129	1.647
IRF-5	Q13568	S437	0.220	1.387	0.415	-1.094
ITK	Q08881	Y512	0.366	1.134	0.040	1.929
Jak1	P23458	Y1022/3	0.120	1.701	0.065	1.835
Jak2	O60674	Y1007/8	0.420	-1.077	0.401	-1.098

Jak3	P52333	Y981	0.090	1.699	0.436	-1.065
JIP1	Q9UQF2	T103	0.043	1.297	0.330	1.175
JNK1	P45983	Y185	0.291	1.217	0.024	-2.219
JNK1	P45983	S377	0.021	-2.023	0.017	2.750
JNK2	P45984	S129	0.427	1.058	0.342	1.242
JNK2	P45984	T404/7	0.415	-1.049	0.355	1.277
JNK3	P53779	T131	0.174	1.406	0.315	1.356
Jun	P05412	S73	0.021	-1.622	0.033	1.645
Jun	P05412	S63	0.474	1.023	0.308	1.173
Kit	P10721	Y721	0.132	-1.341	0.170	1.377
Kit	P10721	S821	0.136	-1.349	0.384	-1.109
LEF-1	Q9UJU2	T155	0.372	1.052	0.042	1.812
LEF-1	Q9UJU2	S166	0.381	1.110	0.138	-1.452
LRRFIP1	O75766	S497	0.457	-1.031	0.440	-1.052
LRRFIP1	O75766	S690	0.378	-1.136	0.240	-1.302
Lyn	P07948	Y507	0.161	1.300	0.008	-2.498
MEK1	Q02750	S217	0.288	1.303	0.056	-1.894
MEK2	P36507	Y216	0.488	1.010	0.137	-1.647
MEK5	Q13163	S311/15	0.193	1.319	0.169	-1.621
MEKK1	Q13233	T1383	0.417	-1.073	0.316	-1.273
Met	P08581	Y1234/5	0.246	1.383	0.234	-1.373
Met	P08581	Y1349	0.070	1.531	0.120	-1.522
MKK3	P46734	T222	0.320	1.237	0.497	1.003
MKP-1	P28562	S296	0.403	-1.044	0.000	3.743
MKP-1	P28562	S359	0.112	-1.432	0.463	-1.024
MKP-1	P28562	S323	0.300	-1.172	0.341	-1.139
MLK3	Q16584	T277	0.010	2.142	0.207	-1.350
Mos	P00540	S25	0.409	-1.053	0.438	-1.051
MSK1	O75582	T581	0.308	-1.172	0.496	-1.003
MSK2	O75676	S347	0.366	-1.103	0.226	1.607
MSK2	O75676	S196	0.231	1.370	0.300	1.265
mucin 1	P15941	T1224/7/9	0.037	1.722	0.005	2.689
NFAT1	Q13469	S168	0.223	-1.310	0.375	1.132
NFAT1	Q13469	S326	0.481	1.016	0.396	1.081
NFAT2	O95644	S294	0.007	-1.953	0.152	-1.191
NFAT2	O95644	S245	0.032	-1.608	0.121	-1.530
NFAT4	Q12968	S163/5	0.450	-1.031	0.069	1.361
NFkB-p100	Q00653	S865	0.199	-1.648	0.064	1.522
NFkB-p100	Q00653	S869/71	0.010	-2.012	0.165	1.396

NFkB-p105	P19838	S337	0.331	-1.176	0.132	1.211
NFkB-p105	P19838	S907	0.117	-1.394	0.474	-1.020
NFkB-p65	Q04206	S276	0.213	1.320	0.110	1.369
NFkB-p65	Q04206	S311	0.169	-1.415	0.382	1.138
NFkB-p65	Q04206	S536	0.049	-1.709	0.450	1.059
NGFR	P08138	Y336	0.126	1.371	0.317	1.236
Nik	Q99558	T559	0.192	1.259	0.449	-1.067
Notch 2	Q04721	S2070	0.121	-1.353	0.261	-1.158
Notch 2	Q04721	T1808	0.411	-1.094	0.057	-1.729
p300	Q09472	S893	0.040	-1.421	0.486	1.011
p300	Q09472	S1834	0.217	-1.239	0.340	-1.174
P38 gamma	P53778	T183/5	0.322	-1.251	0.427	1.116
p38-alpha	Q16539	Y323	0.118	-1.549	0.472	1.020
p38-alpha	Q16539	T180/2	0.280	-1.211	0.489	-1.009
p40phox	P14598	T154	0.069	-1.588	0.430	1.053
p47phox	P14598	S370	0.364	-1.095	0.103	1.649
p53	P04637	S6/9	0.438	1.102	0.178	1.399
p53	P04637	S215	0.258	-1.395	0.140	-1.460
p70S6Kb	Q9UBS0	S473/4	0.477	1.020	0.388	1.135
PDGFRb	P09619	Y579/81	0.058	-1.372	0.076	1.559
PDGFRb	P09619	Y740	0.073	1.733	0.196	1.284
PIK3R1	P27986	S608/7	0.374	-1.114	0.341	-1.117
PKACa	P17612	T195/7	0.386	1.094	0.131	1.577
PKACa	P17612	S338	0.422	1.052	0.204	1.283
PKCA	P17252	Y658	0.188	1.349	0.330	1.109
PKCA	P17252	S656	0.047	-1.714	0.367	1.180
PKCA	P17252	T637	0.137	-1.585	0.265	-1.272
PKCB	P05771	S15/T16	0.346	-1.220	0.355	1.168
PKCB	P05771	T323	0.479	1.022	0.233	-1.339
PKCE	Q02156	T710	0.077	1.522	0.294	-1.273
PKCE	Q02156	S729	0.380	-1.116	0.029	-2.446
PKCT	Q04759	T219	0.473	-1.030	0.300	1.204
PKCT	Q04759	Y90	0.201	1.443	0.314	1.192
PKG1	Q13976	T58	0.374	-1.061	0.320	-1.195
PKR	P19525	T451	0.001	-2.411	0.371	-1.115
PKR	P19525	T446	0.320	-1.091	0.327	-1.128
PLCB1	Q9NQ66	S887	0.310	-1.129	0.012	2.358
PLCB1	Q9NQ66	S887	0.155	1.556	0.099	1.606
PLCG1	P19174	Y472	0.369	1.101	0.172	-1.448

PLCG1	P19174	Y771	0.021	1.863	0.162	-1.582
PLCG1	P19174	Y783	0.489	-1.011	0.000	-2.902
PPARG	P37231	S112	0.459	-1.041	0.477	-1.009
PPP2CA	P67775	T304/7	0.068	1.529	0.434	-1.071
PTP1B	P18031	S50	0.041	1.882	0.458	-1.033
PXN	P49023	Y31	0.121	-1.698	0.188	1.505
Pyk2	Q14289	Y402	0.013	-2.401	0.490	-1.007
RAC1	P63000	S71	0.498	-1.001	0.065	1.367
Raf1	P04049	S499	0.217	-1.330	0.409	-1.097
Raf1	P04049	S259	0.217	-1.410	0.402	-1.130
RasGAP	P20936	Y460	0.350	1.145	0.261	1.446
Rb	P06400	S780	0.223	1.226	0.124	-1.554
Rb	P06400	S795	0.484	-1.010	0.069	-2.440
RelB	Q01201	S573	0.291	1.150	0.116	-1.284
RhoA	P61586	S188	0.253	1.294	0.124	-1.918
RIPK1	Q13546	Y384/7/9	0.098	1.340	0.006	-2.602
ROCK2	O75116	S1134/7	0.321	-1.132	0.077	-1.531
SEK1	P45985	S80	0.314	-1.190	0.355	1.225
SEK1	P45985	S257/0	0.479	-1.023	0.128	-1.833
Shc1	P29353	Y349/0	0.277	1.245	0.496	1.003
Smad1	Q15797	S462/3/5	0.145	-1.209	0.265	-1.160
Smad2	Q15796	S250	0.471	-1.021	0.102	1.772
Smad2	Q15796	S255	0.022	-1.966	0.177	1.425
Smad2	Q15796	T8	0.024	-1.852	0.427	-1.035
Smad3	P84022	S208	0.156	-1.300	0.331	1.123
Smad3	P84022	S422/3/5	0.272	-1.094	0.494	1.002
Smad4	Q13485	T277	0.046	-1.746	0.430	-1.044
smMLCK	Q15746	S1773	0.419	1.068	0.116	1.770
Src	P12931	S96	0.200	1.282	0.486	1.014
Src	P12931	S74	0.188	1.236	0.167	-1.453
SRF	P11831	S77/79	0.138	1.500	0.415	-1.100
STAT1	P42224	S727	0.099	-1.421	0.461	1.026
STAT1	P42224	Y701	0.202	-1.194	0.188	-1.332
STAT2	P52630	Y690	0.082	-1.520	0.110	1.264
STAT3	P40763	Y705	0.104	-1.440	0.300	-1.177
STAT3	P40763	S727	0.321	1.346	0.166	-1.407
STAT4	Q14765	Y693	0.218	-1.234	0.255	-1.205
STAT4	Q14765	S721	0.090	-1.636	0.177	-1.321
STAT5B	P51692	Y699	0.481	1.024	0.473	-1.024

STAT5B	P51692	S731	0.240	1.212	0.464	-1.032
STAT6	P42226	Y641	0.288	-1.250	0.319	-1.095
STMN1	P16949	S62	0.265	-1.168	0.043	1.456
STMN1	P16949	S15	0.364	1.113	0.395	1.094
Syk	P43405	Y525/6	0.039	1.647	0.313	1.282
TAK1	O43318	S192	0.328	1.168	0.019	1.758
TAK1	O43318	T184	0.443	1.059	0.458	1.046
TBK1	Q9UHD2	S172	0.427	1.043	0.492	1.008
TNF-R1	P19438	S274	0.266	-1.288	0.497	-1.003
TNFRSF5	P25942	T254	0.438	1.056	0.231	1.440
TNIK	Q9UKE5	T987	0.240	1.160	0.328	-1.200
TNIK	Q9UKE5	S764	0.017	2.053	0.237	-1.265
TPH1	P17752	S58	0.405	-1.090	0.111	1.878
TRAF6	Q9Y4K3	T	0.182	-1.374	0.274	1.305
TRAF6	Q9Y4K3	T	0.009	-1.830	0.440	-1.086
TRAF6	Q9Y4K3	T	0.121	1.276	0.363	-1.174
TRAF6	Q9Y4K3	T	0.087	-1.236	0.300	-1.211
TRAF6	Q9Y4K3	S	0.026	1.688	0.266	-1.164
TRAF6	Q9Y4K3	S	0.017	1.682	0.006	-2.309
TRAF6	Q9Y4K3	S	0.316	1.169	0.002	-1.705
TrkB	Q16620	Y706/7	0.130	-1.271	0.053	-2.665
TrkC	Q16288	Y516	0.055	1.496	0.280	-1.427
Tyk2	P29597	Y1054/5	0.176	-1.440	0.126	1.717
VASP	P50552	S156	0.197	1.372	0.219	1.344
VEGFR-1	P17948	Y1169	0.052	1.677	0.443	-1.060
VEGFR-2	P35968	Y1214	0.297	1.290	0.137	-1.476
VEGFR3	P35916	Y130/1	0.418	-1.046	0.455	1.051
VEGFR3	P35916	Y1265	0.076	-1.395	0.438	-1.090
WASP	P42768	Y291	0.052	-1.839	0.494	1.007
XIAP	P98170	S87	0.302	1.227	0.309	1.054

Peptide array data which has been transformed with *p*-value and fold change calculated based on the comparisons listed. Name indicates name of protein corresponding to peptide target sequence printed. ID refers to protein UniProt identification number. *p*-value refers to significance value calculated between two treatments indicated. Fold change refers to the differences between the two treatments indicated.

Table A2. Transformed peptide array data: MAP project.

Name	ID	Target	IFN+MAP vs Monocytes		IFN+Monocytes vs Monocytes	
			p-value	Fold Change	*p*-value	Fold Change
4E-BP1	Q13541	T46	0.067	1.234	0.439	1.014
4E-BP1	Q13541	T37	0.361	1.053	0.265	-1.068
ADCY8	P40145	Y406	0.224	-1.090	0.013	-1.104
Akt1	P31749	S473	0.445	1.017	0.384	-1.023
Akt1	P31749	T308	0.213	-1.083	0.046	-1.149
Akt1	P31749	Y326	0.175	1.157	0.030	1.302
Akt1	P31749	S124/9	0.487	-1.005	0.392	-1.042
Akt3	Q9Y243	T447	0.259	1.145	0.108	1.174
Akt3	Q9Y243	S120	0.404	1.027	0.458	1.013
APE1	P27695	S289	0.059	-1.245	0.153	-1.185
Aplp1	P51693	Y643	0.122	-1.327	0.158	1.104
ApoE	P02649	S314	0.488	1.003	0.002	-1.273
A-Raf	P10398	Y301	0.253	1.085	0.279	1.023
ASK1	Q99683	S966	0.147	-1.171	0.266	1.063
ASK1	Q99683	S1033	0.263	-1.082	0.010	-1.232
ASK1	Q99683	S83	0.289	-1.074	0.008	-1.238
ATF-2	P15336	T51/3/5	0.472	-1.016	0.054	1.169
ATF-2	P15336	S44	0.385	1.048	0.404	1.023
ATF-4	P18848	S245	0.462	-1.033	0.033	1.392
axin-1	O15169	S486	0.303	-1.053	0.482	-1.002
Bad	Q92934	S118	0.028	1.259	0.069	1.140
BATF	Q16520	T48	0.027	-1.207	0.207	-1.077
BCAP	Q6ZUJ8	Y281	0.377	1.030	0.113	1.095
BCAP	Q6ZUJ8	Y17	0.311	-1.057	0.094	-1.112
Bcl-2	P10415	S70	0.469	1.026	0.041	1.263
Bcl-2	P10415	T56	0.421	1.043	0.419	1.024
Bid	P55957	T59	0.481	-1.005	0.047	-1.120
BLNK	Q8WV28	Y96	0.209	-1.098	0.133	1.102
BLNK	Q8WV28	Y72	0.336	1.035	0.250	1.043
B-Raf	P15056	T598	0.411	-1.044	0.166	1.090
Btk	Q06187	Y223	0.489	1.004	0.061	1.163
Btk	Q06187	Y551	0.253	1.078	0.068	1.107
Calmodulin	P62158	Y99	0.117	1.144	0.470	-1.007
CaMK2-alpha	Q9UQM7	T286	0.241	-1.085	0.129	1.204
Casp3	P42574	S150	0.116	-1.103	0.406	1.015
Casp8	Q14790	S347	0.060	-1.184	0.150	1.075

caveolin-1	Q2TNI1	Y14	0.420	-1.013	0.068		-1.128
Cbl	P22681	Y371	0.205	-1.139	0.095		-1.113
CBP	Q92793	S2063	0.265	-1.090	0.024		1.203
CCR2	P41597	Y139	0.474	-1.012	0.315		1.094
CCR5	P51681	S336/7	0.108	-1.146	0.161		-1.124
CCR7	P32248	S356/7	0.177	-1.186	0.166		-1.128
CCR7	P32248	T372/3/4/5/7	0.215	-1.071	0.132		-1.114
CD28	P10747	Y206/9	0.276	1.082	0.398		1.021
CD45	P08575	S999/02/03	0.271	1.137	0.062		-1.162
CD45	P08575	Y1216	0.491	1.003	0.053		-1.175
Cdc25A	P30304	S88	0.398	-1.047	0.207		1.108
Cdc25A	P30304	S82	0.270	1.087	0.312		-1.052
Cdc42	P60953	Y64	0.236	-1.071	0.001		-1.227
CDK2	P24941	T14/5	0.199	1.141	0.166		1.127
CDK2	P24941	T160	0.386	1.034	0.237		1.098
CDK7	P50613	T170	0.147	1.119	0.293		1.057
Cot	P41279	S400	0.116	-1.183	0.343		1.072
CREB	P16220	S129	0.422	-1.023	0.063		-1.124
CREB	P16220	S110/1	0.222	1.065	0.058		-1.110
Crk	P46108	Y221	0.151	1.057	0.133		-1.083
CSFR	P07333	Y809	0.226	1.067	0.236		-1.045
CSFR	P07333	Y561	0.241	1.041	0.188		-1.063
CSK	P41240	Y184	0.034	1.247	0.060		1.149
CTLA-4	P16410	Y201	0.297	-1.081	0.364		1.054
CTNNB1	P35222	T41/45	0.153	1.234	0.135		1.114
CTNNB1	P35222	Y142	0.094	1.322	0.264		1.038
CTNNB1	P35222	S675	0.222	1.041	0.102		-1.120
CTSB	P07858	Y219	0.129	1.210	0.358		1.033
CXCR4	P61073	Y157	0.221	1.134	0.252		1.114
cyclin D1	P24385	T286/8	0.413	1.033	0.344		1.046
cyclin E1	P24864	T395	0.354	1.136	0.297		1.067
Cystatin S	P01036	S132	0.288	1.102	0.086		-1.124
DAPK1	P53355	S735	0.306	1.109	0.128		-1.111
DAPK1	P53355	S308	0.065	-1.249	0.009		-1.238
DAPK3	O43293	T180	0.438	-1.024	0.334		1.032
DAPK3	O43293	T225	0.004	1.348	0.375		1.017
DAPP1	Q9UHF2	Y139	0.497	-1.001	0.060		1.159
Daxx	Q9UER7	S668/71	0.464	-1.020	0.487		-1.008
DNA-PK	P78527	T2609	0.500	1.000	0.192		1.110

DNA-PK	P78527	T2638	0.484	1.008	0.429	1.022
Elk-1	P19419	T417	0.426	-1.025	0.038	1.284
Elk-1	P19419	S389	0.121	-1.108	0.320	1.054
eNOS	P29474	S1176	0.325	1.070	0.126	1.088
EphA1	P21709	Y781	0.244	1.088	0.412	-1.015
EphA2	P29317	Y588	0.169	1.171	0.055	1.245
EphA2	P29317	Y772	0.042	1.185	0.195	1.089
EphA2	P29317	Y594	0.173	1.090	0.302	1.025
ERK1	P27361	T202/4	0.304	-1.069	0.403	1.019
ERK2	P28482	Y205	0.019	-1.102	0.088	1.126
ERK3	Q16659	S189	0.037	-1.175	0.094	1.233
Etk	P51813	Y40	0.121	1.139	0.015	1.130
Ezrin	P15311	T566	0.446	1.014	0.048	-1.264
FADD	Q13158	S194	0.402	1.018	0.090	1.104
FADD	Q13158	S196	0.111	1.087	0.015	-1.217
FAK	Q05397	Y397	0.416	1.020	0.405	-1.015
Fas	P25445	Y291	0.130	-1.187	0.192	-1.107
Fas	P25445	Y232	0.480	-1.007	0.009	-1.163
Fes	P07332	Y713	0.433	-1.012	0.002	-1.280
FGFR1	P11362	Y154	0.495	-1.002	0.363	1.023
FGFR1	P11362	Y653/4	0.297	1.068	0.440	1.009
FGFR1	P11362	Y463	0.451	1.014	0.008	-1.171
FGFR3	P22607	Y724	0.213	1.094	0.500	1.000
FGFR3	P22607	Y760	0.247	-1.114	0.303	-1.055
FGFR4	P22455	Y754	0.191	-1.136	0.382	-1.025
FLT3	P36888	Y589/91	0.471	1.012	0.427	1.030
FLT3	P36888	Y597/9	0.377	1.036	0.242	-1.051
Fos	P01100	T232	0.332	-1.051	0.106	1.147
FRS2	Q8WU20	Y196	0.478	1.007	0.447	-1.014
FRS2	Q8WU20	Y436	0.119	-1.151	0.087	-1.179
FRS3	Q8WU20	Y416	0.390	-1.038	0.135	-1.134
Fyn	P06241	Y420	0.463	1.005	0.361	-1.019
Fyn	P06241	Y531	0.266	1.035	0.040	-1.164
GCAP2	Q9UMX6	S200	0.264	-1.117	0.098	1.103
gp130	P40189	S782	0.326	1.040	0.141	1.143
gp130	P40189	Y767	0.355	1.063	0.167	1.152
gp130	P40189	Y814	0.360	1.032	0.448	1.012
Grb10	Q13322	S150	0.281	-1.058	0.148	1.091
Grb2	P62993	Y209	0.416	-1.033	0.312	-1.035

GSK3-beta	P49840	Y216	0.449	-1.017	0.044	1.149
GSK3-beta	P49840	S9	0.348	-1.047	0.067	1.284
HIF1A	Q16665	T796	0.354	1.041	0.397	-1.022
HIF2A	Q99814	T840	0.341	-1.047	0.457	-1.013
HMGA1	P17096	T52	0.344	1.085	0.090	1.093
H-Ras-1	P01112	T35	0.284	-1.065	0.018	-1.247
HSP27	P04792	S78/82/3	0.355	-1.067	0.194	1.117
HSP60	P10809	Y227	0.159	1.110	0.049	-1.115
HSP70	P08107	Y525/6	0.123	1.127	0.147	1.087
IFNAR1	P17181	Y466	0.228	-1.170	0.044	1.141
IFNAR1	P17181	S535	0.411	-1.038	0.246	-1.073
IFNGR1	P15260	Y479	0.467	-1.011	0.243	1.079
IFNGR1	P15260	Y457	0.273	-1.070	0.260	1.092
IGF1R	P08069	Y1166	0.119	-1.148	0.284	1.068
IkB-alpha	P25963	Y42	0.404	-1.031	0.114	-1.121
IkB-alpha	P25963	S32/36	0.406	1.026	0.006	-1.206
IkB-beta	Q15653	S313/15	0.091	1.189	0.357	-1.017
IkB-beta	Q15653	T19/23	0.324	-1.072	0.319	-1.025
IKK-alpha	O15111	T23	0.225	1.067	0.335	-1.028
IKK-beta	O14920	Y199	0.272	1.068	0.086	1.223
IKK-beta	O14920	Y188	0.267	-1.078	0.156	1.103
IKK-gamma	Q9Y6K9	S31	0.289	1.215	0.004	1.366
IKK-gamma	Q9Y6K9	S43	0.326	1.059	0.225	1.065
IL-10R-A	Q13651	Y496	0.146	-1.144	0.192	1.114
IL-16	Q14005	S143/4	0.165	1.174	0.101	1.205
IL1A	P01583	S87	0.245	1.145	0.147	1.135
IL2RB	P14784	Y536	0.272	-1.089	0.237	1.098
IL2RB	P14784	Y364	0.181	-1.119	0.314	1.050
IL4R	P24394	Y713	0.314	1.082	0.140	1.158
IL7R	P16871	Y449	0.178	1.161	0.073	1.156
IL-8R B	P25025	S347	0.451	1.007	0.067	-1.119
IL-8R B	P25025	S351/2/3	0.234	-1.065	0.026	-1.148
iNOS	P35228	Y151	0.089	-1.181	0.027	-1.258
iNOS	P35228	S909	0.305	-1.082	0.016	-1.198
iNOS	P35228	S739	0.180	-1.097	0.001	-1.236
IRAK1	P51617	T100	0.246	-1.134	0.028	1.203
IRAK1	P51617	S376	0.468	1.029	0.296	1.049
IRAK1	P51617	T387	0.310	-1.065	0.453	-1.015
IRAK1	P51617	T209	0.268	1.080	0.275	-1.041

IRAK1	P51617	S568	0.439	-1.031	0.200	-1.088
IRF-3	Q14653	S385/6	0.483	-1.005	0.105	1.123
IRF-3	Q14653	S402/5	0.483	-1.003	0.201	1.054
IRF-3	Q14653	S396/8	0.492	1.002	0.258	1.049
IRF-5	Q13568	S437	0.333	1.043	0.010	1.121
ITK	Q08881	Y512	0.430	1.017	0.372	-1.023
Jak1	P23458	Y1022/3	0.122	-1.161	0.415	1.029
Jak2	O60674	Y1007/8	0.222	-1.085	0.443	-1.010
Jak3	P52333	Y981	0.022	-1.269	0.355	-1.020
JIP1	Q9UQF2	T103	0.478	1.005	0.013	-1.148
JNK1	P45983	Y185	0.277	-1.101	0.070	-1.153
JNK1	P45983	S377	0.380	1.047	0.186	1.149
JNK2	P45984	T404/7	0.193	1.066	0.483	1.003
JNK2	P45984	S129	0.311	-1.069	0.312	-1.046
JNK3	P53779	T131	0.223	1.093	0.079	-1.120
Jun	P05412	S63	0.245	-1.077	0.060	1.332
Jun	P05412	S73	0.392	-1.045	0.395	1.038
Kit	P10721	Y721	0.176	1.096	0.291	1.042
Kit	P10721	S821	0.139	-1.144	0.264	-1.090
LEF-1	Q9UJU2	T155	0.195	1.131	0.246	1.072
LEF-1	Q9UJU2	S166	0.087	-1.159	0.188	-1.055
LRRFIP1	O75766	S690	0.175	1.047	0.449	-1.010
LRRFIP1	O75766	S497	0.226	-1.049	0.185	-1.065
Lyn	P07948	Y507	0.281	1.069	0.074	-1.150
MEK1	Q02750	S217	0.068	-1.255	0.429	1.019
MEK2	P36507	Y216	0.276	1.129	0.063	1.332
MEK5	Q13163	S311/15	0.383	-1.046	0.264	-1.076
MEKK1	Q13233	T1383	0.445	1.015	0.371	-1.032
Met	P08581	Y1349	0.440	1.028	0.233	1.075
Met	P08581	Y1234/5	0.167	1.140	0.453	1.011
MKP-1	P28562	S359	0.066	-1.134	0.049	1.335
MKP-1	P28562	S323	0.221	1.107	0.090	1.172
MKP-1	P28562	S296	0.345	-1.117	0.300	-1.042
MLK3	Q16584	T277	0.417	1.052	0.201	-1.108
Mos	P00540	S25	0.088	-1.319	0.368	-1.036
MSK1	O75582	T581	0.200	-1.139	0.078	-1.095
MSK2	O75676	S347	0.345	1.051	0.072	-1.058
MSK2	O75676	S196	0.399	-1.031	0.008	-1.158
mucin 1	P15941	T1224/7/9	0.367	1.036	0.042	-1.172

NFAT1	Q13469	S326	0.453	1.024	0.051	1.150
NFAT1	Q13469	S168	0.134	-1.168	0.303	1.053
NFAT2	O95644	S294	0.046	1.137	0.137	1.137
NFAT4	Q12968	S163/5	0.439	-1.017	0.228	-1.095
NFkB-p100	Q00653	S865	0.164	1.208	0.086	1.123
NFkB-p100	Q00653	S869/71	0.387	-1.047	0.265	-1.120
NFkB-p105	P19838	S337	0.382	1.045	0.043	1.210
NFkB-p105	P19838	S907	0.330	1.094	0.200	1.110
NFkB-p65	Q04206	S276	0.283	1.152	0.003	1.229
NFkB-p65	Q04206	S311	0.371	-1.071	0.022	1.258
NFkB-p65	Q04206	S536	0.397	1.044	0.235	1.070
NGFR	P08138	Y336	0.275	-1.084	0.399	1.034
Nik	Q99558	T559	0.494	1.001	0.385	1.017
Notch 2	Q04721	T1808	0.446	-1.011	0.420	1.021
Notch 2	Q04721	S2070	0.418	-1.018	0.297	-1.046
p300	Q09472	S893	0.449	1.049	0.054	1.130
p300	Q09472	S1834	0.062	1.212	0.096	1.074
P38 gamma	P53778	T183/5	0.296	1.070	0.091	1.097
p38-alpha	Q16539	Y323	0.234	1.095	0.493	-1.001
p38-alpha	Q16539	T180/2	0.222	1.107	0.329	-1.032
p40phox	P14598	T154	0.376	-1.049	0.268	-1.058
p47phox	P14598	S370	0.498	-1.001	0.447	1.011
p53	P04637	S6/9	0.245	1.060	0.052	-1.135
p53	P04637	S215	0.328	-1.059	0.035	-1.266
p70S6Kb	Q9UBS0	S473/4	0.297	1.060	0.173	-1.092
PDGFRb	P09619	Y579/81	0.175	1.141	0.111	1.100
PDGFRb	P09619	Y740	0.276	1.076	0.415	-1.015
PIK3R1	P27986	S608/7	0.394	-1.042	0.353	-1.038
PKACa	P17612	T195/7	0.121	1.174	0.033	1.165
PKACa	P17612	S338	0.279	1.081	0.246	1.078
PKCA	P17252	S656	0.208	-1.091	0.042	-1.220
PKCA	P17252	T637	0.268	-1.076	0.003	-1.227
PKCB	P05771	T323	0.117	1.190	0.265	-1.075
PKCB	P05771	S15/T16	0.355	1.070	0.162	-1.108
PKCE	Q02156	T710	0.284	1.092	0.416	-1.012
PKCE	Q02156	S729	0.098	-1.179	0.036	-1.213
PKCT	Q04759	T219	0.419	-1.028	0.059	-1.163
PKCT	Q04759	Y90	0.095	-1.191	0.003	-1.293
PKG1	Q13976	T58	0.193	-1.154	0.074	-1.220

PKR	P19525	T451	0.472	-1.009	0.162	1.084
PKR	P19525	T446	0.049	1.370	0.182	1.093
PLCB1	Q9NQ66	S887	0.437	1.027	0.078	1.097
PLCB1	Q9NQ66	S887	0.215	1.196	0.366	1.043
PLCG1	P19174	Y783	0.376	-1.042	0.022	1.137
PLCG1	P19174	Y472	0.490	-1.002	0.407	1.022
PLCG1	P19174	Y771	0.293	-1.057	0.049	-1.103
PPARG	P37231	S112	0.460	1.011	0.047	-1.128
PPP2CA	P67775	T304/7	0.002	-1.730	0.022	-1.328
PTP1B	P18031	S50	0.243	-1.179	0.083	1.146
PXN	P49023	Y31	0.241	1.096	0.096	1.122
Pyk2	Q14289	Y402	0.460	1.016	0.238	1.086
RAC1	P63000	S71	0.372	1.037	0.436	1.006
Raf1	P04049	S499	0.249	1.051	0.018	-1.187
Raf1	P04049	S259	0.297	-1.056	0.012	-1.347
RasGAP	P20936	Y460	0.240	-1.093	0.022	-1.106
Rb	P06400	S780	0.230	1.108	0.241	1.080
Rb	P06400	S795	0.286	1.079	0.298	1.025
RelB	Q01201	S573	0.457	-1.014	0.042	1.196
RhoA	P61586	S188	0.465	1.020	0.090	1.296
RIPK1	Q13546	Y384/7/9	0.126	1.173	0.021	1.293
ROCK2	O75116	S1134/7	0.408	-1.022	0.298	-1.067
SEK1	P45985	S257/0	0.441	1.014	0.187	1.080
SEK1	P45985	S80	0.410	1.038	0.298	1.099
Shc1	P29353	Y349/0	0.478	-1.007	0.029	-1.159
Smad1	Q15797	S462/3/5	0.278	1.164	0.041	1.220
Smad2	Q15796	T8	0.479	-1.013	0.043	1.330
Smad2	Q15796	S255	0.265	1.101	0.043	1.230
Smad3	P84022	S208	0.153	1.163	0.013	1.240
Smad3	P84022	S422/3/5	0.321	1.110	0.123	1.119
smMLCK	Q15746	S1773	0.327	1.068	0.345	1.046
SOD1	P00441	S98	0.290	-1.068	0.267	-1.052
Src	P12931	S96	0.426	-1.033	0.393	-1.029
Src	P12931	S74	0.299	1.044	0.057	-1.129
SRF	P11831	S77/79	0.074	1.116	0.052	-1.098
STAT1	P42224	Y701	0.142	1.203	0.078	1.221
STAT1	P42224	S727	0.207	1.092	0.283	1.050
STAT2	P52630	Y690	0.080	-1.154	0.062	1.133
STAT3	P40763	S727	0.459	-1.018	0.032	1.361

STAT3	P40763	Y705	0.157	-1.116	0.046	1.157
STAT4	Q14765	Y693	0.448	1.017	0.065	1.261
STAT4	Q14765	S721	0.337	-1.060	0.094	1.172
STAT5B	P51692	Y699	0.493	1.003	0.054	1.140
STAT5B	P51692	S731	0.468	1.011	0.450	1.016
STAT6	P42226	Y641	0.139	-1.398	0.004	1.220
STMN1	P16949	S62	0.345	1.049	0.176	1.156
STMN1	P16949	S15	0.208	-1.071	0.410	1.022
Syk	P43405	Y525/6	0.354	-1.036	0.097	1.117
TAK1	O43318	T184	0.325	1.037	0.028	1.120
TAK1	O43318	S192	0.209	1.177	0.283	1.081
TBK1	Q9UHD2	S172	0.377	-1.040	0.224	-1.056
TNF-R1	P19438	S274	0.424	-1.018	0.005	-1.185
TNFRSF5	P25942	T254	0.348	-1.052	0.037	-1.091
TNIK	Q9UKE5	T987	0.218	-1.094	0.005	-1.260
TNIK	Q9UKE5	S764	0.182	-1.135	0.004	-1.353
TPH1	P17752	S58	0.009	-1.407	0.033	-1.239
TrkB	Q16620	Y706/7	0.117	1.155	0.119	1.080
TrkC	Q16288	Y516	0.355	1.081	0.413	1.028
Tyk2	P29597	Y1054/5	0.425	-1.030	0.155	1.040
VASP	P50552	S156	0.305	1.144	0.340	-1.068
VEGFR-1	P17948	Y1169	0.178	-1.203	0.455	1.007
VEGFR-2	P35968	Y1214	0.491	-1.002	0.012	1.215
VEGFR3	P35916	Y130/1	0.437	-1.036	0.032	1.359
VEGFR3	P35916	Y1265	0.063	-1.176	0.121	-1.081
VIM	P08670	S39	0.203	1.077	0.047	-1.146
WASP	P42768	Y291	0.206	-1.075	0.188	1.058
XIAP	P98170	S87	0.169	-1.119	0.018	1.149

Peptide array data which has been transformed with *p*-value and fold change calculated based on the comparisons listed. Name indicates name of protein corresponding to peptide target sequence printed. ID refers to protein UniProt identification number. *p*-value refers to significance value calculated between two treatments indicated. Fold change refers to the differences between the two treatments indicated.